Journal of Power Sources, 2 (1977/78) 3 - 24

REVIEW ON THE LEAD–ACID BATTERY SCIENCE AND TECHNOLOGY

PAUL RUETSCHI
Leclanché S.A., 1400 Yverdon (Switzerland)

Why Still Lead–Acid Batteries?

In spite of extensive and continued efforts aimed at developing new light-weight, low-cost secondary electrochemical power sources, the old "lead–acid" battery, invented 118 years ago, has still not been dethroned as the major battery system. Today, hundreds of millions of lead–acid cells are in use for starting automobiles, to power electric fork-lift trucks, for delivering emergency electric power, for transmitting and signaling operations in telephone central offices, for railway car lighting, for starting diesel engines, to name a few of the more important applications.

A brief look into their history may be helpful in answering the question heading this introduction: Why still lead–acid batteries? First, history teaches us to be patient. More than half a century of exploratory work went by, after Volta's discovery, in 1800, of the first primary "pile" until Planté was able to demonstrate, in 1860, the first practical rechargeable lead–acid battery [1]. Planté used large lead sheet electrodes which he "formed" by cycling in dilute sulphuric acid.

Gautherot had already observed in 1801 the so-called "secondary" current flow, *i.e.* current obtainable in the opposite direction after a preceding "charge". Two years later Ritter reported results with a large number of different "secondary" electrode systems. But only Sinsteden, in 1854, experimented systematically with lead electrodes in sulphuric acid and found them to deliver large "secondary" currents. Previously, from 1836 to 1843 De la Rive had already investigated lead dioxide as a positive electrode in sulphuric acid primary cells. For inventions also, one plants, another waters, and a third reaps.

By the time Planté made his successful demonstration, a large number of various other battery systems had been proposed, as summarized in Tomassi's impressive review [2].

The history of the lead–acid cell may be divided into three chapters. During the *first period* from 1860 to 1910, efforts were concentrated on finding the most suitable electrode structures and practical manufacturing techniques. The endeavour and struggle, mostly by Edison-type trial and error, is reflected in Jumeau's monumental 900-page book [3]. Some examples of early plate structures are shown in Figs. 1 and 2.

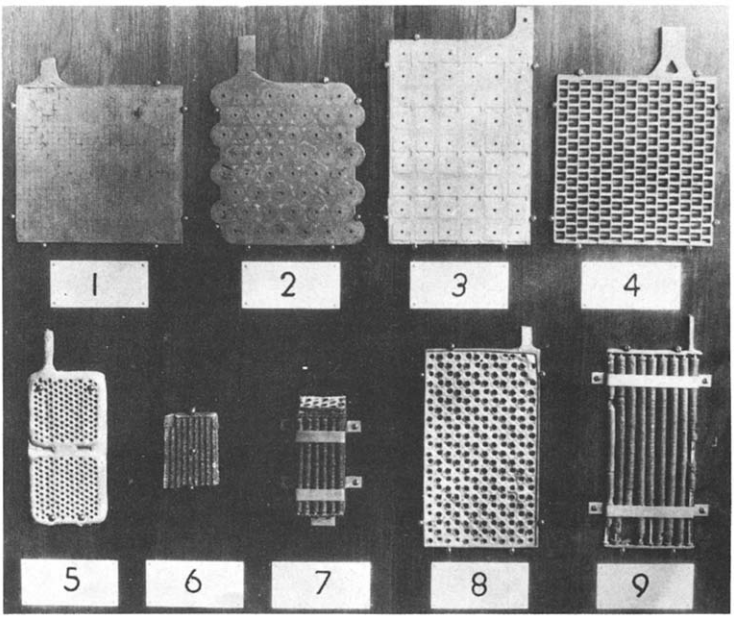

Fig. 1. Collection of plate designs, as used at the beginning of this century. (Courtesy ESB Inc., Philadelphia)

Today, only two types of plate structures have major importance, the *pasted plate*, introduced first by Faure in 1881, and the *tubular plate*, developed at the beginning of this century (Fig. 3). The pasted plate is made by applying a paste, made of (incompletely) oxidized lead powder and sulphuric acid, to a cast lead–alloy grid structure. The tubular plate (also called "iron-clad" plate in the U.S.A.) is made by filling a mixture of oxidized lead powder and minium into porous tubes of glass-, polyester-, or other acid-resistant fibres. The tubes are arranged in parallel fashion to form a plate. A central lead–alloy wire or "spine" serves as current collector in each tube.

The plates are charged (or formed) in dilute sulphuric acid solution to form sponge lead in the negative electrodes and lead dioxide in the positive electrodes.

In 1880 Gladstone and Tribe published the "double sulphate theory" [4]. For many years it was heavily disputed and was only well established many years later [5]. According to this theory, the overall reaction in the lead–acid battery is given by:

$$PbO_2 + Pb + 2H_2SO_4 \rightleftarrows 2PbSO_4 + 2H_2O$$

By 1910, the basic design features, as well as the basic chemical interpretation of the electrochemical cell reactions, had assumed their final forms.

During the *second period* from 1910 to 1950 the technology of plate and cell manufacturing evolved by the use of new machinery allowing the manufacture of finer and purer lead oxides, the more rapid casting of grids,

Fig. 2. Early tubular battery construction, about 1900. The tubes are formed of hard rubber washers, piled upon another. (Courtesy ESB Inc., Philadelphia)

and the mechanized pasting of grids. An important milestone was the introduction of lignin expanders into the negative plates [6]. These had a dramatic effect in improving the cycle-life, by preventing grain coarsening. Microporous rubber separators (introduced in 1927) and resin-bonded paper (introduced in 1948) replaced the old wood separators [7]. Antimony-free grid alloys were first used in 1935 [8]. Arsenic was added to lead antimony alloys to improve greatly their corrosion resistance [9].

Among the scientific progress realized in this period was the establishment of precise thermodynamic data on the lead and lead dioxide electrodes in sulphuric acid [10]. The double sulphate theory was further substantiated [11].

The state of the developments at the end of this period was summarized in Vinal's classic book [12].

Among the technological advances during the *third period*, since 1950, one might mention the use of polypropylene, instead of hard rubber, for

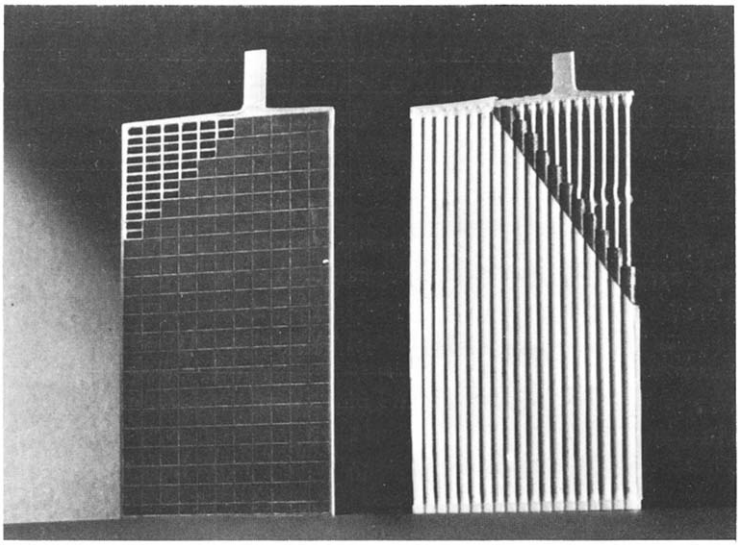

Fig. 3. Modern traction battery plates; (left), pasted negative plate; (right), tubular positive plate.

battery casings, shorter intercell connections (through the cell partitions) for starter batteries, a widespread use of low-antimony or antimony-free grid alloys, the use of thinner plates with optimized grid design and better active mass utilization at high discharge rates, and a more generalized use of dry-charged battery manufacturing technology.

Since 1950 progress in research on lead and lead dioxide electrodes has been spurred by the use of much more sophisticated experimental techniques [13 - 15]. New electronic equipment, such as galvanostats (constant current generators), potentiostats (individual electrode potential regulating means) and sweep generators became available. Considerable progress was made in the mathematical treatment of mass transport phenomena. Rotating disc electrodes were used to separate mass transfer polarization from charge-transfer polarization. Scanning electron microscopy, radioactive tracer methods, X-ray- and neutron-diffraction, nuclear magnetic resonance and electron spectroscopy allowed a better understanding of solid surfaces. Attention turned away from thermodynamics to the kinetics of electrode processes [16].

New stimulus for research came as a result of the discovery of a second polymorph, called α-PbO_2, in positive plates and in corrosion films, by Bode and Voss [17] and Ruetschi and Cahan [18]. This new modification of PbO_2 had been synthesized shortly before by Zaslavsky *et al.* [19] and Katz [20].

Also in recent years, the commercial use of the lead–acid battery has continued unabated, serving many applications. In 1960, in the midst of widespread enthusiasm on fuel cell research, an article had raised the question: "Is the lead–acid battery obsolete?" [21]. It was not obsolete then, and it is not obsolete today, 17 years later. No new battery system is in sight

now, which could do better than the lead–acid battery when it comes to a comparison of those price performance–life ratios which alone are relevant to commercial use. The abundance of lead and its ease of recycling are also helping the lead–acid battery defend its position. Renewed interest in electric automobiles will give lead–acid battery research a new boost [22, 23]. The future will see many new approaches to lead–acid battery technology, including the study of ultra-light grid structures.

In the following, progress in four areas of major interest will be discussed: (1) the kinetics of the electrode processes; (2) side reactions. H_2 and O_2 evolution. Low Sb, and Sb-free grids. Maintenance-free and sealed lead–acid cells; (3) the theory of porous electrodes; (4) anodic corrosion of lead and lead alloys. Emphasis is given to recent progress, not covered in the latest reviews [24 - 26].

The kinetics of the electrode processes

Lead–acid battery electrodes are obviously much more complicated structures than those which a theoretical electrochemist would ideally choose for fundamental studies. In order to characterize and predict the electrochemical behaviour of such complicated porous structures, a number of physical parameters must be determined separately: porosity, surface area, pore size distribution, electrolyte conductivity and viscosity as a function of concentration, solubility and diffusion coefficient of lead sulphate, electrochemical rate constants, transfer coefficients, ohmic resistivity of grids and active materials, and ohmic losses at the solid–solid and solid–liquid interfaces.

In a porous electrode various forms of polarization are coupled: charge transfer (activation) polarization, mass transport (concentration) polarization, ohmic polarization and crystallization polarization [27].

After switching on a current flow to the electrode, double layer charging across the electrolyte resistance in the pores will cause time lags in establishing the pseudo steady-state current distribution throughout the interior of the electrode. Furthermore, as will be discussed later, the pseudo steady-state current density can vary from the surface to the interior of the plates, because of the ohmic resistance in the pores.

The discharge curve for a positive and a negative electrode is illustrated schematically in Fig. 4. The instantaneous potential drop, A, after switching on the current, is due to the electrolyte resistance in the electrolyte-filled pores of the separators, the ohmic resistance in the grids, active material layers and solid–solid and solid–liquid interfaces. The sloping portion, B, arises from double layer capacity discharge, as coupled through the ohmic electrolyte resistance in the pores of the active mass. Supersaturation, nucleation and crystallization phenomena lead to the initial voltage dip, C, in the discharge curve of the positive electrode [28]. This behaviour of the positive electrode may be related to the relatively poor charge acceptance of the positive electrode during recharge at low temperatures and at high rates.

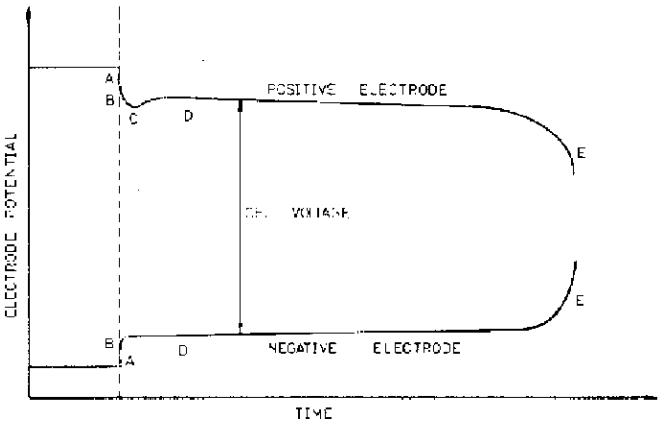

Fig. 4. Schematic discharge curves for positive and negative plates.

Section D in Fig. 4 represents the successive discharge of the active materials to lead sulphate. It is finally followed by rapid polarization at E, due to acid depletion and pore obstruction by lead sulphate crystals.

The basic electrode processes in the positive and in the negative electrodes involve a *dissolution–precipitation mechanism*, and not some sort of solid-state ion transport and film formation mechanism. Thus, during discharge of a lead electrode in sulphuric acid:

$$Pb \rightarrow Pb^{2+} \text{ (in solution)} + 2e^-$$

$$Pb^{2+} + SO_4^{2-} \rightarrow PbSO_4\text{(cryst.)}$$

A micropore undergoing discharge is schematically depicted in Fig. 5. Even though the solubility of lead ions in a 35% sulphuric acid solution is only about 2 mg/l [29] a dissolution–precipitation mechanism may support large currents, because of the high internal surface area of porous electrodes. Vetter [30] has derived a simple equation for the lead ion concentration build-up (Fig. 5). He assumed uniform current distribution throughout the porous electrode, and free availability of the total internal surface area. Nevertheless, the order of magnitude of the calculated concentration build-up must be correct. It is surprisingly small, even at high applied currents per unit of external geometric plate surface. For instance, at 0.1 A/cm^2 one calculates for the increase in surface concentration of lead ions $\Delta C = 4 \times 10^{-7}$ mol/l, a value considerably lower than the equilibrium $PbSO_4$ solubility. The $PbSO_4$ equilibrium solubility decreases with increasing acid concentration and with decreasing temperature. It is apparently high enough in any case to support a diffusion–precipitation mechanism.

Discharge and charge of lead electrodes may be considered as anodic dissolution into, and cathodic electroplating out of, dilute lead ion solutions, respectively. The action of expanders in negative plates may then be understood as inhibition of the growth of large Pb crystals on charge and of large $PbSO_4$ crystals on discharge [31 - 36].

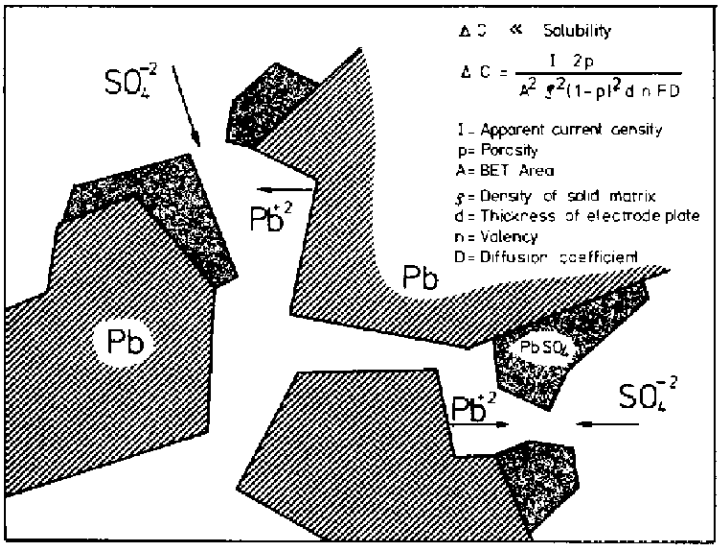

Fig. 5. Schematic illustration of the dissolution–precipitation mechanism in the pores of a negative plate.

The dissolution–precipitation mechanism, illustrated in Fig. 5, is supported by morphological studies using scanning electron microscopy. One observes growth of well-developed lead sulphate crystals which protrude from the surface into the liquid in a manner only explicable by growth from solution, as demonstrated in Fig. 6 [37, 38].

Also for the lead dioxide electrode the discharge reaction proceeds via dissolution–precipitation [39]. This is schematically depicted in Fig. 7. The process may be described by the equations:

$$2e^- + PbO_2 + 4H^+ \rightarrow Pb^{2+} + H_2O$$

$$Pb^{2+} + SO_4^{2-} \rightarrow PbSO_4$$

Discharged PbO_2 electrodes investigated under the scanning electron microscope show well developed $PbSO_4$ crystals whose morphology changes with discharge rate [40 - 45].

Convincing support for a dissolution–precipitation mechanism has been provided by periodic observation of the same pin-point of battery plates with the scanning electron microscope [45]. During discharge the surface of the PbO_2 grains becomes rough but no lead sulphate becomes visible initially. As time proceeds, lead sulphate crystals begin to grow rapidly from solution (Fig. 8). At the end of a 5 h rate discharge a considerable portion of the PbO_2 surface remains still visible. Active mass utilization thus appears to be limited by factors such as acid depletion in the pores and loss of electronic contact to individual PbO_2 grains, rather than by the formation of dense, inert $PbSO_4$ layers.

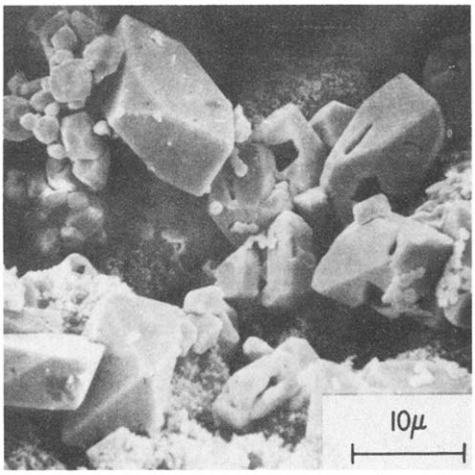

Fig. 6. Electron micrograph of the surface of a cycled negative plate [38].

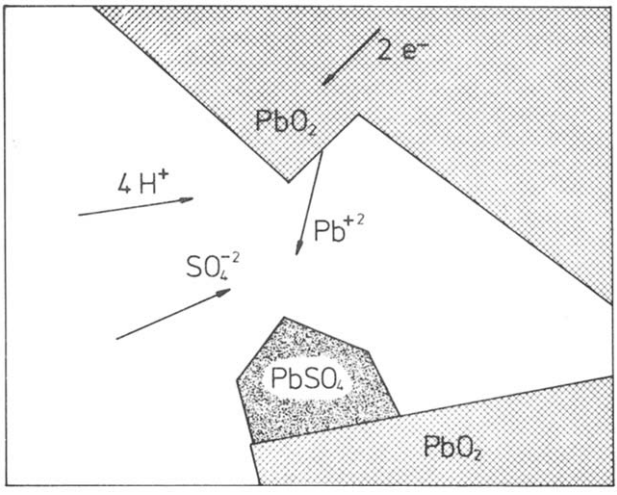

Fig. 7. Schematic illustration of the dissolution–precipitation mechanism in the pores of a positive plate.

It has been proposed that the detailed discharge mechanism may be more complicated than formulated above and may involve further complex intermediates [42, 46 - 50] of 2- or 4-valent lead.

Of interest is the fact that α- and β-PbO_2 show different discharge behaviour, as first discovered by Ruetschi and Cahan [51] and later confirmed by many investigators. The α-PbO_2 modification usually yields smaller discharge capacities than β-PbO_2 [28, 52 - 54]. Only β-PbO_2 produces the initial voltage dip shown in Fig. 4 [28, 52, 55, 56]. Apparently, α-PbO_2 forms a surface having nucleation centres for $PbSO_4$ formation. Thus, during discharge, the α-PbO_2 surface becomes more rapidly covered by $PbSO_4$ crystals. In general, α-PbO_2 forms smaller surface areas than β-PbO_2 [54, 57].

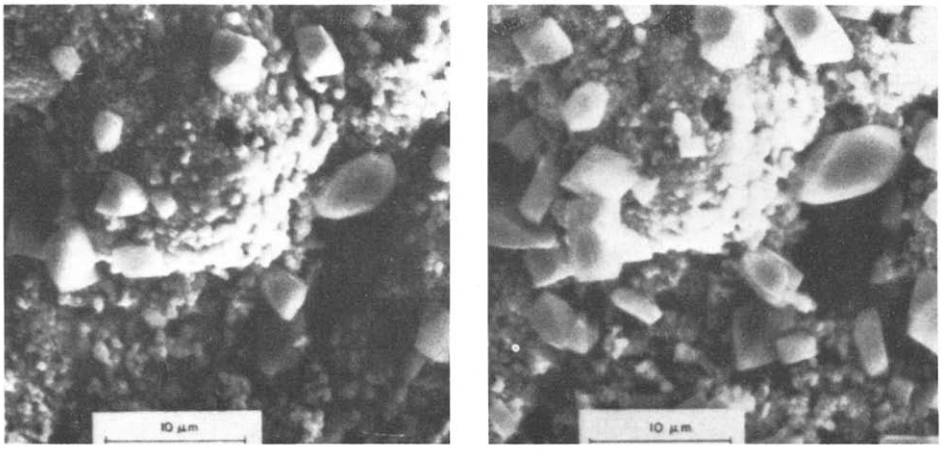

(a) (b)

Fig. 8. Electron photomicrographs of the same pin-point in a positive electrode during discharge at the 5 h rate; (a) after 3 h of discharge; (b) after 5 h of discharge [45].

The mechanism of anodic formation of PbO_2 is influenced by pH and by the type and concentration of anions present. In near neutral or slightly alkaline solutions, lead ions are complexed with OH groups [58]. It may be that in the formation of α-PbO_2 an intermediate complex of tetravalent lead with $(OH)^-$ groups is being formed, *e.g.* $Pb(OH)_2^{2+}$, whereas the formation of β-PbO_2 proceeds via a complex of tetravalent lead with $[HSO_4]^-$ or $[SO_4]^{2-}$ for instance $[Pb(HSO_4)_2]^{2+}$ [17, 46, 51, 59]. Growth of PbO_2 nuclei from $PbSO_4$ follows a cubic rate law, *i.e.* at constant potential, the current increases with the third power of time [60, 61].

The reversible electrode potential of α-PbO_2 in H_2SO_4 is higher than that of β-PbO_2 [51, 52, 54, 62]. The solid state physics of the two PbO_2 modifications have been studied extensively in recent years. X-ray and neutron diffraction, nuclear magnetic resonance, thermal analysis etc. have been used. It would be beyond the scope of this review to discuss also these aspects. In this connection a theoretical study of effective charges on the lead and oxygen atoms is also of interest [63].

Side reactions, self-discharge, gassing, low-antimony and antimony-free grids, maintenance-free and sealed lead–acid cells

In Vinal's book [12], no mention is made of maintenance-free or sealed lead–acid cells. However, since then much interest has developed in this area and during the past 15 years maintenance-free and sealed lead–acid batteries have come into being. This has been possible through the control of side reactions, especially gassing. Self discharge of lead–acid batteries involves seven different reactions [64, 65].

Lead dioxide and lead are thermodynamically unstable in sulphuric acid solution. The potential of the $PbO_2/PbSO_4$ couple (1.698 V *vs.* H_2) is 0.47 V above that of the O_2/H_2O couple, and the potential of the $Pb/PbSO_4$ couple is situated 0.356 V below that of the H_2/H_2O couple. On open circuit, oxygen evolution from the PbO_2 electrode and hydrogen evolution from the Pb electrode must occur. The rates of these gassing reactions depend on the O_2 overvoltage on PbO_2, and the H_2 overvoltage on Pb, respectively.

Oxygen evolution from PbO_2 according to:

$$PbO_2 + H_2SO_4 \rightarrow PbSO_4 + H_2O + 1/2O_2$$

increases with increasing acid concentration [54, 64 - 66]. This is illustrated in Fig. 9.

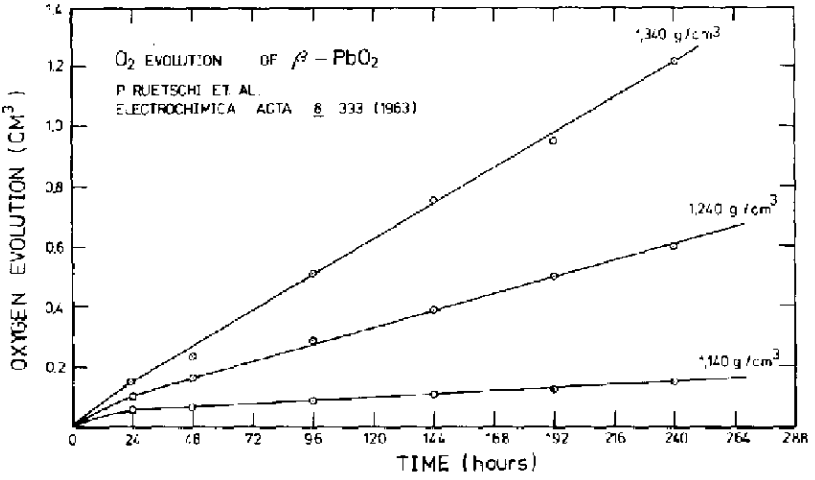

Fig. 9. Oxygen evolved from samples of 1.50 g β-PbO_2 at 30 °C, with sulphuric acid gravity as parameter [54].

The rate of oxygen evolution from PbO_2 is also strongly influenced by the presence of certain impurities. Antimony dissolved out of the positive grids and retained in the positive active material increases O_2 evolution [51]. Also cobalt, silver and copper ions increase the rate of O_2 evolution from PbO_2. Oxygen evolution kinetics from α-PbO_2 differ from those from β-PbO_2 [51, 52, 54, 62]. After current interruption, the oxygen overvoltage decays slowly while O_2 gas continues to be evolved. The large pseudo double-layer capacitance in the O_2 evolution region is due to adsorbed O_2 [62, 67, 68].

Anodic corrosion of the grid alloy is another side reaction which contributes to self-discharge of the positive electrodes. The rate of this reaction depends on the type of grid alloy, as well as on acid concentration [64]. Reaction between the lead–alloy grid and the PbO_2 active material may be described by an equation identical to that of the overall discharge process in the lead acid battery. Figure 10 represents analytically determined lead sulphate

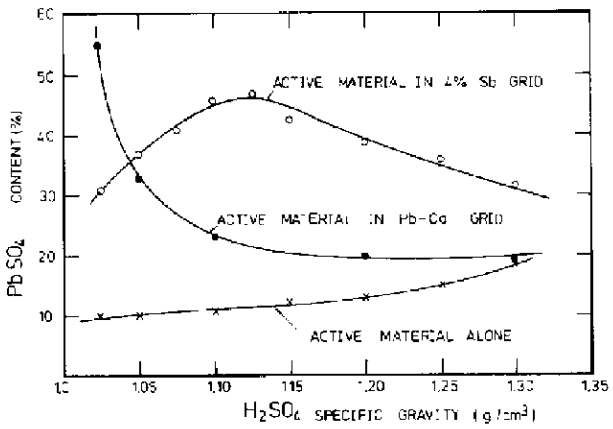

Fig. 10. Analytically determined lead sulphate content (in wt %) in positive active material, after storage of plates, or active material alone, for 16 weeks at 35 °C [64].

content in positive plates, expressed in wt% of the active material, after 16 weeks of open circuit storage at 35 °C. Curve A refers to active material alone, stored in sulphuric acid in the absence of grids. Curve B refers to active material in a positive plate having a 4% antimony grid, and curve C to active material in a calcium alloy grid.

As seen from the difference between curves A and C, sulphation due to interaction between grid and active material proceeds fast in low gravity acid. In the case of active material in 4% Sb grids, sulphation is faster, owing to increased oxygen evolution. However, at low acid gravities, the reaction between grid and active material appears to be slowed down.

Hydrogen is oxidized by PbO_2 according to:

$$PbO_2 + H_2 + H_2SO_4 \rightarrow PbSO_4 + 2H_2O$$

at a very low rate [64, 65, 69].

However, the reaction can be made to proceed very rapidly by means of auxiliary electrodes, whose potential is suitably controlled, as discussed later. The solubility of H_2 in H_2SO_4 decreases strongly with increasing acid concentration because of salting-out effects [70, 71].

Negative plates undergo self-discharge by the reaction:

$$Pb + H_2SO_4 \rightarrow PbSO_4 + H_2$$

whose speed is controlled by the slow step of H_2 evolution. Its rate increases with increasing acid concentration [64, 72]. Owing to the high H_2 overvoltage on lead, the process is quite slow with plates having pure lead or lead-calcium grids. However, if the negative active material is contaminated with Sb, hydrogen evolution is catalyzed considerably [51, 64]. The nature of the antimony species present in sulphuric acid solution has been elucidated only in recent years [73, 74].

Although antimony has a deleterious effect on self-discharge and should therefore be avoided as much as possible in maintenance-free or sealed cells,

it is known to confer beneficial effects on the structure of the positive active mass. In fact, a very large portion of the Sb dissolved anodically from the positive grids is retained in the positive active material and reaches the negative plates only with delay [64, 75].

Antimony retained in the positive active material not only lowers O_2 overvoltage but also seems to act as a binding agent between PbO_2 particles. For this reason, positive plates containing antimony grids may show less shedding of positive active material during cycling. Antimony is possibly present in the positive active material in the form of mixed Sb–Pb oxides [76]. Bismuth appears to show to a lesser extent the same effects as Sb [77].

The presence of antimony in the positive grid may also influence the initial α-β-PbO_2 ratio after formation. Phosphoric acid additions to the electrolyte also tend to influence this ratio [51, 78 - 80].

For maintenance-free lead–acid cells the advantages and disadvantages of having Sb present must be carefully weighed. In the case where Sb-free grids are being used, an addition of phosphoric acid to the electrolyte can be used with advantage to harden the positive plates, at the cost, however, of a slight capacity decrease. In electrolytes containing phosphoric acid, the stability of 4-valent dissolved lead species is increased [81].

The undesirable diffusion of Sb species from the positive plate to the negative plate can be slowed down considerably by using suitable separators [64, 82]. On the negative plate Sb may be removed in the form of stibine by overcharge and vigorous H_2 evolution at cell voltages above 2.4.

Besides Sb, many other contaminants decrease H_2 overvoltage on the negative plates [83, 84]. On the other hand, additives to the electrolyte have been discovered which increase the H_2 overvoltage, and which will at least partly compensate for the effects of Sb on self-discharge [85].

The fact that oxygen is reduced readily on a lead electrode in sulphuric acid, according to the reaction:

$$\tfrac{1}{2}O_2 + Pb + H_2SO_4 \rightarrow PbSO_4 + H_2O$$

contributes to the self-discharge of open cells [64]. In sealed cells this reaction is of basic importance, since it allows removal of oxygen produced during charge, overcharge or storage within the cell. Thus, an "oxygen cycle" may be established [86]. The oxygen reduction appears to be diffusion controlled. Oxygen solubility in H_2SO_4 and the oxygen diffusion coefficient decrease with increasing acid concentration [71].

In order to increase oxygen mass transport, most sealed lead–acid cells make use of semi-dry separator-plate packs in which the sulphuric acid electrolyte is immobilized by gel-formers such as SiO_2. Grids are of Ca–alloy and phosphoric acid additions to the electrolyte are used to improve cycle life [87 93].

For maintenance-free cells, which are not entirely sealed, the use of low-antimony lead alloys has been thought to be a practical compromise. Such grids are characterized by excellent corrosion resistance, as discussed later. In addition, less problems may be expected than with Sb-free grids during cycling

service. A large amount of development work on low-antimony grids, with additions of As, Sn, Se, Te, Co, Ag and Cu has been done in recent years, as reflected by the extensive patent literature and recent reviews [94, 95].

For large, stationary lead–acid cells auxiliary electrodes have been devised to cut watering requirements or to render them completely maintenance-free. Auxiliary electrodes for oxygen reduction, connected to the negative electrodes, consisting of porous carbon, rendered water-proof by sintered Teflon particles, catalyzed with silver and partly immersed into the electrolyte, are able to electrochemically reduce oxygen at high rates [96, 97]. Phthalocyanine has been proposed, instead of silver, as a catalyst in oxygen-consuming auxiliary electrodes [98]. Hydrogen can be removed effectively in large, flooded stationary cells by means of waterproof, partly wetted auxiliary electrodes, held at a suitable electrode potential by such means as solid state diodes [97, 99, 100]. It has also been realized that hydrogen oxidation and oxygen reduction can occur on the same electrode simultaneously [100]. The principle of using potential-controlled auxiliary electrodes is illustrated in Fig. 11. A similar arrangement has been described in a recent patent [101].

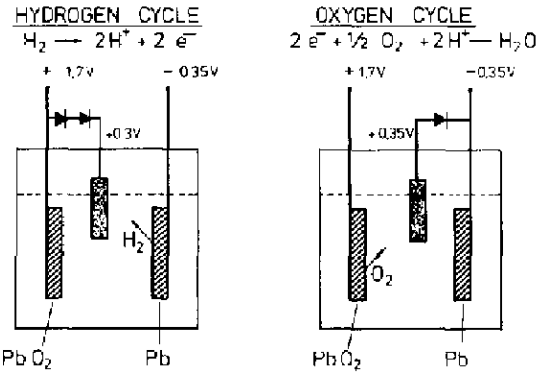

Fig. 11. Auxiliary electrode arrangement for hydrogen or oxygen removal in sealed lead–acid cells. Hydrogen consuming auxiliary electrodes are connected through diodes to the positive electrode. Oxygen removing auxiliary electrodes are connected to the negative electrode.

The pressure-dependence of the hydrogen oxidation, or oxygen reduction current on partly wetted, porous electrodes, held at constant potential, is approximately represented by the equation [97]:

$$\log i = \text{const.} + (1/2)\log p$$

The exchange current density has a maximum at $4N$ H_2SO_4 [71].

Recombination of hydrogen and oxygen on supported catalysts in the gas space above the electrolyte level is another means to reduce water loss due to electrolysis in large lead–acid cells [102, 103].

The development of sealed and semi-sealed lead–acid cells has necessitated the development of safe venting means in case of overpressure (Fig. 12) [90, 104].

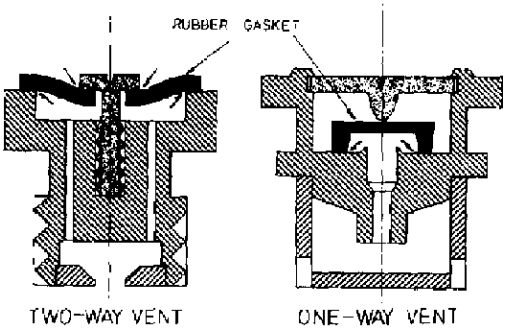

Fig. 12. Venting means for sealed lead–acid cells [90, 104].

Theory of porous electrodes

The positive and negative plates of lead–acid batteries consist of highly porous active masses of lead dioxide, and lead respectively. In order to characterize such electrodes phenomenologically it is necessary to measure the total internal surface area, the porosity and the pore size distribution. Most methods used by electrochemists to determine these quantities are not *in situ* techniques [105]. The electrodes must for instance be freed from electrolyte, washed and dried. This may change the morphology of the surface.

Surface area is usually measured by gas absorption techniques. For positive electrode active material one finds in the charged state typically values of 2 to 10 m^2/g [54, 68, 106, 107]. The surface area is higher for β-PbO_2 than for α-PbO_2 [54].

For metallic sponge lead, the B.E.T. area is much lower, *e.g.* 0.46 m^2/g [106]. The surface area of formed active material depends on the paste consistency used to prepare the plates and on forming conditions, such as temperature, rate and acid concentration [108 - 110]. Total porosity and pore size distribution may be calculated also from gas absorption measurements. Other techniques to study the pore structure are absorption of solute molecules, microscopic evaluation, X-ray diffraction, gravimetric techniques, fluid permeability and mercury intrusion [107].

The measurement of the double layer capacity allows *in situ* surface area determinations. Constant current charging curves [68, 106], a.c. methods and potential-step techniques [111] have been used. Experimental conditions must be chosen so as to diminish interference from Faradaic currents. The electrolyte conductivity should be as high as possible in order to assure that voltage drops in the pores are much smaller than the charge-transfer polarization on the electrode interface, rendering the current distribution as uniform as possible.

From charging curves it was determined that α-PbO_2 has larger specific double layer capacitance ($\mu F/cm^2$ of true surface area) than β-PbO_2 [52]. For technical, pasted PbO_2 electrodes one obtains for the double layer capacitance of the active material in the oxygen evolution region a capacitance of 125 - 140 $\mu F/cm^2$, based on the B.E.T. surface [68, 106].

To what extent the B.E.T. area corresponds really to the electrochemically active area is, of course, rather uncertain.

For the active material in technical negative electrodes one obtains values of 10 - 11 $\mu F/cm^2$ of B.E.T. surface [68, 106].

Much progress has been made in the past few years on the mathematical modelling of porous electrodes with respect to polarization behaviour. Important contributions in this field were made by Ksenzhek and Stender [112], Newman and Tobias [113], de Levie [114], Euler [115] and Dunning *et al.* [116]. A review has been published by Newman and Tiedemann [117].

During discharge of technical battery electrodes the true current density throughout the pore structure is non-uniform. The current density distribution is governed by factors such as resistive voltage drops in the current-carrying grid structure, in the contact-interface grid/active material, in the active material itself and in the electrolyte-filled pores. Electrolyte resistance in the pores is of particular importance since it increases during discharge due to acid depletion. Furthermore, one must take into account electrolyte displacement and pore diameter decrease as $PbSO_4$ crystals, which occupy more space than Pb or PbO_2, precipitate. This latter effect has considerable consequences on the electrolyte resistance in the pores.

Theoretical calculations based on one-dimensional, pseudo steady-state models are able to predict qualitatively characteristic features of current distribution during discharge, state of discharge profiles and acid depletion profiles [118 - 121].

Figure 13 shows a calculated current distribution in a porous PbO_2 electrode during a 5 h rate discharge [120]. As discharge proceeds, a reaction zone advances from the front surface of the plate into the interior.

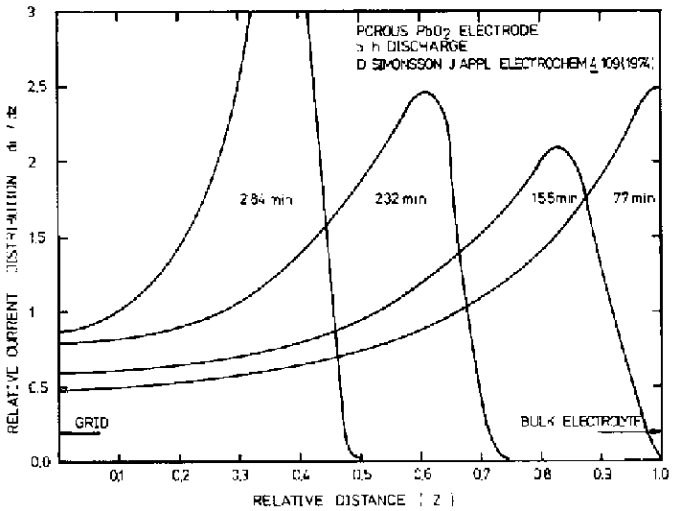

Fig. 13. Relative current distribution in a porous PbO_2 electrode, after 77, 155, 232 and 284 min of discharge, at the 5 h rate, 7.5 mA/cm^2 of plate surface [120].

The state of discharge distribution (degree of conversion of PbO_2 to $PbSO_4$) at various intervals of time during discharge is depicted in Fig. 14, and the local acid concentration profile in Fig. 15.

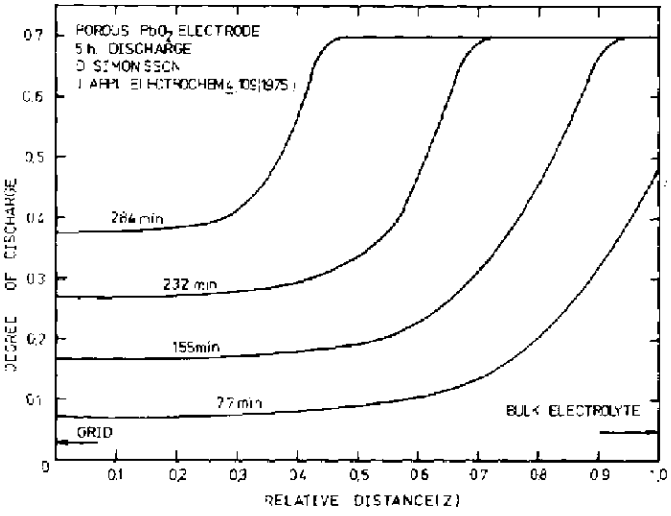

Fig. 14. Relative state of discharge after 4 different time intervals, as in Fig. 13 [120].

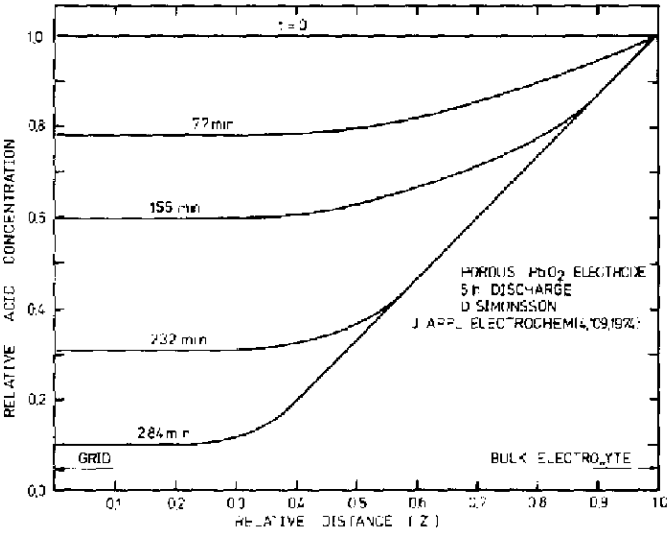

Fig. 15. Relative acid concentration as a function of relative distance from plate centre, at 4 different time intervals, as in Fig. 13 [120].

The following parameters were used for calculating the curves of Figs. 13 - 15. Initial plate porosity, 0.60; initial acid concentration, 5 mol/l; distance from plate centre to surface, 0.9 mm (plate thickness 1.8 mm); maximum active material utilization factor, 0.70.

Characteristic features of porous plate discharge behaviour may thus be accounted for on the basis of a mathematical model. It should be noted that the profiles shown in Figs. 13 - 15 depend strongly on the discharge rate. At very high discharge rates, for instance, the discharge is confined to the surface portions of the plates only [122, 123].

The advances made in the mathematical treatment of porous electrode behaviour might be of use in the future for the design of plates with optimized pore structures for a special use.

Still more accurate calculations could be envisaged, taking into account also the variations of acid concentration in the bulk electrolyte, outside the plates, vertical electrolyte concentration gradients and vertical electrolyte convection, as influenced by the tightness of cell assembly.

Anodic corrosion of lead and lead alloys

Positive grid corrosion is one of the principal reasons why lead–acid batteries wear out in service. Progress in our understanding of structure and growth of anodic corrosion films, as influenced by temperature, electrode potential, acid concentration, grid composition etc., has been paralleled by longer service life of the batteries.

The discovery of α-PbO_2 in corrosion films of lead [18] called for more detailed explanations concerning mass transport in such films. The formation of α-PbO_2 could then be explained by presuming that sulphuric acid does not readily penetrate into the corrosion films and that their interior contained an effectively alkaline medium [51]. It was also found that α-PbO_2 content and thus the degree of blockage against acid penetration depended on grid composition, especially on Sb concentration.

After prolonged constant current anodic oxidation in the potential range of oxygen evolution no divalent lead compounds are observed in the corrosion films [18, 51]. Superimposing an a.c. signal on the anodizing current, the transient behaviour during initial film formation, in particular the transformation of the initial $PbSO_4$, film into PbO_2, may be studied. In the state where the electrode is passivated by a $PbSO_4$ film, the double layer capacitance drops to very low values, *e.g.* 3 $\mu F/cm^2$, while the film resistance is strongly increased [124 - 127].

Using constant potential techniques the composition of the corrosion films may be studied conveniently over a wide range of potentials. In certain potential ranges the films then contain two-valent lead compounds such as PbO, $3PbO.PbSO_4$, $PbO.PbSO_4$ and $PbSO_4$ [128].

Tracing current–time curves at constant potential it was discovered that corrosion could proceed rapidly underneath a covering layer of $PbSO_4$ under certain conditions of potential. The rapid formation of corrosion products such as PbO and α-PbO_2 could be explained by the alkaline pH in the interior of the film.

Treating the covering $PbSO_4$ layer as a perm-selective precipitation membrane, non-permeable for SO_4^{2-} ions, but permeable for H_2O, OH^- and H^+

ions, Ruetschi has developed a multilayer model which accounts quantitatively for the composition of the corrosion films as a function of potential, and for the potentials observed during open-circuit depassivation [129]. According to this model, a diffusion potential due to the pH gradient must occur across the film. It amounts to 59 mV per unit pH difference and can thus reach values of several hundred mV (Figs. 16 and 17).

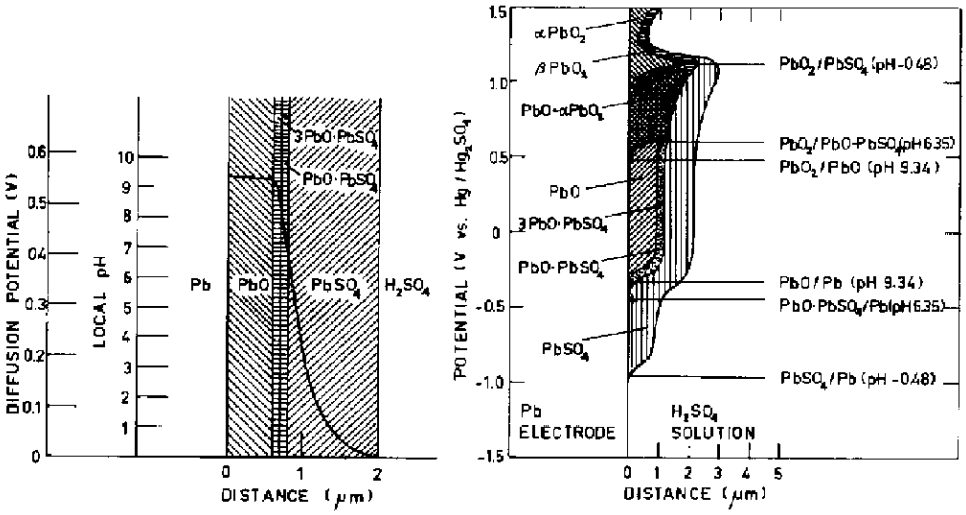

Fig. 16. Schematic representation of the diffusion potential and pH gradient across a multiphase corrosion film [128].

Fig. 17. Composition of anodic corrosion films on lead in sulphuric acid after anodization at various constant potentials for 24 h. [128].

This diffusion potential is to be added to the local potential in the interior of the film in order to calculate potentials which can be compared with experimental values.

The composite film model of Ruetschi also allows for the first time a self-consistent interpretation of the current peaks obtained during potentiodynamic linear anodic sweep [130 - 135].

The model may also be applied to commercial storage battery plates during initial formation in dilute acid. It is known that dense lead sulphate films are formed initially when the plates are immersed into the forming acid. Owing to these films the interior of the plate stays alkaline for a considerable time. This explains not only the formation of α-PbO_2 but also the low formation voltages which are observed initially under low rate formation. Furthermore, the dependence of α-PbO_2 content on paste density and formation rate may be explained by the Ah input into alkaline regions of the plates. [18, 51, 80, 136 - 140].

The multiphase nature of anodic corrosion films on lead in sulphuric acid, as illustrated in Fig. 16 and 17 is in agreement with experimental results

concerning X-ray diffraction [127, 139, 141] and electron microscopy [142 - 145].

The detailed studies of the corrosion phenomena on the positive grids of lead–acid cells have enabled battery engineers to understand the importance of proper float voltage control for longest life stationary batteries [146 - 150].

Conclusion

This review does not make any claim to being complete. In view of the vast subject this would have been hardly possible. It has tried to highlight some aspects of the technological and scientific progress. Also, the reference list had to be limited. I would like to apologize to all authors whose works are not quoted here. Part of the non-English literature was unavailable to me. Obviously, an impressive amount of work has been done on the lead–acid battery. What makes it so hard for new electrochemical power sources to compete with it, is not only its long head start, but also the high degree of sophistication and perfection it has reached.

References

1 G. Planté, C.R. Acad. Sci., 50 (1860) 640.
2 D. Tommasi, Traité des piles électriques, Georges Carré, Paris, 1889.
3 L. Jumeau, Les accumulateurs électriques, Dunod, Paris, 1904.
4 J. H. Gladstone and A. Tribe, Nature, 25 (1882) 221.
5 F. Dolezalek, Die Theorie des Bleiakkumulators, Halle, Paris, 1901.
6 T. A. Willard, U.S. Pat. 1,432,508; 1,505,990 (1920).
7 F. Booth, U.S. Pat. 2,673,889 (1954).
8 H. E. Haring and U. B. Thomas, Trans. Electrochem. Soc., 68 (1935) 293.
9 H. Stoertz, U.S. Pat. 2,678,340 (1953); 2,678,341 (1954).
10 W. J. Hamer, J. Am. Chem. Soc., 57 (1935) 9, 27, 33.
11 W. H. Beck and W. F. K. Wynne-Jones, Trans. Faraday Soc., 50 (1954) 136, 147, 927; 112 (1965) 1133; 55 (1959) 331; J. A. Duisman and W. F. Giauque, J. Phys. Chem., 72 (1968) 562.
12 G. Vinal, Storage Batteries, John Wiley, New York, 1955.
13 P. Delahay, New Instrumental Methods in Electrochemistry, Interscience, New York, 1954.
14 H. R. Thirsk and J. A. Harrison, A Guide to the Study of Electrode Kinetics, Academic Press, London, 1972.
15 E. Yeager and A. J. Salkind, Techniques of Electrochemistry, Vol. 1., Wiley–Interscience, New York, 1972.
16 K. Vetter, Electrochemical Kinetics, Academic Press, New York, 1967.
17 H. Bode and E. Voss, Z. Elektrochem., 60 (1956) 1053.
18 P. Ruetschi and B. D. Cahan, J. Electrochem. Soc., 104 (1957) 406.
19 A. I. Zaslavski, Y. D. Kondrashov and S. S. Tolkachev, Dokl. Akad. Nauk SSSR, 75 (1950) 559; A. I. Zaslavski and S. S. Tolkachev, J. Fiz. Khim. SSSR, 26 (1952) 743.
20 Th. Katz, Ann. Chim., 5 (1950) 5.
21 P. Ruetschi, J. Electrochem. Soc., 108 (1961) 297.
22 F. J. Port, Bull. Schweiz. Elektrotech. Ver., 68 (1977) 129.
23 S. Gross, Battery Council Int. Convention, London, 1974.

24 P. Ness, Electrochim. Acta, 12 (1967) 161.
25 J. Burbank, A. C. Simon and E. Willihnganz, Adv. Electrochem. and Electrochem. Engineering, Vol. 8, Interscience, New York, 1971.
26 J. P. Carr and N. A. Hampson, Chem. Rev., 72 (1972) 679.
27 P. Ruetschi, in C. A. Hampel (ed.), Encyclopedia of Electrochemistry, Reinhold, New York, p. 939.
28 D. Berndt and E. Voss in D. H. Collins (ed.), Batteries 2, Pergamon Press, Oxford, 1965, p. 17.
29 D. N. Craig and G. W. Vinal, J. Res. Natl. Bur. Stand. 22 (1939) 55.
30 K. Vetter, Chem.-Ing. Tech., 45 (1973) 213.
31 E. J. Ritchie, Trans. Electrochem. Soc., 92 (1947) 229.
32 Th. J. Hughel and R. H. Hammer, in D. H. Collins (ed.), Power Sources 3, Oriel Press, Newcastle upon Tyne, 1971, p. 35.
33 M. P. J. Brennan and N. A. Hampson, J. Electroanal. Chem., 48 (1973) 465.
34 E. G. Yampol'skaya, Elektrokhimia, 8 (1972) 1325.
35 A. Simon, S. M. Caulder, P. J. Gurfuski and J. R. Pierson, J. Electrochem. Soc., 121 (1974) 463.
36 G. Archdale and J. A. Harrison, Electroanal. Chem., 34 (1972) 21, 39 (1972) 357; 43 (1973) 321; 47 (1973) 93.
37 J. L. Weininger, J. Electrochem. Soc., 121 (1974) 1454.
38 J. L. Weininger and F. W. Secor, J. Electrochem. Soc., 121 (1974) 1541.
39 K. J. Euler, Bull. Schweiz. Elektrotech. Ver., 61 (1970) 1054.
40 G. Sterr and E. Voss, Aktuelle Batterieforschung, Varta, Frankfurt, 1966, p. 101.
41 A. C. Simon, S. M. Caulder and J. T. Stemmle, J. Electrochem. Soc., 122 (1975) 461.
42 J. L. Weininger and L. R. Morelock, J. Electrochem Soc., 122 (1975) 1161.
43 P. Casson, N. A. Hampson, K. Peters and P. Whyatt, J. Appl. Electrochem., 7 (1977) 257.
44 P. Reinhardt, M. Vogt and K. Wiesener, J. Power Sources, 1 (1976/1977) 127.
45 S. Hattori, M. Yamaura, M. Kohno, Y. Ohtani, M. Yamane and H. Nakashima, in D. H. Collins (ed.), Power Sources 5, Academic Press, London, 1975, p. 139.
46 W. Feitknecht and A. Gäumann, J. Chim. Phys., 49 (1952) 135.
47 L. I. Lyamina, N. I. Korol'kova, E. K. Oshe and K. M. Gorbunova, Elektrokhimia, 10 (1974) 841.
48 N. K. Mikhailova, I. A. Aguf and M. A. Dasoyan, Elektrokhimia, 9 (1973) 439.
49 N. A. Hampson, P. C. Jones and R. F. Phillips, Can. J. Chem., 46 (1968) 1325.
50 H. A. Laitinen and N. H. Watkins, J. Electrochem. Soc., 123 (1976) 804.
51 P. Ruetschi and B. D. Cahan, J. Electrochem. Soc., 105 (1958) 369.
52 R. I. Angstadt, C. J. Venuto and P. Ruetschi, J. Electrochem. Soc., 109 (1962) 177.
53 E. Voss and E. Freundlich, In D. H. Collins (ed.), Batteries, Pergamon Press, London, 1963, p. 73.
54 P. Ruetschi, J. Sklarchuck and R. T. Angstadt, Electrochim. Acta, 8 (1963) 333.
55 H. B. Mark and W. C. Vosburg, J. Electrochem. Soc., 108 (1961) 615.
56 H. B. Mark, J. Electrochem. Soc., 109 (1962) 634; 110 (1963) 945.
57 I. J. Astakhov, I. G. Kiseleva and B. N. Kabanov, Dokl. Akad. Nauk SSSR, 126 (1959) 1041.
58 A. Olin, Acta Chem. Scand., 14 (1960) 126, 314; A. Olin. Sven. Kem. Tidskr., 73 (1961) 482; L. Pajdowski and A. Olin, Acta Chem. Scand., 16 (1962) 983; B. Carell and A. Olin, Acta Chem. Scand., 16 (1962) 2350.
59 M. Fleischmann and M. Liler, Trans. Faraday Soc., 54 (1958) 1370.
60 M. Fleischmann and H. R. Thirsk, Electrochim. Acta, 1 (1959) 146; 2 (1960) 22.
61 M. Fleischmann, J. R. Mansfield, H. R. Thirsk, H. G. E. Wilson and L. Wynne-Jones, Electrochim. Acta, 12 (1967) 967.
62 P. Ruetschi, R. T. Angstadt and B. D. Cahan, J. Electrochem. Soc., 106 (1959) 547.
63 D. E. Parry, J. C. S. Faraday Trans. II, 71 (1975) 193.
64 P. Ruetschi and R. T. Angstadt, J. Electrochem. Soc., 105 (1958) 555.

65 K. R. Bullock and D. H. McClelland, J. Electrochem. Soc., 123 (1976) 327.
66 N. G. Baranova, Elektrokhimia, 8 (1972) 864.
67 B. D. Cahan and P. Ruetschi, J. Electrochem. Soc., 106 (1959) 543.
68 P. Ruetschi, J. B. Ockerman and R. Amlie, J. Electrochem. Soc., 107 (1960) 325.
69 B. K. Mahato, E. Y. Weissman, E. C. Laird, J. Electrochem. Soc., 121 (1974) 13.
70 P. Ruetschi and R. F. Amlie, J. Phys. Chem., 70 (1966) 718.
71 P. Ruetschi, J. Electrochem. Soc., 114 (1967) 301.
72 C. Drotschmann, Bleiakkumulatoren, Verlag Chemie, Weinheim-Bergstrasse, 1951, p. 35.
73 H. E. Hintermann and C. J. Venuto, J. Electrochem. Soc., 115 (1968) 10.
74 J. L. Dawson, M. I. Gillibrand and J. Wilkinson, J. Inorg. Nucl. Chem., 32 (1970) 501; in D. H. Collins (ed.), Power Sources 3, Oriel Press, Newcastle upon Tyne, 1971, p. 1.
75 W. Herrmann and G. Pröpstl, Z. Elektrochem., 61 (1957) 1154.
76 D. E. Swets, J. Electrochem. Soc., 120 (1973) 7.
77 J. L. Devitt and M. Myers, J. Electrochem. Soc., 123 (1976) 1769.
78 R. G. Acton, in D. H. Collins (ed.), Power Sources, Pergamon Press, London, 1966, p. 133.
79 J. Burbank, J. Electrochem. Soc., 111 (1964) 10.
80 V. H. Dodson, J. Electrochem. Soc., 108 (1961) 401.
81 H. Bode and E. Voss, Electrochim. Acta, 6 (1962) 13.
82 F. Zehender, W. Herrmann and H. Leibssle, Electrochim. Acta, 9 (1964) 55.
83 J. R. Pierson, C. E. Weinlein and Ch. E. Wright, in D. H. Collins (ed.), Power Sources 5, Academic Press, London, 1975, p. 97.
84 T. W. Caldwell, U.S. Sokolov and L. M. Bocciarelli, J. Electrochem. Soc., 123 (1976) 1265.
85 P. Ruetschi, U.S. Pat. 2,994,626 (Aug. 1, 1966).
86 J. Atkin, R. Bonnaterre and J.-F. Laurent, in D. H. Collins (ed.), Power Sources 6, Academic Press, London, 1977, p. 91.
87 K. Eberts, Elektrotech. Z., 21 (1969) 297.
88 K. Eberts and O. Jache, 2nd Int. Conf. Lead, 1965, p. 199.
89 J. R. Smyth, J. P. Malloy and D. T. Ferrell, 2nd Int. Conf. Lead, 1965, p. 193.
90 K. Eberts, in D. H. Collins (ed.), Power Sources 2, Pergamon Press, London, 1970, p. 69.
91 J. A. Orsino and H. F. Jensen, Proc. 21st Am. Power Sources Conf., 1967, p. 60.
92 J. R. Thomas and D. R. Walter, Proc. 21st Am. Power Sources Conf., 1967, p. 64.
93 B. K. Mahato and E. C. Laird, in D. H. Collins (ed.), Power Sources 5, Academic Press, London, 1975, p. 23.
94 U. Heubner and H. Sandig, 4th Int. Lead Conf., London, 1971.
95 D. Berndt and S. C. Nijhawan, J. Power Sources, 1 (1976) 1.
96 P. Ruetschi, U.S. Pat. 2,951,106 (Aug. 30, 1960).
97 P. Ruetschi and J. B. Ockerman, J. Electrochem. Soc., 116 (1969) 1222.
98 H. Reber, Busch Tech. Ber., 3 (Aug. 1970).
99 P. Ruetschi and B. D. Cahan, U.S. Pat. 3,080,440 (March 5, 1963).
100 P. Ruetschi and J. B. Ockerman, Electrochem. Technol., 4 (1966) 383.
101 M. Fukuda *et al.*, U.S. Pat. 3,658,591 (1972).
102 S. Sekido *et al.*, U.S. Pat. 3,904,434 (1975).
103 J. I. Dyson and E. Sundberg, in D. H. Collins (ed.), Power Sources 4, Oriel Press, Newcastle upon Tyne, 1973, p. 505.
104 P. Ruetschi, U.S. Pat. 3,124,488 (March 10, 1964).
105 J. Freundlich, Electrochim. Acta, 6 (1962) 35.
106 R. F. Amlie, J. B. Ockerman and P. Ruetschi, J. Electrochem. Soc., 108 (1961) 377.
107 A. Salkind, Techniques of Electrochemistry, Wiley–Interscience New York, 1972, p. 293.
108 D. Pavlov, V. Iliev, G. Papazov and E. Bashtavelova, J. Electrochem. Soc., 121 (1974) 854.

109 D. Pavlov and G. Papazov, J. Appl. Electrochem. 6 (1976) 339.
110 C. W. Fleischmann and W. J. Schlotter, J. Electrochem. Soc., 123 (1976) 969.
111 D. Berndt, Electrochim. Acta, 10 (1965) 1067.
112 O. S. Ksenzhek and V. V. Stender, Dokl. Akad. Nauk SSSR, 107 (1956) 280.
113 J. Newman and C. Tobias, J. Electrochem. Soc., 109 (1962) 1183.
114 R. de Levie, Advances in Electrochemistry and Electrochem. Engineering, Vol. 6, Interscience, New York, 1967, p. 329.
115 K. J. Euler, Electrochim. Acta, 13 (1968) 1533; 15 (1970) 1233.
116 J. S. Dunning, D. N. Bennion and J. Newman, J. Electrochem. Soc., 118 (1971) 1251; 120 (1973) 906.
117 J. Newman and W. Tiedemann, J. Am. Inst. Chem. Eng., 21 (1975) 25.
118 H. Lehning, Elektrotech. Z., 93A (1972) 62.
119 W. Runge, Elektrotech. Z., 93A (1972) 67.
120 D. Simonsson, J. Appl. Electrochem., 3 (1973) 261; 4 (1974) 109.
121 K. Micka and I. Rousar, Electrochim. Acta, 18 (1973) 629; 19 (1974) 499.
122 H. Haebler, H. Panesar and E. Voss, Electrochim. Acta, 15 (1970) 1421.
123 H. Bode, H. Panesar and E. Voss, Naturwissenschaften, 55 (1968) 541; Chem.-Ing. Tech., 41 (1969) 878.
124 B. N. Kabanov and D. I. Leikis, Z. Elektrochem. Ber. Bunsenges., 62 (1958) 660.
125 B. D. Cahan and P. Ruetschi, J. Electrochem. Soc., 106 (1959) 543.
126 R. P. Vasil'eva and E. A. Mendzheritskii, Elektrokhimia, 8 (1972) 526.
127 D. Pavlov and N. Iordanov, J. Electrochem. Soc., 117 (1970) 1103.
128 P. Ruetschi and R. T. Angstadt, J. Electrochem. Soc., 111 ((1964) 1323.
129 P. Ruetschi, J. Electrochem. Soc., 120 (1973) 331.
130 H. S. Panesar, in D. H. Collins (ed.), Power Sources 3, Oriel Press, Newcastle upon Tyne, 1971, p. 79.
131 J. P. Carr, N. A. Hampson and R. Taylor, J. Electronal. Chem., 33 (1971) 109.
132 M. P. J. Brennan, B. N. Stirrup and N. A. Hampson, J. Appl. Electrochem., 4 (1974) 49.
133 T. F. Sharpe, J. Electrochem. Soc., 122 (1975) 845; 124 (1977) 168.
134 T. G. Chang, M. M. Wright and M. L. Valeriote, in D. H. Collins (ed.), Power Sources 6, Academic Press, London, 1977, p. 69.
135 W. Visscher, J. Power Sources, 1 (1976/1977) 257.
136 J. Burbank and E. J. Ritchie, J. Electrochem. Soc., 116 (1969) 125; 117 (1970) 299.
137 W. O. Butler, C. J. Venuto and D. V. Wisler, J. Electrochem. Soc., 117 (1970) 1339.
138 A. C. Simon, C. P. Wales and S. M. Caulder, J. Electrochem. Soc., 117 (1970) 987.
139 D. Pavlov, G. Papazov and V. Iliev, J. Electrochem. Soc., 119 (1972) 8.
140 S. Ikari, S. Yoshizawa and S. Okada, J. Electrochem. Soc. Jap., (overseas edn.), 27E (1959) 186.
141 D. Pavlov, C. N. Poulieff, E. Klaja and N. Iordanov, J. Electrochem. Soc., 116 (1969) 316.
142 W. Feitknecht, Z. Elektrochem., 62 (1958) 795.
143 D. Pavlov, Z. Elektrochem., 71 (1967) 398.
144 D. Pavlov, Electrochim. Acta, 13 (1968) 2051.
145 D. Pavlov and R. Papova, Electrochim. Acta, 15 (1970) 1483.
146 Th. Gerber, Tech. Mitl. PTT (Switzerland), No. 5 (1967).
147 Th. Gerber, Tech. Mitl. PTT (Switzerland, No. 6/7 (1977).
148 E. Willihnganz, Electrochem. Technol., 6 (1968) 338.
149 A. G. Cannone, P. O. Feder and R. V. Biagetti, Bell Syst. Tech. J. 49 (1970) 1279.
150 N. J. Maskalick, J. Electrochem. Soc., 127 (1975) 19.

2. WEIGHT ANALYSIS OF THE LEAD-ACID BATTERY

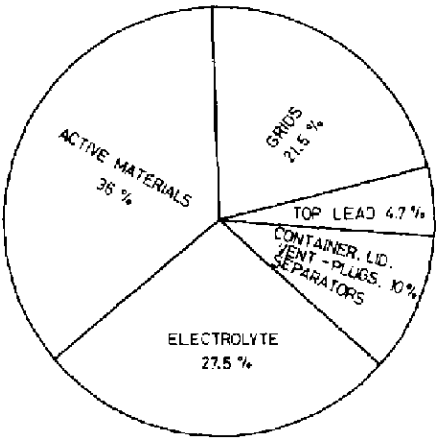

Fig. 18. Weight analysis of a typical SLI battery.
(Source: Ed. Proc. Symp. on Lead Acid Batteries, ILZIC, 1971, p. 12.)

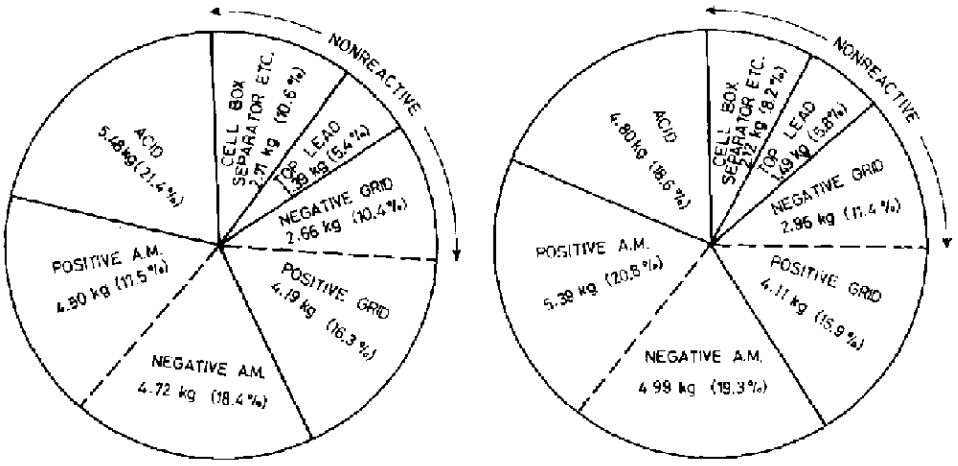

Fig. 19. Weight analysis of (a) typical tubular and (b) flat plate traction cells.
(Source: Ed. Proc. Symp. on Lead Acid Batteries, ILZIC 1971, p. 12.)

3. LEAD AND LEAD OXIDES

TABLE 1

PROPERTIES OF ELEMENTAL LEAD

Atomic weight	207.2
Atomic number	82
Valences	2 and 4
Crystal structure	Face centred cubic
a, Å	4.949
Bond length, Pb–Pb, at 25 °C, Å	3.499
Ionization potential, eV	
First electron	7.42
Second	15.03
Third	32.08
Fourth	42.25
Fifth	69.7
Specific gravity	
20 °C	11.34
327 °C (solid)	11.005
327 °C (liquid)	10.686
650 °C	10.302
850 °C	10.078
Specific heat, cal g^{-1}	
0 °C	0.0297
20 °C	0.0306
100 °C	0.0320
327 °C	0.0390
500 °C	0.037
Vapour pressure, mm Hg	
987 °C	1.0
1167 °C	10.0
1417 °C	100.0
1508 °C	200.0
1611 °C	400.0
Viscosity, cP	
441 °C	2.12
551 °C	1.70
703 °C	1.35
844 °C	1.19
Surface tension, dyne/cm, 327.4 °C	444
Melting point, °C	327.4
Boiling point, °C	1751
Electric resistivity, μohm cm, at 20 °C	20.65
Thermal conductivity, cal s^{-1} cm^{-2} (°C/cm), 20 °C	0.083
Magnetic susceptibility, 10^{-6} cgs units	−0.12
Tensile strength, kg cm^{-2}	126.55 — 175.77
Modulus of elasticity, 10^6 kg cm^{-2}	0.155
Latent heat of vaporization, cal g^{-1}	204
Latent heat of fusion, cal g^{-1}	5.89
Superconductivity	below 7.23 K
Linear coefficient of expansion, °C 10^{-6} units	29.3
Brinell hardness (cast)	4.2
Electrolytic solution potential, *vs.* NHE	0.122

(Continued)

TABLE 1 *(continued)*

Thermodynamic properties	
Heat of fusion, cal $atom^{-1}$	1,225
Heat of vaporization, cal $atom^{-1}$	42,880
Entropy at 25 °C, cal $atom^{-1}$ deg^{-1}	15.49
Heat capacity at 327 °C, cal $atom^{-1}$ deg^{-1}	6.80

(Source: Kirk and Othmer, Encyclopaedia of Chemical Technology, Vol. 12, Interscience, New York, 1967.)

TABLE 2

STANDARD AND FORMAL POTENTIALS OF LEAD AT 25 °C

Half-cell reaction	*Potential* (V)	*Conditions*
$Pb^{2+} + 2e = Pb$	−0.126	
	−0.280	0.1 - 1.3 *M* NaCl
	−0.204	0.1 *M* $NaNO_3$
	−0.334	0.1 *M* KBr
	−0.472	0.1 *M* NaF
	−0.393	0.2 *M* Na_2SiO_3
	−0.180	0.01 *M* $NaHCO_3$
	−0.250	0.2 *M* $NaHCO_3$
	0.128	0.3 *M* H_3PO_4
	−0.259	0.1 *M* Na_2SO_4
	−0.356	0.1 *M* NaAc
	−0.177	H_2S (satd.)
	−0.230	5×10^{-4} to 2 *M* H_3PO_4 in $HClO_4$, pH 1.05
	−0.280	Phthalate buffer, pH 5.0
$Pb^{2+} + Hg + 2e^- = Pb(Hg)$	−0.195	1 *M* $Pb(Ac)_2$, pH 5.6
	−0.239	1 *M* $Pb(Ac)_2$, 1 *M* HAc, pH 3.9
	−0.193	1 *M* $Pb(Ac)_2$, 1 *M* NaAc, 1 *M* HAc, pH 4.72
$PbCl_2 + 2e^- = Pb + 2Cl^-$	−0.268	
$PbBr_2 + 2e^- = Pb + 2Br^-$	−0.284	
$PbI_2 + 2e^- = Pb + 2I^-$	−0.365	
$PbHPO_4 + 2e^- = Pb + HPO_4^{2-}$	−0.465	
$Pb_3(PO_4)_2 + 6e^- = 3Pb + 2PO_4^{3-}$	−0.658	
$PbSO_4 + 2e^- = Pb + SO_4^{2-}$	−0.353 to −0.359	
$PbSO_4 + Hg + 2e^- = Pb(Hg) + SO_4^{2-}$	−0.351	
$PbO_r + H_2O + 2e^- = Pb + 2OH^-$	−0.580	
$PbO_2 + H_2O + 2e^- = PbO_r + 2OH^-$	0.247	
$PbO_2 + 4H^+ + 2e^- = Pb^{2+} + 2H_2O$	1.455	
α-$PbO_2 + SO_4^{2-} + 4H^+ + 2e^- = PbSO_4 + 2H_2O$	1.697 to 1.698	
	1.709	4.4 *M* H_2SO_4, 31.8°
β-$PbO_2 + SO_4^{2-} + 4H^+ + 2e^- = PbSO_4 + 2H_2O$	1.690	
	1.692	4.4 *M* H_2SO_4, 31.8°

(Source: "Encyclopaedia of Electrochemistry of the Elements", Ed. by A. J. Bard, Vol. 1, Chapter 5, Marcel Dekker, New York, 1973.)

TABLE 3

CHEMICAL REACTIVITY OF LEAD

Reactant	*Condition*	*Product*
Air	Cold	Oxide or carbonate coating
	800 °C	PbO
Water	Free of oxygen	No reaction
	Oxygenated	$Pb(OH)_2$
	1000 °C, H_2O vapour	PbO
Hydrochloric acid	Any concentration, cold or warm	$PbCl_2$ forms slowly
Hydrogen halides	Cold	No reaction
	Heated	No reaction, or very little to form PbX_2
Sulphuric acid	Concentrated, cold	No reaction
	Concentrated, above 200 °C	$PbSO_4$
Nitric acid	Any concentration	$Pb(NO_3)_2$
Carbon, nitrogen, phosphorus, arsenic	Heated	No reaction
Chlorine	Heated	$PbCl_2$
Fluorine	25 °C	PbF_2
Sulphur vapour	-	PbS
Selenium or tellurium	Fused	PbSe or PbTe
Alkalies	Fused	No reaction

TABLE 4

COMPOSITION OF DIFFERENT GRADES OF PIG LEAD

Element	UNITED STATES ASTM Pig Lead Specification B 29 - 1955				GERMANY DIN 1719 - 1951				UNITED KINGDOM BS 334 - 1934		INDIA IS 27 - 1965	
	Corroding	Chemical	Acid Copper	Common Desilverized	Pure Pb 99.99	Pure Pb 99.985	Smelter Lead	Pure Copper Lead	Chemical Type A	Chemical Type B	Pb 99.99	Pb 99.94
Ag, max%	0.0015	0.020	0.002	0.002	0.001	0.001	0.001	0.0025	0.002	NS	0.001	0.001
Ag, min%	–	0.002	–	–	–	–	–	–	–	NS	–	–
Cu, max%	0.0015	0.080	0.080	0.0025	0.001	0.001	0.001	0.08	0.003	NS	0.001	0.001
Cu, min%	–	0.040	0.040	–	–	–	–	0.04	–	NS	–	–
Ag + Cu, max%	0.0025	–	–	–	–	–	–	–	–	NS	–	–
As, max%	–	–	–	–	0.001	0.001	0.001	0.001	Trace	NS	0.001	0.001
Sb, max%	–	–	–	–	0.001	0.002	0.002	0.002	0.002	NS	0.001	0.002
Sn, max%	–	–	–	–	0.001	0.001	0.001	0.001	Trace	NS	0.001	0.001
As + Sb + Sn, max%	0.002	0.002	0.002	0.005	–	–	–			NS		–
Zn, max%	0.001	0.001	0.001	0.002	0.001	0.001	0.001	0.001	0.002	NS	0.001	0.001
Fe, max%	0.002	0.002	0.002	0.002	0.001	0.001	0.001	0.001	0.003	NS	0.001	0.001
Bi, max%	0.050	0.005	0.025	0.150	0.005	0.01	0.05	0.01	0.005	0.005	0.005	0.05
Cd, max%	–	–	–	–	–	–	–		Trace	NS	–	–
Co, max%	–	–	–	–	–	–	–	–	0.001	NS	–	–
Ni, max%		–	–	–	–	–	–	–	0.001	NS	–	–
Lead, min%	99.94	99.90	99.90	99.85	99.99	99.985	99.94	99.90	99.99	NS	99.99	99.94

NS = Not specified. Open to negotiation between supplier and customer.
(Source: American Society for Testing Materials, Committee B29.)

TABLE 5

BINARY MELTS OF SEVERAL METALS WITH LEAD

Metal	*Crystal structure*	*Atomic radius (Å)*	*Radius ratio*	*Relative EMF**	*Lead-rich eutectic*		*Lead-rich compound*	*Room temperature solid solubility in Pb*	
					% Pb	*Temp. (°C)*		*Solubility (%)*	*Temp. (°C)*
Pb	fcc	1.74	100.0	0	–	–	–	–	–
Sr	fcc	2.15	123.5	+13	–	–	$SrPb_3$	Slight	–
Ca	fcc	1.97	113.2	+11	–	–	$CaPb_3$	0.01	20
Tl	fcc	1.73	99.5	+4	–	–		Completely miscible	–
Ag	fcc	1.44	82.8	−6	95.3	304	–	0.02	100
Al	fcc	1.43	82.2	+8	99.84	326.8	–	Almost nil	–
Cu	fcc	1.27	73.0	−4	99.94	326	–	⩽0.007	–
K	bcc	2.31	132.6	+14	98.1	277	KPb_4	Very low	–
Ba	bcc	2.17	124.8	+12	95.5	293	$BaPb_3$	0.02	20
Na	bcc	1.84	106.0	+10	97.3	307	$NaPb_3$	0.20	20
Li	bcc	1.50	86.3	+15	99.3	235	LiPb	0.01	20
Mg	hcp	1.60	92.0	+9	97.8	253	Mg_2Pb	0.36	232
Cd	hcp	1.49	85.8	+5	82.6	248	–	⩽0.04	100
Zn	hcp	1.33	76.4	+6	99.5	318.2	–	⩽0.05	318.2
Co	hcp	1.26	72.5	+3			–	Very low	–
Ni	hcp	1.24	71.3	+2	–	–	–	0.023	20
Sn	dia.	1.40	80.5	+1	38.1	183	–	1.9	20
Bi	Rhomb.	1.55	89.0	−2	–	–	–	19.05	100
Hg	Rhomb.	1.49	85.7	−7	–	–	–	23.4	93
Sb	Rhomb.	1.439	82.8	−1	88.9	252	–	0.44	100
As	Rhomb.	1.25	71.8	−3	97.2	288	–	0.01	20
Te	hex	1.44	82.8	−5	99.975	326.3	PbTe	0.0015	300
Se	hex	1.16	66.7	−?	79.5	860	PbSe	0.004	300

*Under EMF, the relative electronegativity of the elements with respect to lead have been listed. The values were obtained from a list of EMF series of elements by setting lead = 0, and counting the position of each metal in the list.
(Source: Max Hansen, Constitution of Binary Alloys, McGraw-Hill, New York, 1958.)

TABLE 6

PHYSICAL PROPERTIES OF LEAD OXIDES

Property	PbO	PbO_2	Pb_3O_4
1. Molecular weight	223.21	239.19	685.57
2. Colour	α: Red β: Yellow	Dark brown or black	Orange to brick red
3. Structure	α: Tetragonal β: Orthorhombic	α: Orthorhombic β: Tetragonal	Spinel
4. Density (g/cm^3)	α: 9.2 - 9.5 β: 9.5 - 9.9 Fumed litharge: 0.7 (max) Black (grey): 1.4 - 1.8 Ground calcined oxide: 1.6 - 2.0	Reported 9.165, 9.375 and 9.40 for $PbO_{1.919}$	9.1
5. Transition temperature	488.5 °C	–	–
6. Melting point	897 °C, sublimes before melting	Decomposes at 290 °C	830 °C (in oxygen pressure) decomposes in atm. at 500 °C
7. Electrical properties	p or n type semiconductor	semiconductor (resistivity at 20 °C, 91 MΩ cm)	non-conductor
8. Solubility	α: 0.05 $g\,l^{-1}$ in H_2O at 25 °C β: 0.107 $g\,l^{-1}$ in H_2O at 25 °C	Insoluble in cold or hot water. Soluble in HCl. Slightly soluble in HNO_3 and H_2SO_4	Insoluble in cold or hot water. Soluble in HCl and HNO_3 and warm con. H_2SO_4
9. Thermal stability (See Fig. 23)	Stable upto 250 °C oxidized to PbO_{1-2} at 300 - 350 °C and to Pb_3O_4 at higher temperatures	Decomposes to lower oxides above 290 °C	Stable upto 500 °C decomposed to PbO at higher temperatures.

TABLE 7

CHEMICAL PROPERTIES OF LEAD OXIDES

Reagent	PbO	PbO_2	Pb_3O_4
1. Hydrogen	Reduction is slow	Reduced at 150 °C to lower oxides and water	Reduced above 200 °C
2. Carbon	–	Reduced at 260 °C	Reduced above 300 °C
3. Chlorine or Bromine vapour	Dihalide is formed	Dihalide or oxy-halide is formed	Dihalide is formed
4. Aqueous solutions of halogens	Oxidized to dioxide	Diiodide & iodic acid are formed in presence of moisture	
5. Hydrogen halides		Oxidized to halogens	–
6. Sulphuric and nitric acids	–	Tetravalent salts are formed	Divalent salts are formed
7. Hydrochloric acid		Tetrachloride is formed	Dichloride is formed
8. Sulphur	Sulphide is formed	Oxidized to sulphur dioxide	
9. Hydrogen sulphide	–	Sulphide is formed	–
10. Sulphur dioxide	–	Reacts violently forming $PbSO_4$	Sulphide is formed
11. Ammonia	–	Nitrogen is formed	–
12. Nitrous oxide	–	Decomposed to PbO and oxygen	–
13. Phosphorus	–	Reacts explosively	–
14. Metallic oxides	Fuses readily to form double oxides	Plumbates are formed	

TABLE 8

THERMODYNAMIC PROPERTIES OF LEAD OXIDES AT 25 °C

Property	α-PbO (Red)	β-PbO (Yellow)	PbO_2	Pb_3O_4
1. Heat of formation ΔH° (kcal mole^{-1})	−52.41	−52.07	−64.55	−175.50
2. Free energy of formation ΔF° (kcal mole^{-1})	−45.13	−44.95	−50.77	−147.50
3. Entropy S° (cal deg^{-1} mole^{-1})	15.60	16.10	18.28	50.50
4. Heat capacity C_p (cal deg^{-1} mole^{-1})	10.94	10.96	14.87	34.00 (0 °C)
5. Heat of sublimation ΔH_s (kcal mole^{-1})	63.88	63.54	–	–

(Source: Lead Chemicals, ILZRO, 1975)

TABLE 9

TYPICAL LIMITING PERCENTAGES OF IMPURITIES IN LEADY OXIDE

This table refers to a typical impurity specification in U.S.A. The specification of impurities and free lead in leady oxide is generally agreed to between the manufacturer and user.

Impurity	*Percent*	*Impurity*	*Percent*
Antimony, arsenic, tin	0.005	Nickel, cobalt	0.002
Bismuth	0.10	Silver	0.01
Copper	0.01	Zinc, cadmium	0.002
Iron	0.02	Calcium	0.04
Silica	0.05	Platinum	None
Pb_3O_4	0.25	$PbSO_4$	0.20

(Source: Storage Battery Manufacturing Manual, IBMA, p. 11.)

TABLE 10

THEORETICAL WEIGHT PERCENT OF LEAD IN LEAD OXIDES

Formula	*Oxygen/lead ratio*	*% Lead*
Pb_2O	0.500	96.282
PbO	1.000	92.831
	1.100	92.170
	1.130	91.974
Pb_3O_4	1.333	90.664
Pb_5O_7	1.400	90.243
	1.410	90.181
$Pb_{12}O_{17}$	1.417	90.137
	1.420	90.117
$5\ PbO.2H_2O$	-	89.928
	1.470	89.805
Pb_2O_3	1.500	89.619
	1.516	89.519
	1.550	89.310
Pb_7O_{11}	1.571	89.179
$Pb_{12}O_{19}$	1.583	89.105
Pb_5O_8	1.600	89.004
Pb_3O_5	1.667	88.597
Pb_8O_{15}	1.875	87.352
	1.910	87.146
	1.950	86.912
PbO_2	2.000	86.621
	2.12	85.932
$Pb(OH)_2$	-	85.896

(Source: Lead Oxides, IBMA 1974, p. 14.)

TABLE 11

X-RAY CRYSTALLOGRAPHIC DATA OF OXIDES OF LEAD

	System structure type	*Space group*	*Lattice constants* a, b, c, (Å)	*Molecules/ unit cell*
α-PbO (red)	Tetragonal	D_{4h}^{7}	3.98, . . ., 5.01	2
β-PbO (yellow)	Orthorhombic	V_h^{19}	5.50, 4.72, 5.88	4
α-PbO_2	Orthorhombic	-	4.98, 5.95, 5.44	-
β-PbO_2	Tetragonal	D_{4h}^{14}	4.97, . . ., 3.40	2
$PbSO_4$	Orthorhombic	V_h^{16}	8.45, 5.38, 6.93	4

(Source: Handbook of Physics and Chemistry, Chemical Rubber Co., 1953.)

TABLE 12

STANDARD DIFFRACTION PATTERNS FOR α- AND β-LEAD DIOXIDES

α-lead dioxide			*β-lead dioxide*		
Interplanar spacing	*Relative intensity*	*Indices hkl*	*Interplanar spacing*	*Relative intensity*	*Indices hkl*
3.83	12	110	3.50	100	110
3.12	100	111	2.80	100	101
2.97	15	020	2.48	70	200
2.74	70	002	2.21	10	210
2.63	70	021	1.856	100	211
2.48	20	200	1.754	60	220
2.23	6	112	1.693	40	002
2.02	6	022	1.569	60	310
1.89	30	220	1.527	70	112
1.84	45	130,202	1.486	70	301
1.79	30	221	1.399	50	202
1.64	15	113	1.276	70	321
1.56	17	222,023	1.240	20	400
1.53	30	311,132	1.220	50	222
1.43	20	041,312	1.170	20	330
1.37	15	312	1.152	70	312
1.31	15	233			
1.26	20	330			
1.24	30	241,400			
1.20	40	204,313			

(Source: J. P. Carr and N. A. Hampson, Chem. Rev., 72 (1972) 679.)

TABLE 13

TYPICAL PROPERTIES OF BATTERY OXIDES MANUFACTURED BY DIFFERENT METHODS

Property	*Barton pot*	*Rotating drum*
1. Particle size	8 - 16 μm (normal oxide) 4 - 16 μm (ground oxide) 2 - 16 μm (fine oxide) 0 - 5 μm (finer oxide)	4 - 16 μm (Hardinge oxide) 0 - 2 μm (Shimadzu oxide)
2. Particle shape	Tetragonal and Rhombohedral	Tetragonal
3. PbO content	70 - 78% (normal & ground oxides) 75 - 83% (fine & finer oxides)	65 - 75% (Hardinge oxide) 70 - 78% (Shimadzu oxide)
4. Allotropic modification*	5 - 15% β-PbO balance α-PbO	1 - 3% β-PbO balance α-PbO
5. Water absorption (ml/100 g of oxide)	12 - 13 (finer oxides)	9 - 10 (Hardinge oxide) 10 - 12 (Shimadzu oxide)
6. Material utilization (g/Ah at 20 h rate)	9	9 - 10

*α, tetragonal; β, rhombohedral.

TABLE 14

DENSITIES OF LEAD COMPOUNDS

Compound	*Density*
Pb_2O	8.34
α-PbO	9.32
β-PbO	9.67
Pb_3O_4	9.10
PbO_2	9.37
$PbSO_4$	6.32
$PbO.PbSO_4$	7.02
$3PbO.PbSO_4.H_2O$	6.50
$4PbO.PbSO_4$	8.15
$PbO.Pb(OH)_2$	7.59

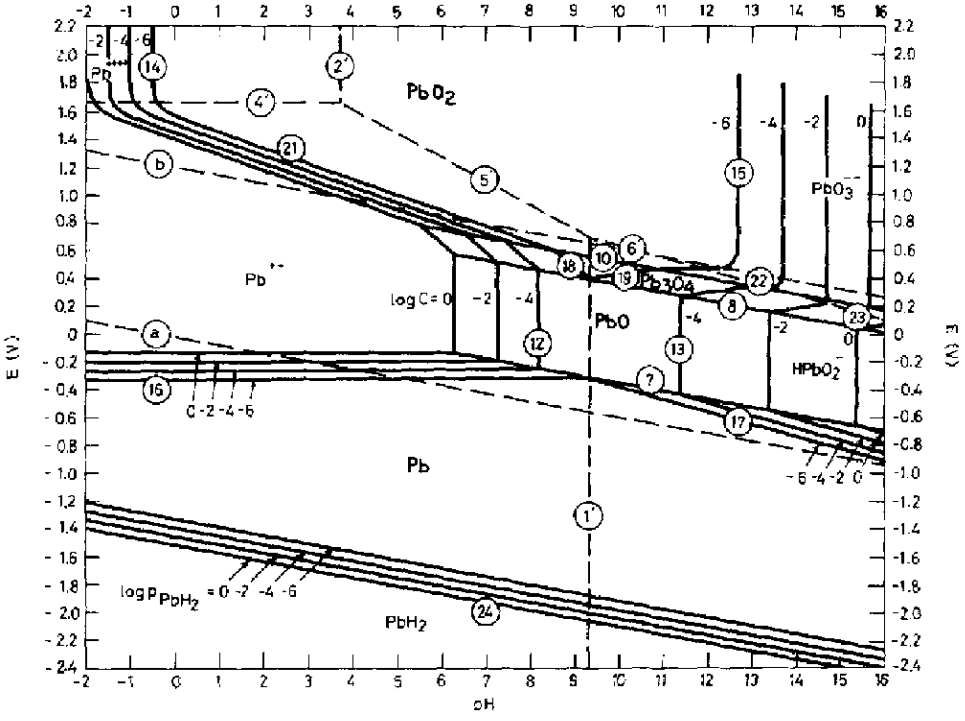

Fig. 20. Potential–pH diagram of lead.
(Source: Atlas of Electrochemical Equilibria in Aqueous Solutions, M. Pourbaix, Pergamon Press, London, 1966.)

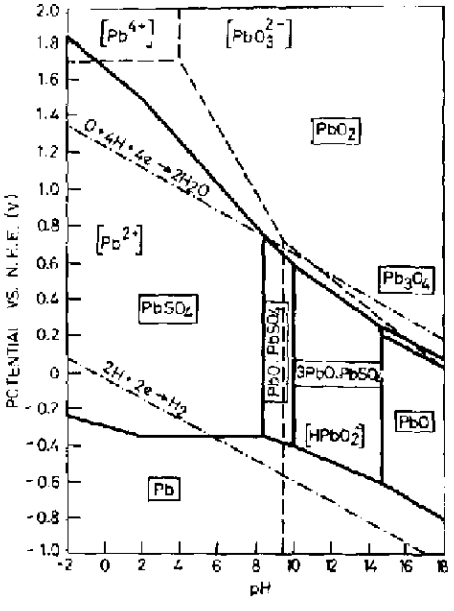

Fig. 21. Potential–pH diagram of lead in the presence of sulphate ions at unit activity. (Source: S. C. Barnes and R. T. Mathieson, in D. H. Collins (ed.), Batteries 2, Pergamon Press, Oxford, 1965, p. 41.)

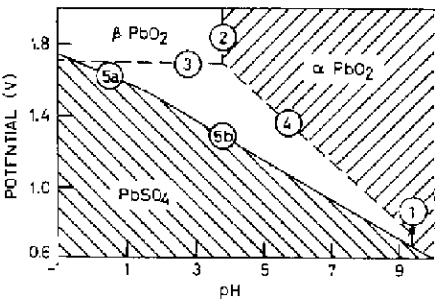

1. $HPbO_2^- + 3H^+ = Pb^{2+} + 2H_2O$
2. $PbO_3^{2-} + 6H^+ = Pb^{2+} + 3H_2O$
3. $Pb^{2+} + 2e^- = Pb$
4. $PbO_2^{2-} + 6H^+ + 2e^- = Pb^{2+} + 3H_2O$

5a. $PbO_2 + HSO_4^- + 3H^+ + 2e = PbSO_4 + 2H_2O$

5b. $PbO_2 + SO_4^{2-} + 4H^+ + 2e^- = PbSO_4 + 2H_2O$

Fig. 22. Portion of potential–pH diagram showing stability regions for α- and β-PbO_2. (Source: J. Burbank, J. Electrochem. Soc., 104 (1957) 693.)

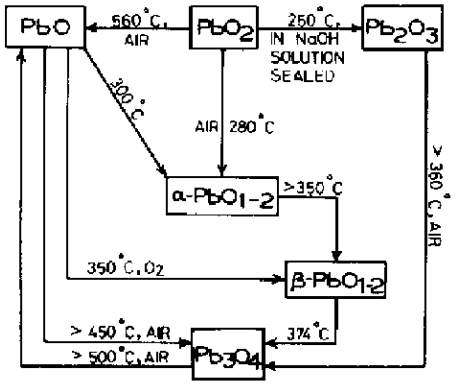

Fig. 23. Thermal stability of lead oxides. (Source: A. F. Wells, Structural Inorganic Chemistry, Oxford Univ. Press, London, 3rd edn., 1962.)

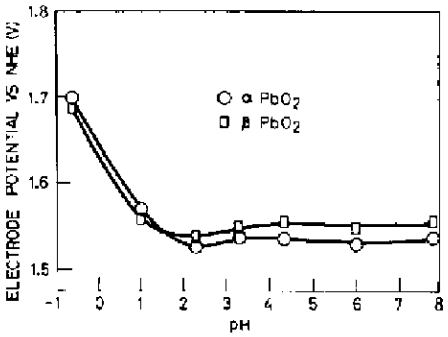

Fig. 24. Electrode potentials of α- and β-PbO_2 as a function of pH. (Source: P. Ruetschi *et al.*, J. Electrochem. Soc., 106 (1959) 547.)

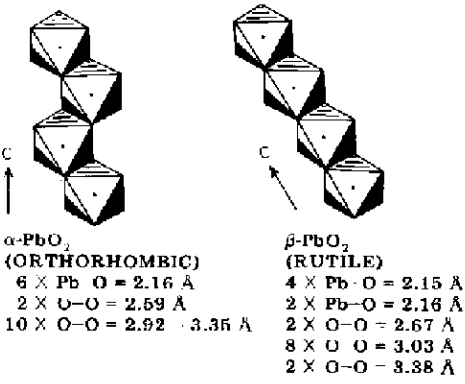

Fig. 25. Packing of octahedra in α- and β-PbO_2

(Source: W. Mindt, J. Electrochem. Soc., 116 (1968) 1076.)

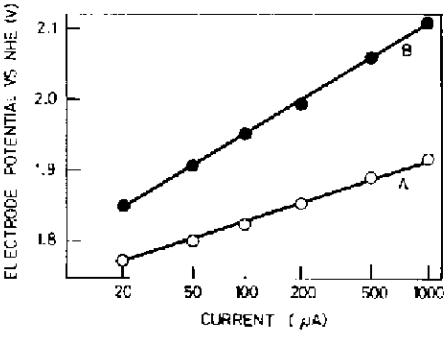

Fig. 26. Oxygen overvoltage on α- and β-PbO_2 (A — α-PbO_2, B — β-PbO_2). (Source: P. Ruetschi, R. T. Angstadt and B. D. Cahan, J. Electrochem. Soc., 106 (1959) 547.)

4. ALLOYS AND GRIDS

TABLE 15

MANUFACTURERS' TYPICAL GRID METAL SPECIFICATIONS*

Metals	*1*	*2*	*3*	*4*	*5*	*6*	*7*	*8*	*9*	*10*
Antimony	5.25% to 5.75%	4.75% to 5.25%	4.75% to 5.25%	4.50% to 4.75%	3.10% to 3.50%	5.85% to 6.20%	5.75% to 6.25%	4.35% to 4.65%	4.35% to 4.65%	2.75% to 3.25%
Arsenic	0.35% to 0.40%	0.15% to 0.19%	0.45% to 0.55%	0.14% to 0.18%	0.45% to 0.60%	0.085% to 0.115%	0.05% to 0.10%	0.14% to 0.18%	0.32% to 0.35%	0.12% max
Tin	0.25% to 0.50%	0.35% to 0.65%	0.40% to 0.50%	0.20% to 0.30%	0.30% to 0.50%	0.02% max	0.15% to 0.25%	0.25% to 0.45%	0.25% to 0.45%	0.20% to 0.40%
Silver	0.005% max	<0.10%	–	0.02% max	0.005% max	0.005% max	0.01% max	0.02% max	0.02% max	0.02% max
Iron	0.005% max	<0.002%	0.01% max	0.005% max	0.005% max	0.01% max	0.005% max	0.005% max	0.005% max	0.005% max
Copper	0.06% max	0.01% max	0.06% max	0.02% max	0.07% to 0.12%	0.02% max	0.03% to 0.07%	0.07% max	0.07% max	0.07% max
Nickel	0.01% max	<0.0015%	0.002% max	Trace	0.01% max	0.001% max	–	0.001% max	0.001% max	0.001% max
Cobalt	0.005% max	–	–	Trace	0.005% max	–	–	–	–	–
Zinc	0.005% max	<0.0015%	0.002% max	Trace	0.006% max	0.001% max	0.002% max	–	–	–
Bismuth	0.05% max	0.05% max	0.05% max	0.035% max	0.05% max	0.02% max	0.05% max	0.05% max	0.05% max	0.05% max
Cadmium	–	–	–	0.02% max	0.05% to 0.10%	0.01% max	–	–	–	
Manganese	0.005% max	–	–	Trace	0.005% max	–	–	–	–	–
Sulphur		<0.001%	0.002% max	–	–	–	–	–	–	–

*A number of these specifications are covered by patents of US and elsewhere.
(Source: Grid Metal Manual, IBMA, USA, 1973, p. 12.)

TABLE 16

PROPERTIES OF CAST LEAD–ANTIMONY ALLOYS

Antimony (%)	*Temp. of complete liquefaction* (°C)	*Density* (g cm^{-3})	*Tensile strength* (kg mm^{-2})	*Elongation* (%)	*Hardness Brinell number*	*Expansivity coefficient*	*Resistivity at 20 °C* (ohm-cm)
0	327	11.34	1.2515	–	3.0	0.0000292	0.0000212
1	320	11.26	–	–	4.2	0.0000288	0.0000220
2	313	11.18	–	–	4.8	0.0000284	0.0000227
3	306	11.10	3.3046	15	5.3	0.0000281	0.0000234
4	299	11.03	3.9795	22	5.7	0.0000278	0.0000240
5	292	10.95	4.4717	29	6.2	0.0000275	0.0000246
6	285	10.88	4.8092	24	6.5	0.0000272	0.0000253
7	278	10.81	5.0482	21	6.8	0.0000270	0.0000259
8	271	10.74	5.2170	19	7.0	0.0000267	0.0000265
9	265	10.66	5.3294	17	7.2	0.0000264	0.0000271
10	261	10.59	5.3927	15	7.3	0.0000261	0.0000277
11	256	10.52	5.3576	13	7.4	0.0000258	0.0000283
12	252	10.45	5.2591	12	7.4	0.0000256	0.0000289

(Source: G. W. Vinal, Storage Batteries, Wiley, New York, 1955, p. 16.)

TABLE 17

PROPERTIES OF GRID ALLOYS USED IN SLI AND SEALED LEAD BATTERIES

Alloy composition (%) (balance lead)			*Brinell hardness* ($kg\ mm^{-2}$)	*Tensile strength* ($kg\ mm^{-2}$)	*Elongation (%) at fracture* $\delta 5$	*Electrical conductivity* ($mmho\ mm^{-2}$)
Sb 8	As 0.01	Cu 0.01	9.6	2.3	10.2	3.52
Sb 7	As 0.12	Cu 0.04	10.59	4.05	8.4	3.36
Sb 7	As 0.17	Cu 0.05	12.8	1.9	2.9	3.58
Sb 6	As 0.15	Cu 0.04	11.2	3.1	3.8	3.80
Sb 6	As 0.25	Cu 0.01	11.1	3.1	4.2	3.45
Sb 5	As 0.1	Cu 0.04	11.8	4.3	4.2	3.50
Ca 0.07			9.25	–	–	3.68

(Source: U. Heubner and H. Sandig, LEAD 71, Ed. Proc. 4th Intern. Conf. on Lead, p. 34.)

TABLE 18

ULTIMATE TENSILE STRENGTH OF LEAD ALLOYS

Alloy composition	*As-cast* ($kg\ mm^{-2}$)	*Aged 1 week at room temperature* ($kg\ mm^{-2}$)
4.5 Sb–Pb	3.5858	3.7967
0.07 Ca–Pb	2.9530	3.7264
0.01 Li–Pb	2.3203	2.1796
0.02 Li–Pb	3.3045	2.9881
0.03 Li–Pb	4.0077	3.5155

The specimens were cast in sheets.
(Source: G. W. Mao *et al.*, J. Electrochem. Soc., 117 (1970) 1327.)

TABLE 19

RAGONE FLUIDITY OF LEAD–CALCIUM–TIN ALLOYS

(90 mm vacuum; liquidus 25 °C)

Weight percent (balance lead)		*Fluidity** (cm)
Calcium	*Tin*	
0.06	0	50.03
0.06	0.01	52.57
0.06	0.05	50.03
0.06	0.10	58.42
0.06	0.25	58.92
0.06	1.0	58.42
Corroding grade lead		45.46
3.5% antimonial lead		9.14
6% antimonial lead		17.52

*Average of three tests ±6.3 mm
(Source: M. Myers, Tin and Bismuth in Lead–Calcium Alloy, BCI Con., 1975.)

TABLE 20

PROPERTIES OF LEAD–ANTIMONY–CADMIUM ALLOYS

Hardness measurements were carried out using a Hounsfield tensometer with a 25-kg load on a 5-mm dia ball for 15 s. Creep tests were carried out on specimens of dia 0.64 cm and gauge length 15 cm with an initial stress of 1.4 kg mm^{-2}. Anodic weight loss tests were carried out on specimens immersed in 1.25 SG sulphuric acid at a current density of 155 mA cm^{-2} for 24 h. Stress corrosion tests were made on specimens of dia 0.32 cm and gauge length 12 cm, using an initial stress of 1.4 kg mm^{-2} and a current density of 8.5 mA cm^{-2} in 1.25 SG sulphuric acid.

Composition (wt.%)			*Hardness (BHN)*		*Creep strain (%) after 2 years*	*Anodic weight loss* (g)	*Stress corrosion life* (h)
Antimony	*Cadmium*	*Silver*	*After 1 day*	*After 20 days*			
0.3	0.3	–	8.5	10.5	N.T.	1.4	N.T.
0.5	0.5	–	10.7	12.5	N.T.	1.4	N.T.
1.0	1.0	–	12.4	14.5	N.T.	1.1	600
1.25	1.25	–	13.2	15.7	N.T.	1.3	N.T.
1.5	1.5	–	13.9	16.5	0.36	1.1	2,500
2.0	2.0	–	15.7	18.3	0.15	1.1	1,800
2.5	2.5	–	18.0	19.5	0.47	1.1	2,600
3.0	3.0	–	17.4	19.2	N.T.	1.2	2,700
4.0	4.0	–	17.0	17.7	N.T.	1.3	N.T.
4.5	4.5	–	15.8	16.1	N.T.	1.4	N.T.
5.0	5.0	–	16.8	16.5	N.T.	1.5	2,000
2.0	2.0	0.05	15.8	17.5	0.3	0.9	3,000
2.0	2.0	0.1	14.1	16.4	0.14	0.6	3,300
2.0	2.0	0.25	16.5	18.5	0.4	0.5	3,400
2.5	2.5	0.05	17.9	18.0	0.32	0.8	4,000
2.5	2.5	0.1	16.3	17.0	0.41	0.6	5,000

N.T. = Not Tested.

(Source: N. E. Bagshaw, LEAD 68, Ed. Proc. 3rd Int. Conf. on Lead, Pergamon, Oxford, p. 210, 211.)

TABLE 21

ADHESION SCORES* ON TEST GRIDS

Grid metal	*Paste density* ($g\ cm^{-3}$)	*Acid Sp. Gr.*	*Adhesion score after:*			
			Plate curing	*Formation*	*Cycling and stand*	*Final inspection*
Ca–Pb	4.27	1.250	100	100	100	100
Ca–Pb	4.27	1.300	90.2	89.7	89.7	87
Ca–Pb	4.63	1.250	95.1	93.4	93.4	75.8
Ca–Pb	4.63	1.300	90.2	89.3	86.7	75.2
DS–Pb	4.27	1.250	74.5	72.9	72.9	68.7
DS–Pb	4.27	1.300	70.3	70.3	70.3	58.4
DS–Pb	4.63	1.250	77.9	73.2	73.2	68.7
DS–Pb	4.63	1.300	70.4	69.2	68.3	30.8
4% Sb	3.90	1.250	87.0	85.8	85.8	84.2
7% Sb	3.90	1.250	98.8	98.8	98.8	95.6

*Determined according to the test procedure described in ILZRO Report LE 82-84, as given below:
The adhesion tests were conducted on a test grid with 7 each of smooth and threaded holes of diameters from 1/8″ to ½″ in increments of 1/16″. The scores were related to the areas of the pellet and the total score for smooth holes was arbitrarily placed at 60 and 40 for threaded holes. The appropriate score, full or half, was subtracted for each missing (full or half) pellet after several stages, viz. curing, forming, cycling (and stand) and final inspection. The adhesion scores are in fact averages of 12 replicates for each of the 10 grid/paste combinations. (DS = Dispersion Strengthened lead.)
(Source: ILZRO Project LE 82-84 Final Report, Dec. 31, 1971, p. 1/51.)

TABLE 22

TENSILE PROPERTIES OF DISPERSION STRENGTHENED LEAD

Oxide content (wt.%)	1.8	2.9	3.2	3.6	4.4	5.4	6.1	6.7
Limit of proportionality ($kg\ mm^{-2}$)	1.125	1.125	1.167	1.068	1.258	1.167	1.195–1.335	1.349
Modulus of elasticity ($kg\ mm^{-2}$) $\times 10^8$	0.112–0.129	0.126–0.134	0.131	0.139–0.148	0.159–0.161	0.206–0.210	0.175–0.203	0.200
Proof stress ($kg\ mm^{-2}$)								
0.05%	1.884–1.968	2.249–2.285	2.285–2.334	2.334–2.376	2.706	2.390–2.847	1.968–2.531	2.692–2.742
0.1%	2.144–2.285	2.706–2.777	2.601–2.742	2.882–2.917	3.058–3.093	3.058–3.325	2.474–3.023	3.410–3.445
0.2%	2.461–2.601	3.136–3.234	3.028–3.164	3.410–3.466	3.515	3.677–3.937	3.163–3.410	4.134–4.183
Elongation (%) on 2.5 cm	15	13–11	11–10	12–10	11	10–8	9	7–5
Ultimate tensile strength ($kg\ mm^{-2}$)	3.586–3.726	4.205–4.359	4.676–4.901	4.920–5.182	5.344–5.414	5.653–5.836	5.386–5.484	6.398–6.679

(Source: D. H. Roberts et al., Powder Metallurgy, Nov. 1962.)

TABLE 23

MECHANICAL AND ELECTRICAL PROPERTIES OF LEAD ANTIMONY ALLOY AND DISPERSION STRENGTHENED LEAD

		Lead–6% antimony alloy	*Dispersion strengthened lead*
Ultimate tensile strength,	kg mm^{-2}	3.37	4.22
	(psi)	(4800)	(6000)
Tensile yield strength 0.5% offset,	kg mm^{-2}	1.97	4.08
	(psi)	(2800)	(5800)
Elongation, %		35	18.5
Proportional limit,	kg mm^{-2}	1.41	3.59
	(psi)	(2000)	(5100)
Modulus of elasticity,	kg $mm^{-2} \times 10^{6}$	0.0017–0.0025	0.0014–0.0015
	(psi $\times 10^{-6}$)	(2.4 3.6)	(2.0–2.2)
Ultimate compressive strength,	kg mm^{-2}	–	4.57
	(psi)	–	(6500)
Unnotched Charpy impact strength, kg m			2.76
Brinell hardness, 10 mm ball, 100 kg load		10	13.5
Creep rate, % per year at room temperature	kg mm^{-2}	0.9 at 0.28	0.1 at 1.41
	(psi)	(400)	(2000)
Stress to rupture in 1000 hours,	kg mm^{-2}	0.81	2.39
	(psi)	(1150)	(3400)
Electrical resistivity, μohm-cm, 20 °C		25.3	24.3

(Source: M. V. Rose, LEAD 68, Ed. Proc. 3rd Int. Conf. on Lead, Pergamon, Oxford, p. 273.)

TABLE 24

CASTABILITY OF GRID ALLOYS

Ref. No.	*Composition %*						
	Sb	*As*	*Sn*	*Cu*	*Bi*	*Pb*	*Others*
1	0.0016	< 0.0001	< 0.0005	0.00021	0.0051	Balance	
2	7.31	0.015	-	0.03	0.0035	Balance	
3	6.21	0.16	-	0.011	0.002	Balance	
4	5.83	< 0.01	< 0.01	0.011	0.003	Balance	
5	6.05	0.21	0.13	0.007	0.0018	Balance	
6	4.43	0.18		0.0025	0.003	Balance	0.046 Ag
7	4.43	0.21	0.09	0.0025	0.003	Balance	0.046 Ag
8	9.63	0.025		0.0044	0.0012	Balance	
9	5.7	0.03	-	0.0038	0.0028	Balance	
10	3.36	0.02	-	0.0029	0.0033	Balance	
11	6.97	0.026	-	0.077	0.0053	Balance	
12	6.91	0.026	-	0.038	0.0053	Balance	
13	5.15	0.20	0.23	0.003	0.0026	Balance	
14	1.7	0.14	0.015	0.015	0.003	Balance	
15	5.87	0.13	0.17	0.078	0.003	Balance	
16	6.05	0.10	-	0.049	0.004	Balance	
17	5.84	0.14	0.15	0.049	0.003	Balance	
18	1.07	0.02	-	0.0064	0.004	Balance	1.5 Cd, 0.18 Ag
19		0.143	-	0.0045	0.006	Balance	0.17 Ag, 0.065 Te
20	9.62	-	0.15			Balance	
21	8.92	0.15				Balance	
22	5.54	-	0.15			Balance	
23	5.11	0.15	-			Balance	
24	2.77	-	0.15			Balance	
25	2.62	0.17	-			Balance	
26	9.31	0.14	0.15	0.007		Balance	
27	5.51	0.146	0.16	0.0038	0.003	Balance	
28	2.96	0.15	0.16	0.0021	0.0039	Balance	
29	6.03	0.16	0.11	0.007	0.026	Balance	
30	5.94	0.18	0.02	0.009	0.026	Balance	
31	0.0019	< 0.0001	< 0.0005	0.003	0.024	Balance	
32	6.42	0.14	-	0.035	0.0036	Balance	

(continued)

TABLE 24 *(continued)*

Ref. No.	*Average castability score*									
	Casting temperature (°C)					*Mould temperature (°C)*				
	400	*425*	*450*	*475*	*500*	*100*	*125*	*150*	*175*	*200*
1	28	29	36	39	43	29	30	37	39	42
2	28	30	32	37	41	28	28	33	44	59
3	29	32	34	43	48	27	29	33	46	59
4	14	19	21	22	28	13	18	21	27	30
5	26	29	30	31	33	24	26	30	32	44
6	19	25	26	27	32	16	23	26	30	46
7	26	27	27	29	33	15	28	28	30	37
8	33	38	39	42	48	27	30	39	55	59
9	14	17	24	25	27	14	17	24	27	28
10	15	21	26	26	26	13	24	26	25	28
11	27	26	27	26	27	20	26	26	28	29
12	25	28	27	28	28	23	27	27	28	31
13	17	21	28	28	28	16	24	28	29	36
14	14	26	26	26	29	14	19	26	28	28
15	9	15	16	21	23	15	16	15	26	60
16	20	22	26	27	27	18	25	26	26	28
17	17	22	28	29	29	16	19	27	29	51
18	20	27	28	29	33	26	26	29	31	37
19	12	17	22	23	25	0	4	22	24	22
20	21	28	27	30	29	26	28	28	34	61
21	28	28	28	35	38	28	29	28	34	55
22	27	28	28	29	29	27	28	28	29	37
23	23	26	28	28	28	19	24	27	27	29
24	15	19	24	28	28	15	18	24	28	28
25	15	19	24	23	27	15	23	24	25	27
26	26	27	32	37	40	28	30	34	52	68
27	16	27	28	28	28	25	28	27	29	32
28	15	24	26	28	28	17	26	26	27	28
29	28	28	29	29	32	28	28	30	34	51
30	23	28	28	31	37	28	28	29	36	62
31	27	30	36	36	41	23	29	36	35	40
32	27	26	30	29	31	26	26	30	34	45
	Constant mould temp. 150 °C					Constant casting temp. 450 °C				

The castability score was determined with a "tree mould" with arbitrarily assigned points to each portion of the mould.

(Source: BHAS paper appearing in edited proceedings of Lead 74 Conference.)

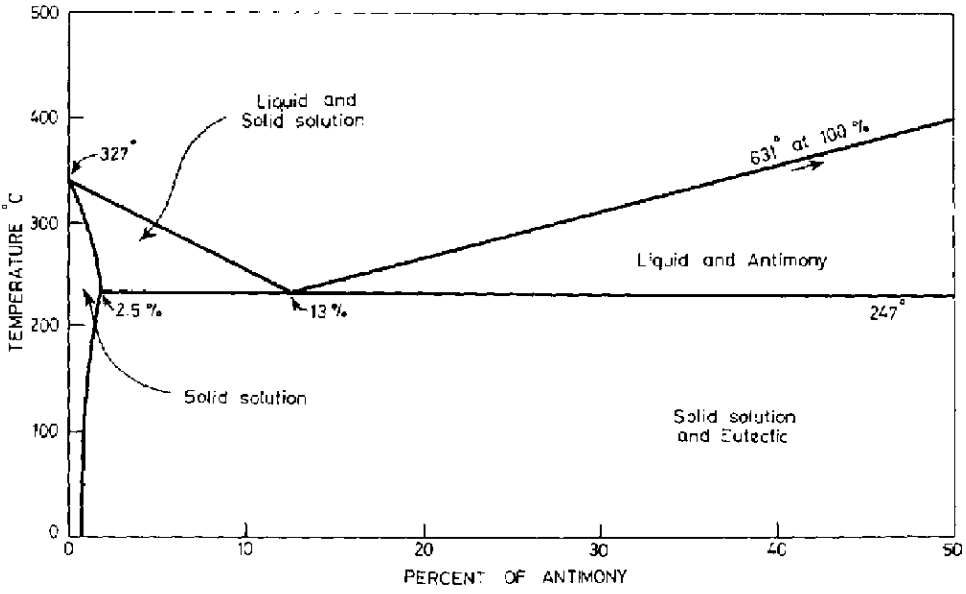

Fig. 27. Equilibrium diagram of lead–antimony.
(Source: G. W. Vinal, Storage Batteries, Wiley, New York, 1955, p 18.)

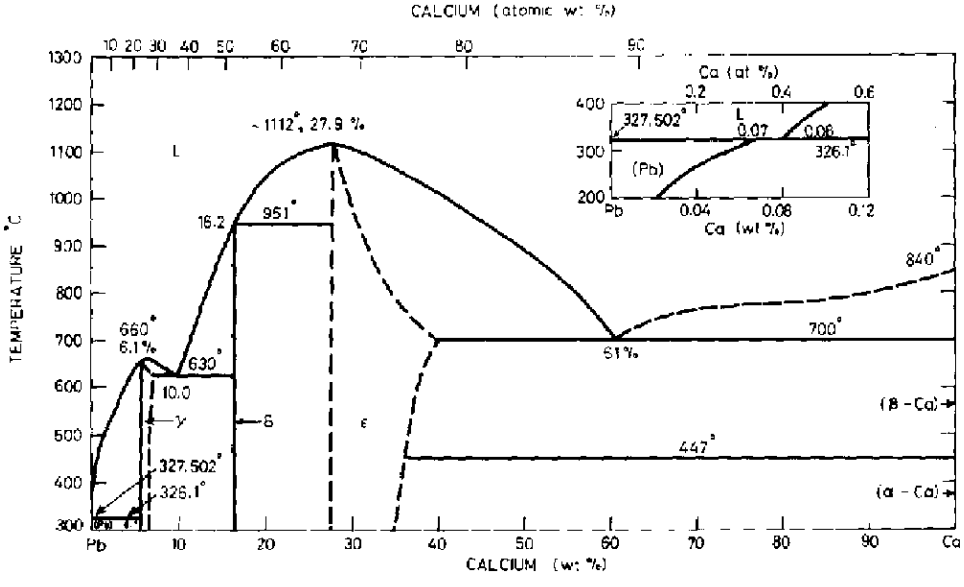

Fig. 28. Phase diagram of lead–calcium.
(Source: Metals Handbook, 8th edn., Vol. 8, American Society for Metals, Cleveland, Ohio, 1973, p. 280.)

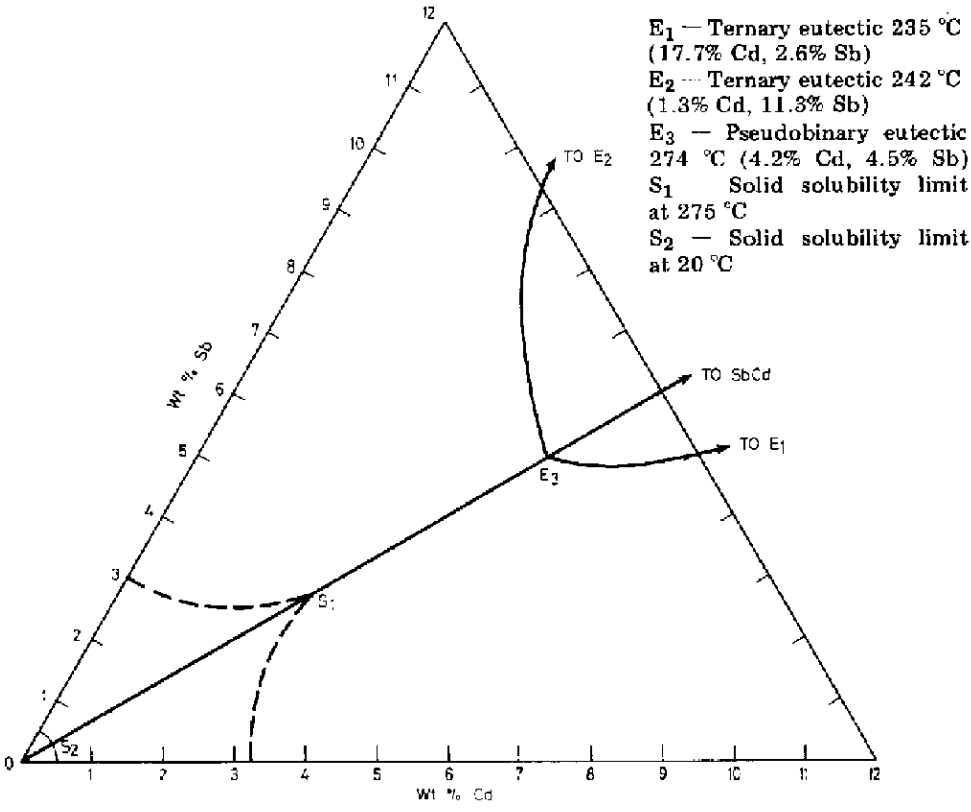

Fig. 29. Phase diagram of lead–antimony–cadmium.
(Source: N. E. Bagshaw, LEAD 68, Ed. Proc. Third Intern. Conf. on Lead, Venice, Pergamon Press, Oxford, 1969, p. 215.)

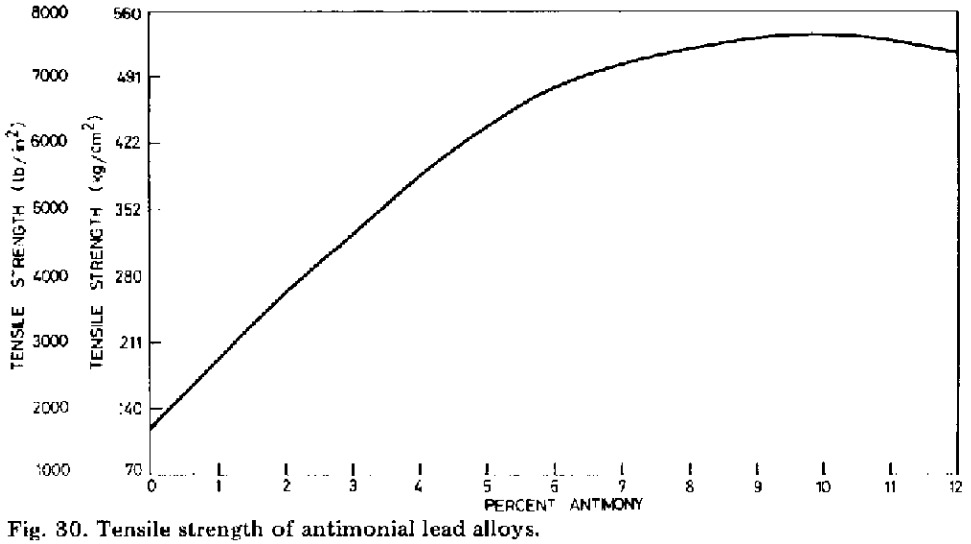

Fig. 30. Tensile strength of antimonial lead alloys.
(Source: Grid Metal Manual, IBMA 1973, p. 4.)

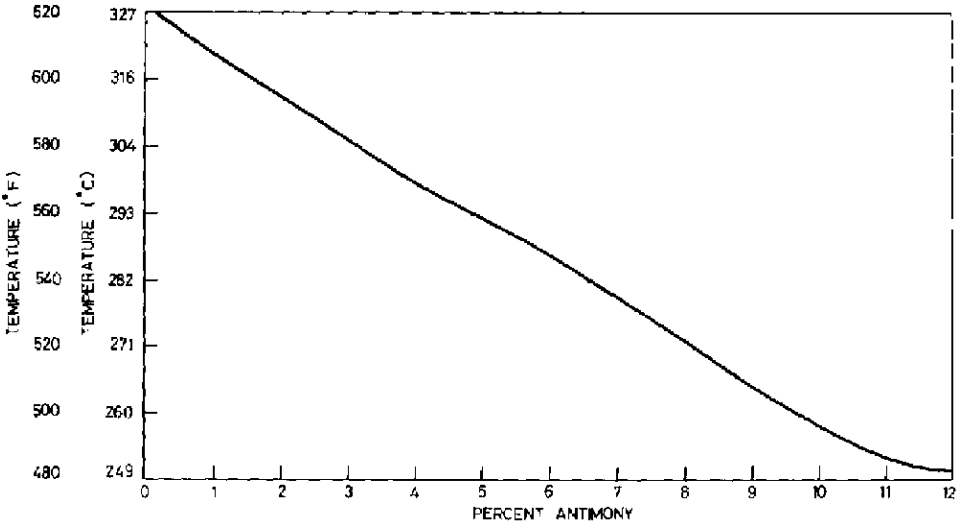

Fig. 31. Melting point of antimonial lead alloys.
(Source: Grid Metal Manual, IBMA 1973, p. 5.)

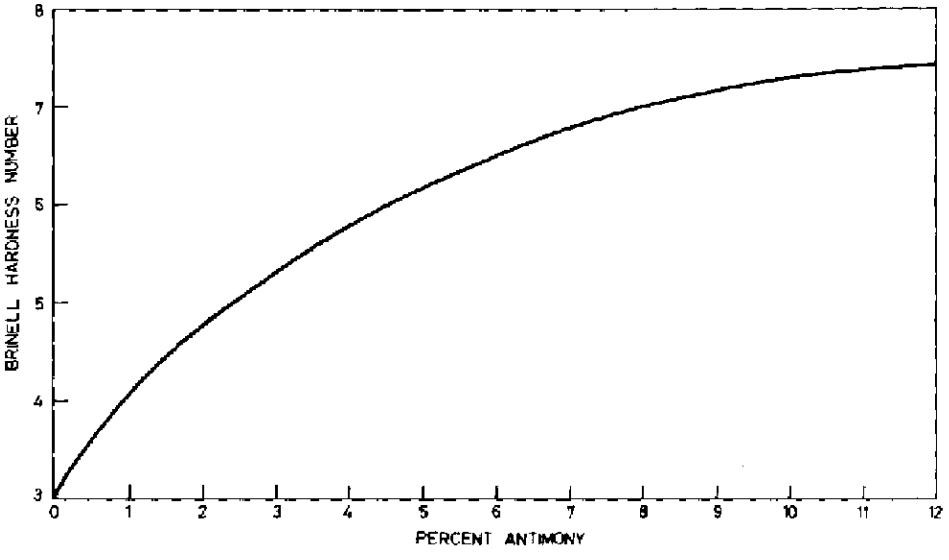

Fig. 32. Brinell Hardness of antimonial lead alloys.
(Source: Grid Metal Manual, IBMA 1973, p. 3.)

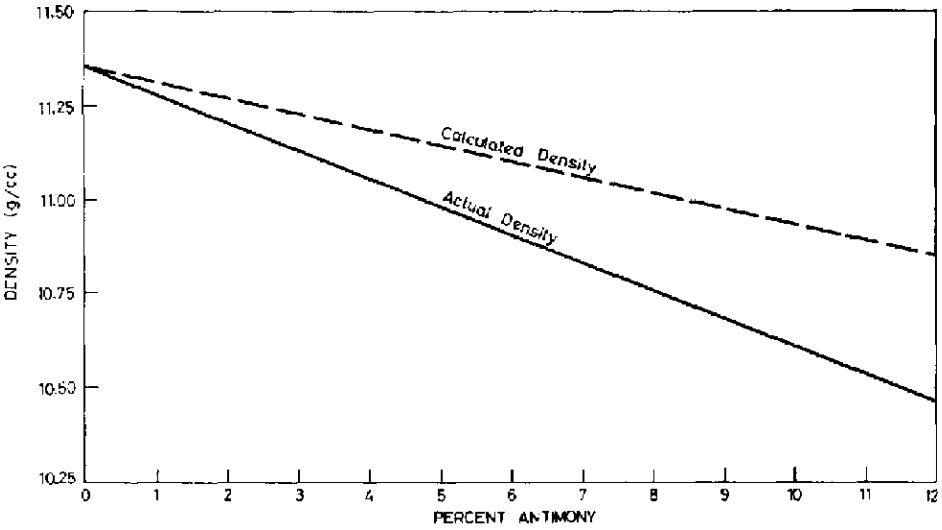

Fig. 33. Density of antimonial lead alloys.
(Source: Grid Metal Manual, IBMA 1973, p. 5.)

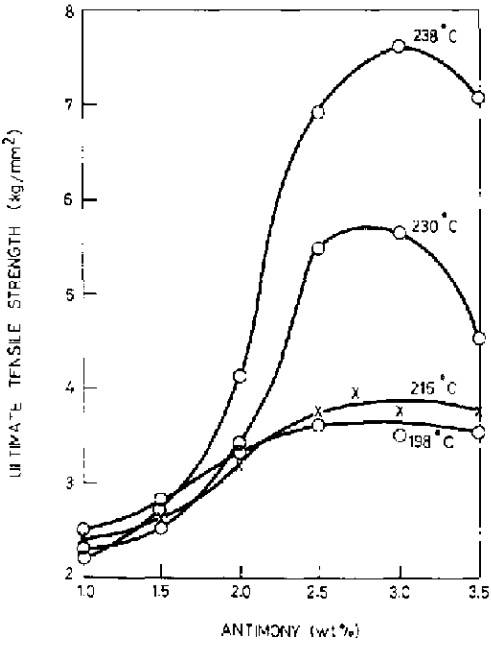

Fig. 34. Age hardening of lead antimony alloys in relation to quenching temperature. Storage time: 1 day.
(Source: L. Zickrick and F. C. Nix, Trans. AIME, 73 (1962) 505.)

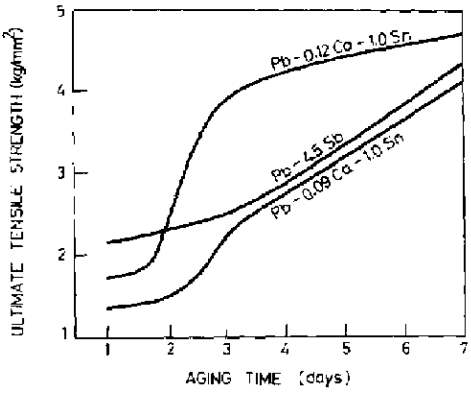

Fig. 35. The ageing of grids after casting. (Source: J. A. Young et al., Paper presented at the BCI Convention, 1973, p. 46.)

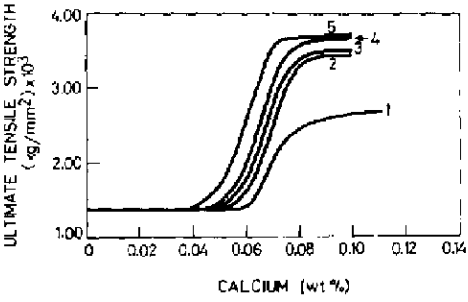

Fig. 36. Tensile strength *vs.* calcium content of Pb Ca showing the effect of ageing time. Period of ageing: 1, 1 min; 2, 6 min; 3, 11 min; 4, 21 min; 5, 60 min. All specimens were solution-treated for 5 h at 300 °C and water quenched.

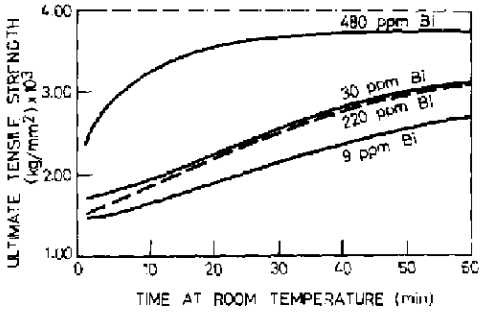

Fig. 37. Tensile strength *vs.* ageing time for Pb–0.06%Ca at varying bismuth levels.

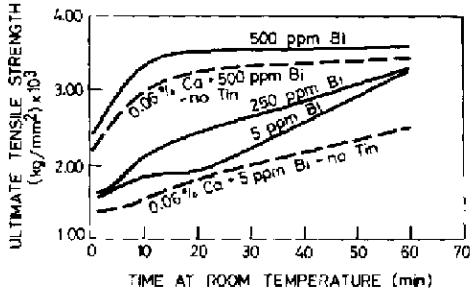

Fig. 38. Tensile strength *vs.* ageing time for Pb–0.06%Ca–0.25%Sn at varying bismuth levels.

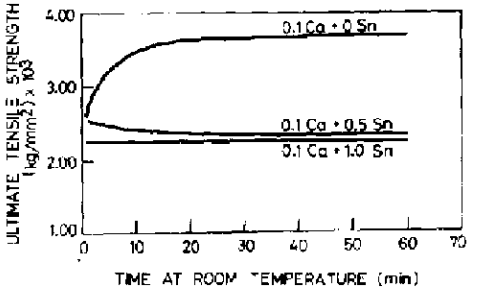

Fig. 39. Tensile strength *vs.* ageing time for Pb–0.1%Ca at varying Sn levels.

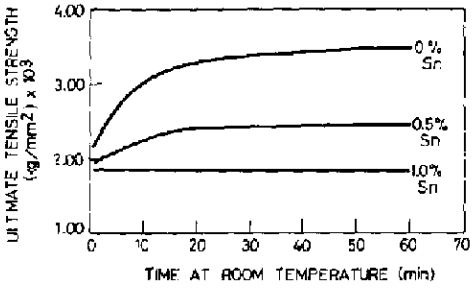

Fig. 40. Tensile strength *vs.* ageing time of Pb–0.06%Ca 500 ppm Bi at varying Sn levels.

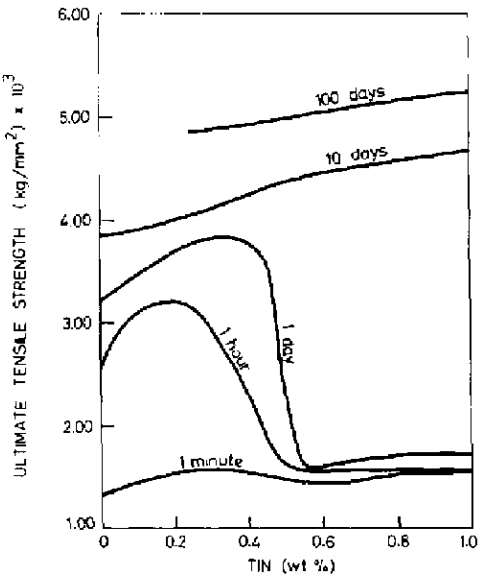

Fig. 41. Tensile strength *vs.* Sn content of Pb–0.06%Ca–5 ppm Bi alloys after different periods of ageing. The alloy was solution-treated at 300 °C for 5 h and water quenched and aged at room temperature.

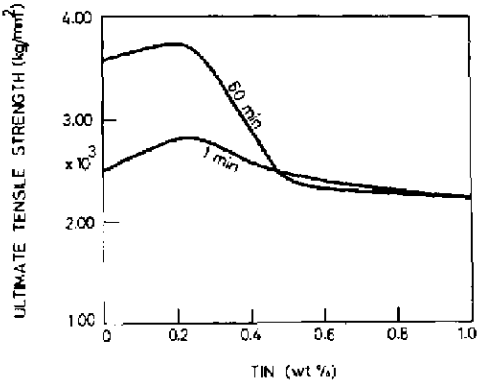

Fig. 42. Tensile strength *vs.* Sn content of Pb–0.1%Ca–5 ppm Bi alloys after different periods of ageing. The alloy was solution-treated at 300 °C for 5 hours and water quenched and aged at room temperature.

(Source of Figs. 37 - 42: M. Myers, Proc. BCI Convention 1975, P. 135.)

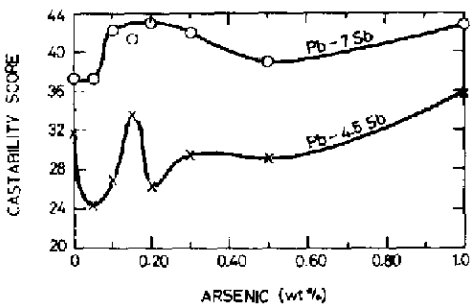

Fig. 43. Influence of arsenic additions on castability of antimonial lead. The castability score was determined with a "tree mould" with arbitrarily assigned points to each portion of the mould, the mould and metal temperatures being 204 °C and 482 °C. (Source: G. W. Mao and J. G. Larsen, Metallurgia, Dec. 1968, p. 244.)

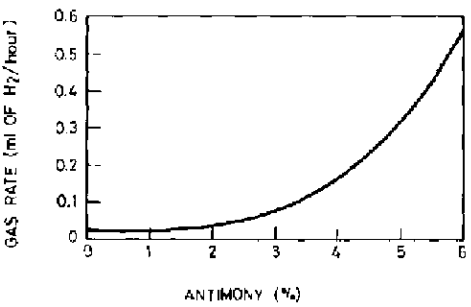

Fig. 44. Gassing rate *vs.* antimony content of grid alloy. The experiments were carried out with laboratory cells which were given pretreatment equivalent to two DIN (German Standards) cycles.

(Source: H. Niklas, Proc. BCI Convention, 1974, p. 51.)

5. PASTING AND FORMING

TABLE 25

HEATS OF REACTION OF LEAD OXIDE AND HYDROXIDES

Reactants	*Products*	*Heat of reaction**	
		(kcal)	(Watt-min)
$PbO + H_2O$	$Pb(OH)_2$	+ 2.64	184.2
$4\ PbO + PbSO_4$	$4\ PbO.PbSO_4$	+ 4.89	341.2
$Pb(OH)_2 + PbSO_4$	$PbO.PbSO_4 + H_2O$	+ 5.15	359.3
$PbO + PbSO_4$	$PbO.PbSO_4$	+ 7.79	543.5
$3\ PbO + PbSO_4$	$3\ PbO.PbSO_4$	+11.91	830.9
$Pb(OH)_2 + H_2SO_4$	$PbSO_4 + 2H_2O$	+38.66	2697.3
$PbO + H_2SO_4$	$PbSO_4 + H_2O$	+41.30	2881.5
$5\ PbO + H_2SO_4$	$4\ PbO.PbSO_4 + H_2O$	+46.19	3222.6
$2\ PbO + H_2SO_4$	$PbO.PbSO_4 + H_2O$	+49.09	3425.0
$4\ PbO + H_2SO_4$	$3\ PbO.PbSO_4 + H_2O$	+53.21	3712.4

*The heat of formation of liquid sulphuric acid rather than its standard state at infinite dilution was used in calculating the heat of reaction (1 kcal = 69.769 Watt-min).

(Source: ILZRO Project LE-82-84 Final Report, Dec. 31, 1971, p. 2/27.)

TABLE 26

HEAT OF REACTION OF SULPHURIC ACID WITH EXCESS PbO

Sp. Gr.	*Millimoles H_2SO_4 per cm^3*	*Heat of reaction in Watt min per cm^3 of acid for the products*			
		$PbSO_4$	*$PbO.PbSO_4$*	*$3PbO.PbSO_4$*	*$4PbO.PbSO_4$*
1.250	4.31	7.548	8.972	9.725	8.442
1.283	4.93	8.826	10.491	11.371	9.871
1.300	5.26	9.384	11.154	12.090	10.495
1.307	5.40	9.788	11.634	12.611	10.947
1.325	5.74	10.352	12.304	13.338	11.578
1.336	5.96	10.973	13.043	14.138	12.272
1.371	6.64	12.467	14.818	16.062	13.943
1.400	7.21	13.431	15.964	17.305	15.021
1.416	7.52	14.460	16.000	18.630	16.172
1.473	8.67	17.191	20.433	22.149	19.226
1.500	9.20	17.889	21.263	23.048	20.007

(Source: ILZRO Project LE-82-84 Final Report, Dec. 31, 1971, p. 2/35.)

TABLE 27

HEAT OF REACTION: $PbO + H_2SO_4 = PbSO_4 + H_2O$

Acid dilution			*Millimoles H_2SO_4*		*Heat of prior dilution from 100 % acid*			*Reaction heat per mole reacted H_2SO_4* (kcal)
Moles	*H_2O/SO_3 Sp. Gr.*	*Heat of formation per mole of H_2SO_4* (kcal)	*per gram*	*per cm^3*	*Enthalpy* (kcal)	*Entropy* (cal)	*Total* (kcal)	
1	1.830	194.55	-	-	-	-	-	41.295
5	1.473	207.43	5.58	8.67	12.878	14.99	12.893	28.417
6	1.416	208.39	5.31	7.52	13.738	15.03	13.753	27.557
7	1.371	208.94	4.84	6.64	14.394	13.16	13.407	26.901
8	1.336	209.46	4.46	5.96	14.908	12.76	14.921	26.387
9	1.307	209.86	4.13	5.40	15.315	11.57	15.327	25.980
10	1.283	210.19	3.84	4.93	15.640	10.52	15.651	25.655
∞	1.000	217.32	-		22.770		-	18.525

(Source: ILZRO Project LE-82-84 Final Report, Dec. 31, 1971, p. 2/34.)

TABLE 28

HEAT OF REACTION PER KG OF PbO AT VARIOUS SULPHATE CONTENTS

Moles PbO per mole SO_3	*Moles SO_3* per kg PbO*	*Weight percent $PbSO_4$ in paste*	*Heat of reaction*	
			(kcal)	(Watt-min)
5	0.896	25.35	37.00	2581.4
6	0.747	21.38	30.85	2152.4
7	0.640	18.46	26.43	1844.0
8	0.560	16.25	23.13	1613.8
9	0.498	14.52	20.57	1435.1
10	0.448	13.12	18.50	1290.7
11	0.407	11.95	16.81	1172.8
12	0.373	10.98	15.40	1074.4

*The heat of formation of sulphuric acid is taken as 194.55 kcal per mole in this table.

(Source: ILZRO Project LE-82-84 Final Report, Dec. 31, 1971, p. 2/35.)

TABLE 29

WEIGHT AND MOLAR PERCENTAGE DATA FOR THE PbO H_2O SYSTEM

Moles H_2O per mole PbO	*Mole percentage*		*Weight percentage*		*Volume of H_2O per unit weight PbO* (cm^3 $kg.^{-1}$)
	PbO	*H_2O*	*PbO*	*H_2O*	
0.027	97.34	2.66	99.78	0.22	2.20
0.333	75.00	25.00	97.38	2.62	26.89
0.400	71.43	28.57	96.87	3.13	32.19
0.500	66.67	33.33	96.12	3.88	40.34
0.819	54.97	45.03	93.80	6.20	66.14
1.000	50.00	50.00	92.53	7.47	80.69
1.100	47.62	52.38	91.84	8.16	88.78
1.200	45.46	54.54	91.17	8.83	96.85
1.300	43.48	56.52	90.50	9.50	104.90
1.400	41.67	58.33	89.85	10.15	113.0
1.500	40.00	60.00	89.20	10.80	121.0
1.600	38.46	61.54	88.56	11.44	129.4
1.700	37.04	62.96	87.93	12.07	137.2
1.800	35.72	64.28	87.31	12.69	145.3
1.900	34.45	65.55	86.70	13.30	153.3
2.000	33.33	66.67	86.10	13.90	161.4
2.100	32.26	67.74	85.51	14.49	169.5
2.200	31.25	68.75	84.92	15.08	177.6
2.300	30.30	69.70	84.34	15.66	185.6
2.400	29.41	70.59	83.77	16.23	193.7
2.500	28.57	71.43	83.21	16.79	201.7
3.000	25.00	75.00	80.51	19.49	242.1
3.500	22.22	77.78	77.97	22.03	282.6

(Source: ILZRO Project LE-82-84 Final Report Dec. 31, 1971, p. 2/93A.)

TABLE 30

WEIGHT AND MOLAR PERCENTAGE DATA FOR THE PbO–SO_3 SYSTEM

Moles PbO per mole SO_3	*Mole %*		*Weight %*		*Weight % as*		*Volume (cm^3) acid per kg PbO*		*Grams H_2SO_4 per kg PbO*
	PbO	*SO_3*	*PbO*	*SO_3*	*$PbSO_4$*	*$4PbO.PbSO_4$*	*Specific gravity*		
							1.336	*1.416*	
1	50.00	50.00	73.60	26.40	100.00	-	751.70	595.70	439.40
2	66.67	33.33	84.97	15.21	57.61	–	375.80	297.80	219.70
3	75.00	25.00	89.32	10.68	40.46	–	250.50	198.60	146.50
4	80.00	20.00	91.77	8.23	31.17	-	187.90	148.90	109.90
5	83.33	16.67	93.31	6.69	25.34	100.00	150.30	119.10	87.86
6	85.71	14.29	94.35	5.64	21.36	84.28	125.30	99.28	73.24
7	87.50	12.50	95.12	4.87	18.45	72.83	107.40	85.10	62.77
8	88.89	11.11	95.71	4.29	16.25	64.09	93.96	74.46	54.91
9	90.00	10.00	96.17	3.83	14.51	57.22	83.33	66.04	48.80
10	90.91	9.09	96.54	3.46	13.11	51.69	75.16	59.57	43.91
11	91.67	8.33	96.84	3.16	11.97	47.21	68.33	54.15	39.97
12	92.31	7.69	97.10	2.90	10.98	43.32	62.64	49.64	36.59
13	92.86	7.14	97.31	2.69	10.19	40.19	57.82	45.82	33.87
14	93.33	6.67	97.50	2.50	9.47	37.35	53.69	42.55	31.41
15	93.75	6.25	97.66	2.34	8.86	34.96	50.11	39.71	29.36

(Source: ILZRO Project LE 82-84 Final Report, Dec. 31, 1971, p. 2/93C.)

TABLE 31

WEIGHT AND MOLAR PERCENTAGE DATA FOR THE H_2O–SO_3 SYSTEM

Sp. Gr. 20 °C	*Moles H_2O per mole SO_3*	*Mole %*		*Weight %*		*Weight % H_2SO_4*	*Moles H_2SO_4 per litre*	*Volume (cm^3) acid per mole H_2SO_4*
		SO_3	*H_2O*	*SO_3*	*H_2O*			
1.900	0.50	66.67	33.33	89.89	10.11	–	–	–
1.600	3.34	23.04	76.96	57.10	42.90	69.95	11.41	87.6
1.500	4.61	17.83	82.17	49.11	50.89	60.16	9.20	108.7
1.400	6.34	13.62	86.38	41.21	58.79	50.50	7.21	138.7
1.300	9.29	9.72	90.28	32.39	67.61	39.68	5.26	190.1
1.250	11.64	7.91	92.09	27.60	72.40	33.82	4.31	232.0
1.228	13.00	7.14	92.86	25.48	74.52	31.21	3.91	255.7
1.200	15.19	5.92	94.08	22.63	77.37	27.72	3.39	295.0
1.178	17.32	5.46	94.54	20.41	75.59	25.00	3.00	333.0
1.150	21.03	4.54	95.46	17.45	82.55	21.38	2.51	398.4
1.100	32.53	2.98	97.02	12.02	87.98	14.73	1.65	606.1
1.050	66.45	1.48	98.52	6.27	93.73	7.68	0.82	1216.5
1.025	131.60	0.75	99.25	3.26	96.74	4.00	0.42	2392.3

(Source: ILZRO Project LE-82-84 Final Report, Dec. 31, 1971, p. 2/93D.)

TABLE 32

MIXING DATA ON LEAD SULPHATE/LEAD OXIDE PASTES

PbO/SO_3	*Heat of Mixing* (Watt-min)	*Max. mix Temp.* (°C)	*Paste*		*Second cycle*			*10th discharge*, Ah	*Last cycle*	*Final condition*
			Consistency	*Density* ($g\ cm^{-3}$)	*Voltage on charging* (V)	Ah	Ah g^{-1}			
PbO	693	43	21	3.66	2.84	7.4	0.114	1.0	11	Good appearance
12	96	50	18	4.27	2.76	7.0	0.104	4.6	18	Badly shed
8	385	50.5	22	3.66	2.79	7.4	0.131	0.6	11	Good appearance
5	758	80	23	3.14	2.86	2.3	0.050	0.7	11	Good appearance

The last three mixes in this table were made by adding 161 cm^3 of initial water to 1 kg of oxide, and no acid was used in any mix. Final water amounting to 150 and 60 cm^3 respectively, had to be added to the last and the last but one mixes to obtain a pastable mix. 74.5 cm^3 of 1.416 SG acid was used in the control mix. The pasted plates were subjected to cycling. At ten cycles the cells had received six capacity tests plus four weeks of trickle charging at the gassing level. At 18 cycles, they had received six capacity tests and 12 weeks of trickle charge. (Source: ILZRO Project LE-82-84 Final Report, Dec. 31, 1971, pp. 2/67 and 2/68.)

TABLE 33

DATA ON RED LEAD MIXES*

Oxide	Pb_3O_4 (%)	*Specific surface* ($m^2\ kg^{-1}$)	*Heat of Mixing* (Watt min)	*Paste*	
				Consistency	*Density* ($g\ cm^{-3}$)
H1 (1969 production material)	25	790	150	26	3.60
H2 (1968 production material)	25	790	451	19	3.69
H3 (1971 production material)	25	410	561	22	3.69
Blend (very fine particle 98.1% Pb_3O_4, and very fine PbO)	25	1172	351	17	3.75
Furnaced (25% very severely milled)	25	670	540	18.5	3.75
Furnaced (75% very severely milled)	75	890	205	17	3.75
Control (severely milled chemical PbO)	0	1080	890	18	3.84

*The H1 mix was made with 113.5 cm^3 of 1.283 SG acid, while 93.5 cm^3 of 1.336 SG acid was used for making other mixes. The above table is intended to show that replacing a part of litharge with red lead results in less chemical reaction heat being generated during mixing.

(Source: ILZRO Project LE-82-84, Final Report, Dec. 31, 1971, p. 2/69.)

TABLE 34

AMPERE-HOURS TO FORM POSITIVE PLATES OF DRY CHARGED BATTERIES*

Plate type	*Thickness* (mm)	*Ampere hours for formation per positive plate*
Regular	2.03	46
Low	2.03	42
High	2.03	50
Narrow	2.03	37
Utility	2.03	25
Bus truck	4.00	90
Regular thin	1.78	40
Low thin	1.78	36
High thin	1.78	43
Narrow thin	1.78	32

*The data in the above table apply specifically to plate types employed in U.S.A.

(Source: Storage Battery Manufacturing Manual, IBMA, p. 36.)

TABLE 35

SOME COMMONLY USED GRID SIZES AND SUGGESTED PLATE PASTE WEIGHTS*

Grid type	*Width* (cm)	*Height* (cm)	*Thickness* (mm)	*No. of Wires*		*Feet height* (mm)	*Approx weight* (g)	*Dry paste weight* (g)					
				Horizontal	*Vertical*			*Positive paste*			*Negative paste*		
								Max	*Min*	*Average*	*Max*	*Min*	*Average*
Regular	14.29	12.39	1.78	30	7	3.2	71	101	91	96	108	97	101
Regular	14.29	12.39	2.03	30	7	3.2	79	117	106	111	123	108	113
Low	14.29	11.28	1.78	28	7	2.4	68	91	82	86	99	88	92
Low	14.29	11.28	2.03	28	7	2.4	75	106	95	99	–	–	–
High	14.29	13.32	1.78	34	7	3.2	76	109	99	104	117	105	109
High	14.29	13.32	2.03	34	7	3.2	86	127	114	119	132	119	124
Narrow	10.80	13.32	1.78	34	5	2.4	60	84	77	80	86	79	81
Narrow	10.80	13.32	2.03	34	5	2.4	66	95	85	90	–	–	–
Utility	12.20	11.42	1.78	26	6	2.4	56	–	–	–	82	74	78
Utility	12.20	11.42	2.03	26	6	2.4	61	89	80	84	93	84	87
Bus-Truck	14.29	12.39	3.20	30	7	3.2	136	–	–	–	184	165	173
Bus-Truck	14.29	12.39	4.00	30	7	3.2	181	221	201	209	–	–	–
Regular Thin	14.29	12.39	1.53	30	7	3.2	63	–	–	–	94	84	88
Low Thin	14.29	11.28	1.53	28	7	2.4	61	–	–	–	85	76	80
High Thin	14.29	13.32	1.53	34	7	3.2	66	–	–	–	101	90	94
Narrow Thin	10.80	13.32	1.53	34	5	2.4	54	–	–	–	76	67	71

*The data presented in this table specifically apply to grid and plate types employed in U.S.A.

(Source: Storage Battery Manufacturing Manual, IBMA, 1970, p. 3.)

TABLE 36

CONTAINER PLATE FORMING SCHEDULE. RATE IN AMPERES*
(High rate, 24 hours; low rate, approx. 12 hours)

Plates per cell	*Plate type*				*For thickness of positive and negative plates, see Table 34*											
	Low and narrow		*Regular and high*		*Regular*		*Low*		*High*		*Narrow*		*Utility*		*Bus-Truck*	
	Pos. 1.78 mm Neg. 1.52 mm		*Pos. 1.78 mm Neg. 1.52 mm*		*High*	*Low*	*High*	*Low*	*High*	*Low*	*High*	*Low*	*High*	*Low*	*High*	*Low*
	High	*Low*	*High*	*Low*												
5	3	1	3	1	4	1.5	4	1.5	4	2	4	-	4	-	–	–
7	4	1	4	1	4	3	4	2	5	3	4	1	4	–	7	5
9	5	3	5	3	6	3	5	3	6	4	5	3	4	3	9	6
11	6	3	6	4	7	4	6	4	8	5	6	4	5	4	11	8
13	7	3	7	5	8	5	7	5	9	5	7	5	6	5	13	9
15	7	5	8	6	9	6	8	6	10	7	8	6	7	5	15	10
17	8	6	10	6	11	7	10	6	12	8	10	6	8	5	17	12
19	10	6	11	7	12	8	11	7	13	9	11	7	–	–	19	13
21	–	–	–	–	13	9	12	8	15	10	12	8	–	–	20	14
23	–	–	–	–	14	10	13	9	17	11	13	9	–	–	–	–
25	–	–	–	–	16	11	14	10	18	12	14	10	–	–	–	–

*The data presented in this table specifically apply to grid types employed in U.S.A.

(Source: Storage Battery Manufacturing Manual, IBMA, 1970, p. 31.)

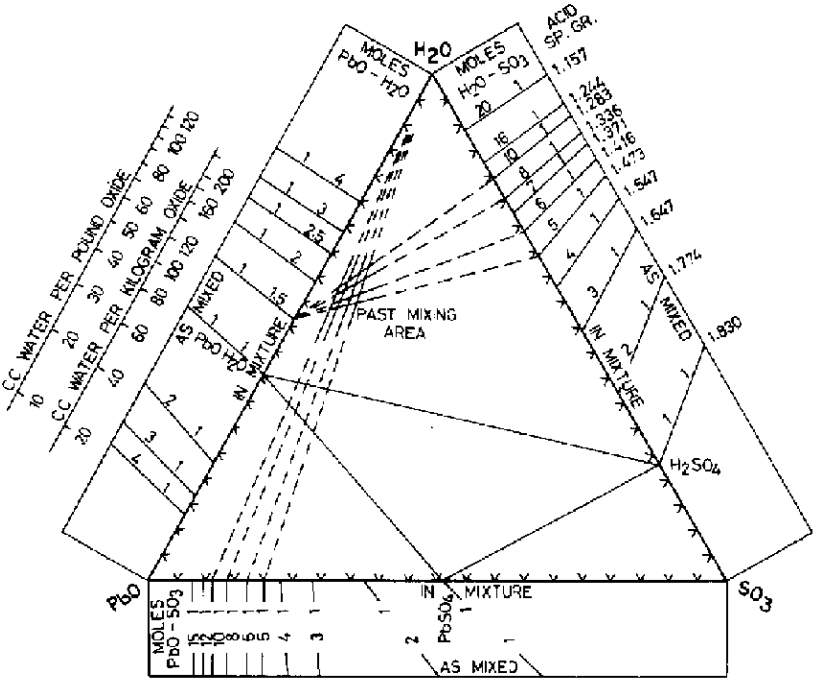

Fig. 45. Molar relations in battery pastes.
(Source: ILZRO Project LE 82-84 Final Report, Dec. 31, 1971, pp. 2/39.)

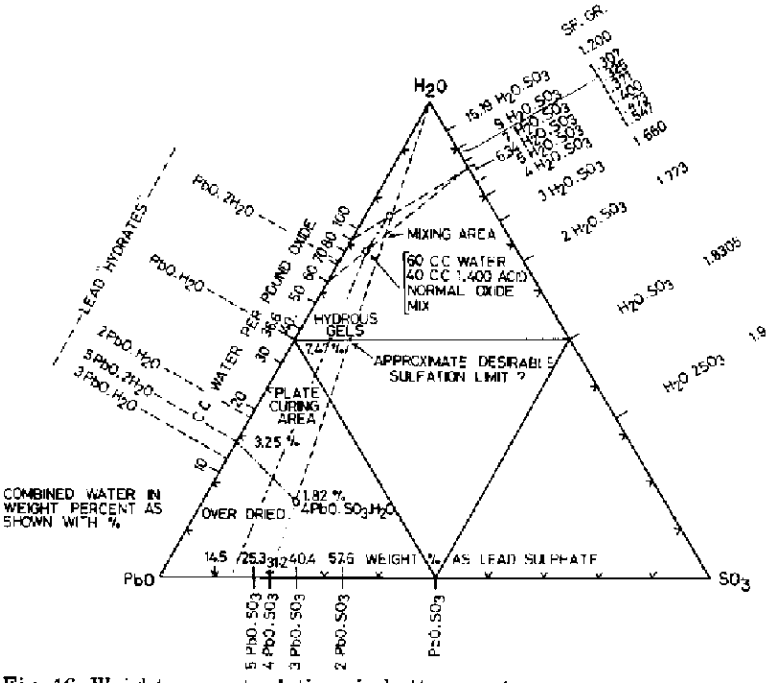

Fig. 46. Weight percent relations in battery pastes.
(Source: ILZRO Project LE 82-84 Final Report, Dec. 31, 1971, pp. 2/40.)

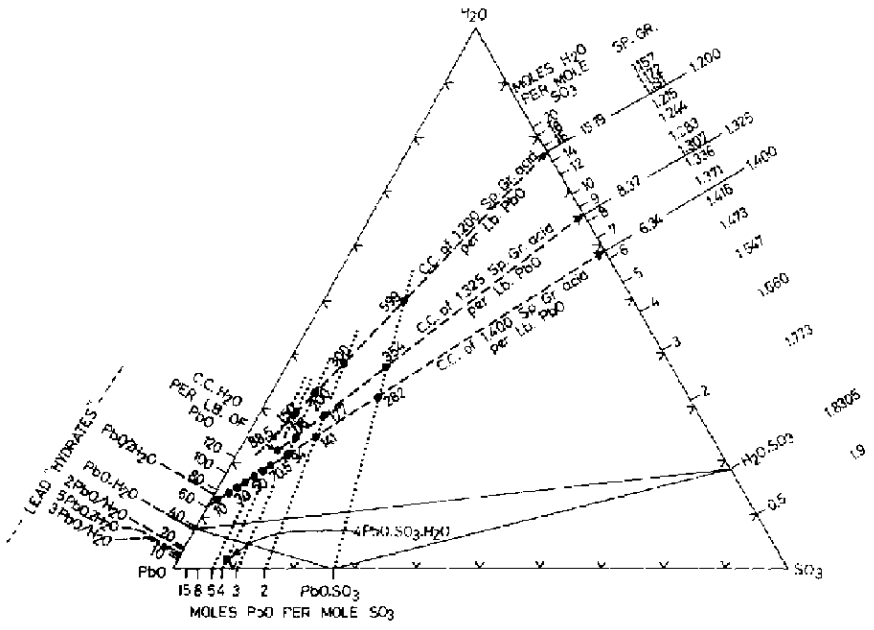

Fig. 47. Volume relations in battery pastes.
(Source: ILZRO Project LE 82-84 Final Report, Dec. 31, 1971, p. 2/41.)

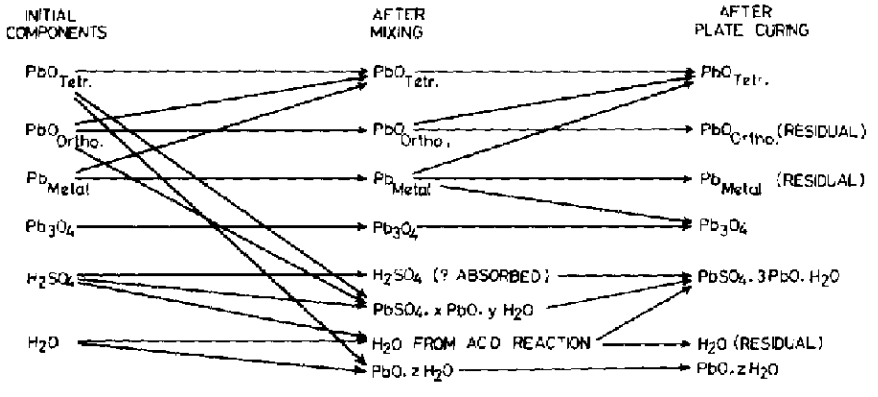

Fig. 48. Transitions of battery paste components.
(Source: ILZRO Project LE 82-84 Final Report, Dec. 31, 1971, p. 2/26.)

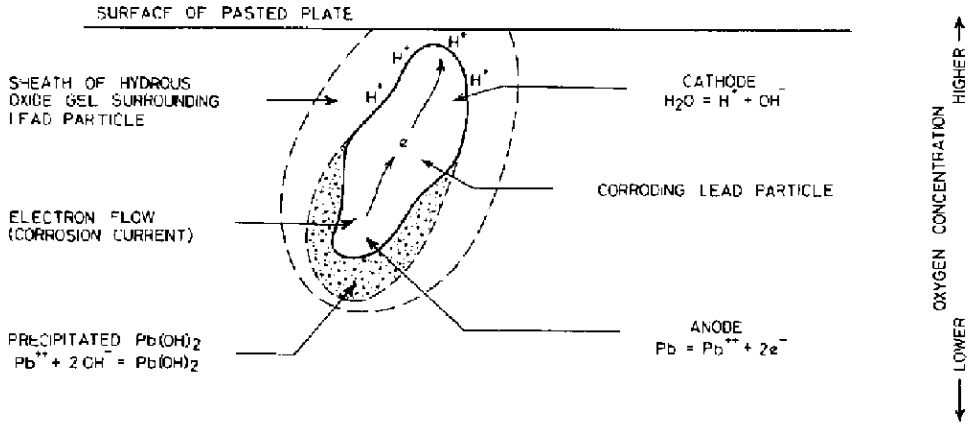

Atmospheric oxygen diffuses into the paste, through the sheath, and depolarizes the cathode areas by combining with the hydrogen ions, and electrons furnished by the lead anode.

$$O + 2H^+ + 2e^- = H_2O$$

Fig. 49. Electrochemical oxidation of lead particles during curing.
(Source: ILZRO Project LE 82-84 Final Report, Dec. 31, 1971, p. 3/5.)

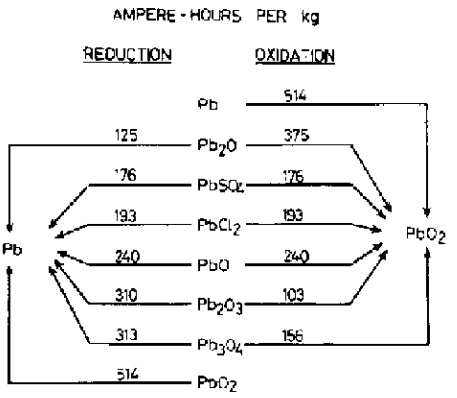

Fig. 50. Quantity of electricity required to reduce or oxidise lead compounds.

6. ELECTROLYTE

TABLE 37

PROPERTIES OF SULPHURIC ACID SOLUTIONS

Specific Gravity		*Temp. coef. of Sp. Gr. at 15 °C (10^{-5})*	H_2SO_4		*Baume degrees*	*Twaddell degrees*
at 15 °C	*at 25 °C*		*(wt.%)*	*(vol.%)*		
1.000	1.000	—	0.0	0.0	0.0	0
1.020	1.019	22	2.9	1.6	2.8	4
1.040	1.039	29	5.9	3.3	5.6	8
1.060	1.058	36	8.7	5.0	8.2	12
1.080	1.078	43	11.5	6.7	10.7	16
1.100	1.097	48	14.3	8.5	13.2	20
1.120	1.117	53	17.0	10.3	15.5	24
1.140	1.137	58	19.6	12.1	17.8	28
1.160	1.156	62	22.1	13.9	20.0	32
1.180	1.176	65	24.7	15.8	22.1	36
1.200	1.196	68	27.2	17.7	24.2	40
1.220	1.216	70	29.6	19.6	26.1	44
1.240	1.235	72	32.0	21.6	28.1	48
1.260	1.255	73	34.4	23.6	29.9	52
1.280	1.275	74	36.8	25.6	31.7	56
1.300	1.295	75	39.1	27.6	33.5	60
1.320	1.315	76	41.4	29.7	35.2	64
1.340	1.335	76	43.6	31.8	36.8	68
1.360	1.355	77	45.8	33.9	38.4	72
1.380	1.375	78	47.9	35.9	39.9	76
1.400	1.395	79	50.0	38.0	41.4	80
1.420	1.415	80	52.0	40.1	42.9	84
1.440	1.435	81	54.0	42.2	44.3	88
1.460	1.455	83	55.9	44.4	45.7	92
1.480	1.475	84	57.8	46.5	47.0	96
1.500	1.495	85	59.7	48.7	48.3	100
1.520	1.515	87	61.5	50.8	49.6	104
1.540	1.535	88	63.3	53.0	50.8	108
1.560	1.554	89	65.1	55.2	52.1	112
1.580	1.574	91	66.8	57.4	53.2	116
1.600	1.594	92	68.6	59.7	54.4	120
1.620	1.614	93	70.3	61.9	55.5	124
1.640	1.634	95	72.0	64.2	56.6	128
1.660	1.654	96	73.7	66.5	57.7	132
1.680	1.674	98	75.4	68.8	58.7	136
1.700	1.694	100	77.1	71.2	59.7	140
1.720	1.713	102	78.8	73.6	60.7	144
1.740	1.733	105	80.6	76.2	61.7	148
1.760	1.753	109	82.4	78.8	62.6	152
1.780	1.773	110	84.4	81.7	63.5	156
1.800	1.793	110	86.7	84.8	64.4	160
1.820	1.813	108	89.8	88.9	65.3	164
1.840	1.834	103	94.8	94.8	—	168

The values of temperature coefficient strictly apply to specific gravity referred to water at 15 °C. However, for practical purposes, these may be used for 25 °C basis also. To calculate SG (S_t) for any temperature t °C, the following equation may be used:

$$S_t = S_{15} + \alpha(15 - t)$$

where S_{15} is the specific gravity at 15 °C, and α is the temperature coefficient in column 3 of this table.

(Source: G. W. Vinal, Storage Batteries, Wiley, New York, 1955, p. 123.)

TABLE 38

RESISTIVITY OF SULPHURIC ACID SOLUTIONS

Temp. (°C)	*Resistivity* (Ohm cm)				*For minimum resistivity*	
	15%	*25%*	*35%*	*45%*	(%)	(Ohm cm)
30	1.596	1.180	1.140	1.312	31.5	1.129
25	1.689	1.261	1.231	1.422	31.1	1.213
20	1.800	1.357	1.334	1.549	30.6	1.310
10	2.090	1.606	1.602	1.885	29.8	1.562
0	2.510	1.961	1.998	2.371	28.8	1.928
−10	—	2.500	2.600	3.100	27.9	2.480
−20	—	3.350	3.570	4.310	26.9	3.340
−30	—	—	5.290	6.350	—	—
−40	—	—	8.390	9.890	—	—

(Source: G. W. Vinal, Storage Batteries, Wiley, New York, 1955, p. 111.)

TABLE 39

FREEZING POINTS OF SULPHURIC ACID SOLUTIONS

Sp. Gr. at 15 °C	*Freezing Point* (°C)	*Sp. Gr. at 15 °C*	*Freezing Point* (°C)
1.00	0	1.450	−29
1.050	−3.3	1.500	−29
1.100	−7.7	1.550	−38
1.150	−15	1.600	indeterminate
1.200	−27	1.650	indeterminate
1.250	−52	1.700	−14
1.300	−70	1.750	+5
1.350	−49	1.800	+6
1.400	−36	1.835	−34

(Source: G. W. Vinal, Storage Batteries, Wiley, New York, 1955, p. 110.)

TABLE 40

VAPOUR PRESSURE OF SULPHURIC ACID SOLUTIONS

Sp. Gr. at 15 °C	*Percentage of* H_2SO_4	*Vapour pressure* (mm of Hg)			
		0 °C	*15 °C*	*25 °C*	*35 °C*
1.0	0.0	4.6	12.8	23.8	42.2
1.1	14.3	4.2	12.0	21.8	39.0
1.2	27.2	3.6	10.2	18.7	33.8
1.3	39.1	2.6	7.5	13.8	25.0
1.4	50.0	1.6	4.5	8.5	15.4
1.5	59.7	0.8	2.0	4.1	7.3
1.6	68.6	0.2	0.6	1.3	2.6
1.7	77.1	—	0.2	0.4	0.8

(Source: G. W. Vinal, Storage Batteries, Wiley, New York, 1955, p. 113.)

TABLE 41

VISCOSITY OF SULPHURIC ACID SOLUTIONS

Temp. (°C)	*Viscosity* (Centipoise)				
	10%	*20%*	*30%*	*40%*	*50%*
30	0.976	1.225	1.596	2.16	3.07
25	1.091	1.371	1.784	2.41	3.40
20	1.228	1.545	2.006	2.70	3.79
10	1.595	2.010	2.600	3.48	4.86
0	2.160	2.710	3.520	4.70	6.52
−10	—	3.820	4.950	6.60	9.15
−20	—	—	7.490	9.89	13.60
−30	—	—	12.200	16.00	21.70
−40	—	—	—	28.80	—
−50	—	—	—	59.50	—

(Source: G. W. Vinal, Storage Batteries, Wiley, New York, 1955, p. 119.)

TABLE 42

ELECTROCHEMICAL EQUIVALENT OF SULPHURIC ACID SOLUTIONS

Sp. Gr. at 25 °C	Amp hrs*
1.05	22
1.10	44
1.15	67
1.20	90
1.25	115
1.30	141
1.35	167

*Calculated per litre of acid, assuming that all the acid is used up in the battery reaction.

TABLE 43

CONVERSION OF DENSITIES TO SPECIFIC GRAVITIES*

	Sp. Gr. $\frac{15\,°C}{15\,°C}$	*Sp. Gr.* $\frac{20\,°C}{20\,°C}$	*Sp. Gr.* $\frac{25\,°C}{25\,°C}$
Density $\frac{25\,°C}{4\,°C}$	+0.0011	+0.0019	+0.0029
Density $\frac{20\,°C}{4\,°C}$	+0.0010	+0.0018	+0.0028
Density $\frac{15\,°C}{4\,°C}$	+0.0009	+0.0017	+0.0027

*This table gives the multiplying factors (MF) used to convert density (D) to specific gravity (SG) and vice versa, employing the relationship SG = D (1 + MF)
The numerator in the above expression for specific gravity or density denotes the temperature of the solution and the denominator the temperature of water.
(Source: G. W. Vinal, Storage Batteries, Wiley, New York, 1955, p. 121.)

TABLE 44

SPECIFIC HEAT OF DILUTED SULPHURIC ACID

Sp. Gr.	*Dilution* (Moles H_2O per mole SO_3)	*Specific Heat*			
		Calories per		Watt minutes per	
		$g\ °C^{-1}$	$cm^3\ °C^{-1}$	$g\ mV^{-1}$	$cm^3\ mV^{-1}$
1.000	∞	1.000	1.000	1.327	1.327
1.100	32.53	0.870	0.957	1.155	1.271
1.200	15.19	0.787	0.945	1.047	1.256
1.283	10.00	0.707	0.907	0.938	1.204
1.325	8.37	0.664	0.880	0.879	1.165
1.350	7.53	0.636	0.859	0.844	1.140
1.400	6.34	0.585	0.819	0.776	1.087
1.450	5.40	0.542	0.786	0.720	1.044
1.500	4.61	0.507	0.761	0.673	1.010
1.550	3.92	0.479	0.743	0.637	0.987
1.650	2.98	0.435	0.718	0.578	0.954
1.750	2.23	0.391	0.684	0.519	0.908
1.830	1.00	0.330	0.608	0.438	0.807

(Source: ILZRO Project LE-82-84 Final Report, Dec. 31, 1971, p. 231, based on data from A. M. Fairlie, Sulphuric Acid Manufacture, A.C.S. Monograph No. 69, 1936, pp. 308 and 602.)

TABLE 45

RANGE OF SPECIFIC GRAVITIES FOR DIFFERENT TYPES OF BATTERIES WHEN FULLY CHARGED

Type of Battery	*Specific Gravity*	
	Temperate climate	*Tropical climate*
Stationary batteries	1.200–1.225	1.200–1.225
Heavy vehicle batteries	1.260–1.280	1.210–1.240
SLI batteries	1.260–1.280	1.210–1.240
Aircraft batteries	1.260–1.285	1.260–1.285
Car-lighting batteries	1.210–1.230	1.210–1.230

TABLE 46

RELATIVE HEAT CONTENT AND HEAT OF DILUTION OF SULPHURIC ACID SOLUTIONS

Sp. Gr. at 25 °C	*Relative molal heat content at 25 °C* (kg cal)	*Heat of dilution at 25 °C* (kg cal)
1.835	20.35	3.19
1.774	16.72	6.82
1.648	13.58	9.96
1.548	11.66	11.88
1.416	9.45	14.09
1.262	7.30	16.24
1.150	6.23	17.31
1.066	5.78	17.76
1.034	5.62	17.92
1.017	5.41	18.13
1.009	5.02	18.52
1.002	4.04	19.50
1.001	2.90	20.64
1.0005	1.54	22.00
1.000	0.00	23.54

The heat liberated when ordinary concentrated acid (1.835 SG) is diluted can be calculated by subtracting the respective molal heat contents in column 3 from 20.35 kcal.
(Source: G. W. Vinal, Storage Batteries, Wiley, New York, 1955, p. 107.)

TABLE 47

SPECIFIC GRAVITY OF SULPHURIC ACID AT DIFFERENT STATES OF CHARGE FOR SLI BATTERIES

State of charge for discharge at reserve capacity rate	*Specific Gravity*	
	in tropical climate	*in temperate climate*
100%	1.225	1.265
75%	1.185	1.225
50%	1.150	1.190
25%	1.115	1.155
Discharged	1.080	1.120

(Source: Battery Service Manual, BCI 1972, p. 25.)

TABLE 48

'HIDDEN' WATER VOLUME IN SULPHURIC ACID

Sp. Gr.	*'Hidden' water** ($cm^3\ l^{-1}$)
1.600	92.2
1.500	90.6
1.473	87.0
1.416	81.1
1.400	79.2
1.336	70.9
1.325	69.4
1.283	63.6

*Hidden water is the amount of water released when concentrated acid is allowed to react with the paste during mixing. This amount of water recovered from a given volume of acid during mixing is higher for the more concentrated acid.
(Source: ILZRO Report LE-82-84, Dec. 31, 1971, pp. 2–36.)

TABLE 49

SOLUBILITY OF LEAD SULPHATE IN SULPHURIC ACID SOLUTIONS

Sp. Gr. at 25 °C	*Weight of $PbSO_4$* ($mg\ l^{-1}$)	
	at 25 °C	*at 0 °C*
1.102	6.28	2.63
1.140	5.18	2.21
1.179	3.76	1.76
1.219	2.75	1.27
1.260	2.02	0.84
1.303	1.52	0.53

(Source: G. W. Vinal, Storage Batteries, Wiley, New York, 1955, p. 183.)

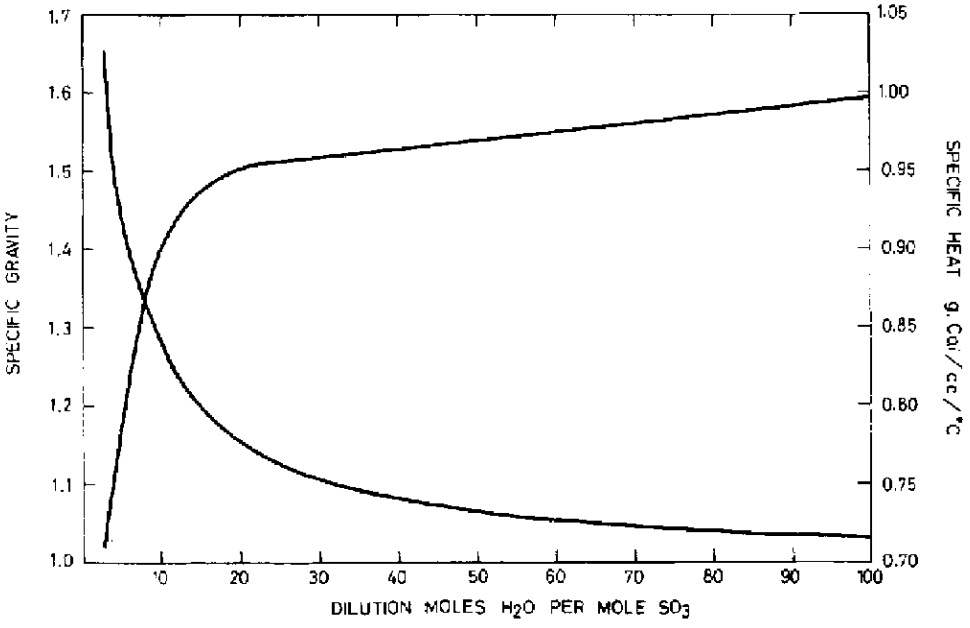

Fig. 51. Specific gravity and specific heat of diluted sulphuric acid.
(Source: ILZRO Project LE 82-84 Final Report, Dec. 31, 1971, p. 2/32, based on data from "Sulphuric Acid Manufacture", by A. M. Fairlie, ACS Monograph No. 69, 1936, pp. 308 and 602.)

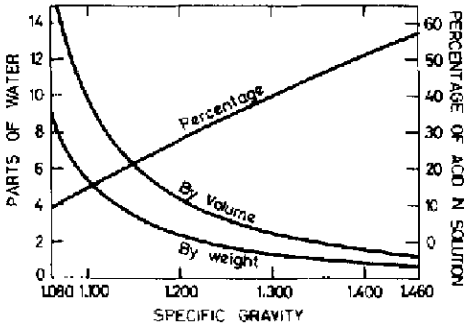

Fig. 52. Preparation of electrolyte of any specific gravity from concentrated sulphuric acid.
(Source: G. W. Vinal, Storage Batteries, Wiley, New York, 1955, p. 129.)

7. TESTING AND CHARGING

TABLE 50

ELECTROMOTIVE FORCE AND TEMPERATURE COEFFICIENT OF THE LEAD BATTERY AS A FUNCTION OF THE SPECIFIC GRAVITY OF THE ACID

Sp. Gr. at 25 °C	*EMF at 25 °C** (V)	*Temp. coef.*** ($mV\,°C^{-1}$)
1.020	1.855	—0.06
1.030	1.878	+0.02
1.040	1.893	+0.06
1.050	1.907	+0.10
1.100	1.961	+0.25
1.150	2.006	+0.28
1.200	2.049	+0.26
1.250	2.095	+0.23
1.280	2.125	+0.20
1.300	2.144	+0.17

The EMF (E_t) of a lead battery at a temperature t °C, and a given electrolyte specific gravity can be calculated from the relationship $E_t = E_{25} + \alpha(t - 25)/1000$ where E_{25} is the EMF at 25 °C at the same electrolyte specific gravity and α is the temperature coefficient in column 3.

*Mean of four directly measured values and three values calculated from electrode potential measurements.

**Mean of three directly measured values and three values calculated from electrode potential measurements.

(Source: G. W. Vinal, Storage Batteries, Wiley, New York, 1955, pp. 192, 194.)

TABLE 51

TIME IN HOURS TO RECHARGE ANTIMONY-FREE STATIONARY LEAD BATTERIES* AT VARIOUS POTENTIALS

Constant potential (V per cell)	*Charger capacity* (A)	*10% discharged*			*50% discharged*			*100% discharged*		
		% Ah returned			*% Ah returned*			*% Ah returned*		
		90	*100*	*110*	*90*	*100*	*110*	*90*	*100*	*110*
2.17	0.15 C**	9.6	21.7	105	44	97	516	75	163	972
	0.3 C	7.5	19.7	103	36	89	508	55	145	952
	0.5 C	7.1	19.3	102	33	86	506	49	139	946
	1.0 C	6.9	19.0	101	32	85	504	45	135	942
2.22	0.15 C	5.9	9.0	46	29	44	231	58	82	448
	0.3 C	3.5	6.6	44	17	31	218	32	56	422
	0.5 C	2.7	5.8	43	13	27	214	24	47	413
	1.0 C	2.3	5.3	43	13	27	212	18	42	408
2.33	0.15 C	5.8	6.5	15	29	33	72	58	65	142
	0.3 C	2.9	3.3	11.5	14	17	56	28	33	111
	0.5 C	1.8	2.2	10.4	9.0	10.9	50	18	22	99
	1.0 C	1.0	1.4	9.6	4.8	6.7	46	9.8	13.5	91

*These cells are being used by Telecom Commission of Australia.

**C = Nominal ampere hour capacity at 10-hour rate.

(Source: Lead Batteries for Auxiliary Power Supply, ALDA, Sep. 1973, p. 26.)

TABLE 52

RELATIVE CAPACITY OF LEAD ACID STORAGE BATTERIES AT VARIOUS RATES OF DISCHARGE AND TEMPERATURES

Temp. (°C)	*Relative capacity in percent for rates of discharge and cut-off voltages specified below**									
Rate of discharge (min):	600	300	180	120	60	40	30	20	10	5
Cut-off voltage (V)	1.77	1.75	1.73	1.71	1.64	1.60	1.54	1.46	1.26	0.95
27	120	100	88	78	65	58	53	46	38	30
10	95	78	68	60	49	44	40	35	29	23
0	79	65	56	50	41	37	33	29	23	18
−10	64	52	45	40	32	28	26	22	17	13
−20	50	40	34	30	24	21	18	15	11	6
−30	36	28	23	20	15	13	11	8	4	—
−40	23	17	13	10	6	4	3	1	—	—
−50	11	5	2	0	—	—	—	—	—	—

*Percentages based on the capacity at the 5-hour rate and 27 °C taken as 100%. These data are based on observations made on a group of small cells with 9 plates and wood separators. The table is intended to illustrate how one can calculate the constants n and c in Peukerts' equation which can then be used to compute either the time of discharge or current. For example, the currents at the 1-hour and 10-hour rates respectively are 65 and 12 amperes as given in the table. Peukerts' equation reads $i^n t = c$, where i is the current and t is the time of discharge, and n and c are constants for a given cell or battery from which it follows that

$$n = \frac{\log t_2/t_1}{\log i_2/i_1} = 1.360$$

and $c = (65)^{1.36} = 291.4$. Knowing n and c, the time of discharge or current can be calculated from Peukerts' equation.

(Source: G. W. Vinal, Storage Batteries, Wiley, New York, 1955, p. 217.)

TABLE 53

MODIFIED CONSTANT-POTENTIAL CHARGING OF LEAD ACID BATTERIES*

Time available for recharge hours	*Bus volts per cell*	*Resistance values per cell* (ohm)		*Ampere rates per 100 Ah*		*Control adjustment*	
		Normal	*Maximum*	*Start of charge*	*Resistor capacity*	*Voltage time relay*	*Ah meter % overcharge*
7.0	2.60	0.016	0.027	27.5	32.5	2.5–3.0	10
7.5	2.61	0.018	0.029	25.5	30.0	2.5–3.0	10
8.0	2.63	0.022	0.031	22.5	26.0	2.5–3.0	10
8.5	2.65	0.026	0.035	20.0	23.0	2.0–2.5	10
9.0	2.67	0.030	0.039	18.5	21.0	2.0–2.5	10
9.5	2.69	0.034	0.043	17.0	19.5	2.0–2.5	10
10.0	2.72	0.040	0.049	15.5	17.5	2.0–2.5	10
12.0	2.84	0.064	0.073	12.0	13.5	2.0–2.5	10
14.0	3.00	0.096	0.105	10.0	11.0	2.0–2.5	10
16.0	3.27	0.150	0.160	8.5	9.0	2.0–2.5	10

*Based on 100 ampere hour capacity at the 6-h rate; Specification of The Electric Industrial Truck Association.

This table is intended to illustrate how one can calculate the value of the modifying resistance (normal and maximum values) to be used. The modifying resistance per cell is multiplied by the number of cells in the battery and this product is divided by the number of hundreds of ampere hours of the battery-rated capacity. The required bus voltage is determined by multiplying the bus volts per cell by the number of cells in the battery.

(Source: G. W. Vinal, Storage Batteries, Wiley, New York, 1955, p. 249.)

TABLE 54

GASSING OF LEAD–ANTIMONY BATTERIES

Cell voltage (V)	*Composition* (vol.%)		*Ratio* H_2/O_2
	Hydrogen	*Oxygen*	
2.2	—	—	—
2.3	52	47	1.1
2.4	60	38	1.6
2.5	67	33	2.0

(Source: G. W. Vinal, Storage Batteries, Wiley, New York, 1955, p. 262.)

TABLE 55

AVERAGE WEIGHT LOSSES FOR BARE GRID AND PASTED GRID SAMPLES

Composition (%)	*Weight losses* (mg cm^{-2}) *at constant current in 56 days*							
	Bare grid samples				*Pasted grid samples*			
	0.14 mA cm^{-2}		*0.84 mA* cm^{-2}		*0.14 mA* cm^{-2}		*0.84 mA* cm^{-2}	
	Coarse grained	*Fine grained*	*Coarse grained*	*Fine grained*	*Coarse grained*	*Fine grained*	*Coarse grained*	*Fine grained*
Pb (pure)	6.3	4.6	24.1	19.5	3.9	3.0	12.7	5.9
Pb-0.46Ag	4.0	9.2	6.7	19.5	4.3	4.2	3.3	4.1
Pb-11.6Sb	43.5	37.8	78.3	73.9	41.6	27.1	86.6	67.7
Pb-6Sb	34.8	28.9	69.7	64.7	22.6	20.6	70.1	57.0
Pb-0.09Ca	5.6	5.8	25.5	27.0	3.3	4.0	6.9	11.7
Quinary alloy*	17.5	25.6	38.4	41.3	12.1	18.4	12.9	26.2

The above samples were subjected to anodic corrosion in sulphuric acid of SG 1.25. The grid pasting was done by hand with a paste containing 23.6% free lead and cured for 48 hours at 40 - 50 °C in saturated humidity. The pasted grids were dried for 1 - 2 days at room temperature before they were tested. The structural characteristics (coarse or fine grained) were determined according to the following table:

Material	*Structural characteristics*		
	Parameter selected	*Coarse structure* (mm)	*Fine structure* (mm)
Pb (pure)	Grain size (mean dia.)	2.45	0.45
Pb-0.46%Ag	Grain size (mean dia.)	0.93	0.47
Pb-11.6%Sb	Interlamellar spacing	2.85×10^{-3}	0.97×10^{-3}
Pb-6%Sb	Size of dendritic cells	15.2×10^{-3}	9.0×10^{-3}
Pb-0.09%Ca	Grain size (mean dia.)	1.96	0.33
Quinary alloy*	Size of dendritic cells	12.5×10^{-3}	7.8×10^{-3}

*Sn 0.5%, Ag 0.2%, Sb 6%, As 0.24%.
(Source: ILZRO LE-130 Report No. 9, p. 25 - 26.)

TABLE 56

AVERAGE WEIGHT LOSSES AT CONSTANT CURRENT FOR GRID ALLOY SAMPLES

Composition (%)	*Weight loss in 4 weeks at 84 mA cm*$^{-2}$ (mg cm^{-2})
Pb–4.50Sb	590.16
Pb–0.13Sn–4.50Sb	602.52
Pb–0.46Sn–4.50Sb	610.88

Sulphuric acid of SG 1.115 was used in the above experiments. The samples were cast in the form of rods.
(Source: G. W. Mao *et al.*, J. Inst. Metals, 97 (1969) 348.)

TABLE 57

WEIGHT LOSSES OF GRID ALLOY SAMPLES AT CONSTANT VOLTAGE

Composition (%)	*Weight loss in 4 weeks at 2.8 V* (mg cm^{-2})
Pb–4.5Sb	135.4
Pb–0.07Ca	49.5
Pb–0.01Li	46.8
Pb–0.02Li	48.0
Pb–0.03Li	63.1
Pure Pb	61.1

Sulphuric acid of SG 1.115 was used in the above experiments. The samples were cast in the form of rods.
(Source: G. W. Mao *et al.*, J. Electrochem. Soc., 117 (1970) 1325.)

TABLE 58

STANDARDS ON LEAD BATTERIES

Description	*Indian Standards*	*British Standards*	*Australian Standards*	*American Standards*	*Japanese Standards*	*German Standards*	*International Electrotechnical Commission Standards*
1 Lead–acid batteries for motor vehicles	7372–1974	3911–1965	D2–1968	SAE J 537h SAE J 240a and SAE J 930a	C 8701–1969		95-1 (1972) 95-2 (1965) 95-3 (1963)
2 Lead–acid traction batteries	5154–1969	2550–1971	—	—	—	—	254–1967
3 Lead–acid batteries for motorcycles, auto-rickshaws and similar vehicles	1146–1962	—	—		—	—	—
4 Stationary lead–acid cells and batteries with tubular positive plates	1651–1970	—		—	C 8704–1973	DIN 40736 DIN 40737	—
5 Stationary lead–acid cells and batteries with Plante positive plates	1652–1972	440–1964	—	—	—	DIN 40731 DIN 40732 DIN 40733 DIN 40738	—
6 Stationary lead–acid cells and batteries with pasted plates	6304–1971	—	—	—	—	—	—
7 Lead–acid batteries for aircraft	1846–1961	2G 205 Pt.I (1975)	U2–1952	—	—	—	—
8 Miner's cap lamp lead–acid batteries	2512–1963	4946–1973	—	—	—	—	—
9 Lead–acid batteries for train lighting and air conditioning	6848–1972	—	—		—	DIN 43579 DIN 43567	—

Description	Indian Standards	British Standards	Australian Standards	American Standards	Japanese Standards	German Standards	International Electro-technical Commission Standards
10 Rubber and plastic containers for lead acid batteries	1146–1972	—	D 23–1973	ASTM D639 –60T	—	—	—
11 Separators for lead–acid batteries	6071–1970 (synthetic)	—	AS 1320–1975	—	—	DIN 43577	
12 Sulphuric acid for battery use	266–1961	3031–1972	C 60–1961	F.S.O.-S801b F 4-14-65	—	—	—
13 Water for battery use	1069–1964	4974–1975	C 59-1961	—	—	—	—
14 Battery terminals and terminal lugs	—	—	C 300–1947	—	—	DIN 40746 DIN 40748 DIN 43569	

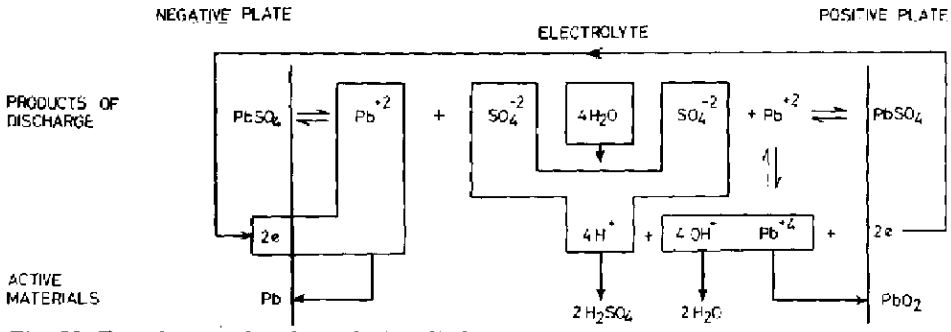

Fig. 53. Reactions at the plates during discharge.

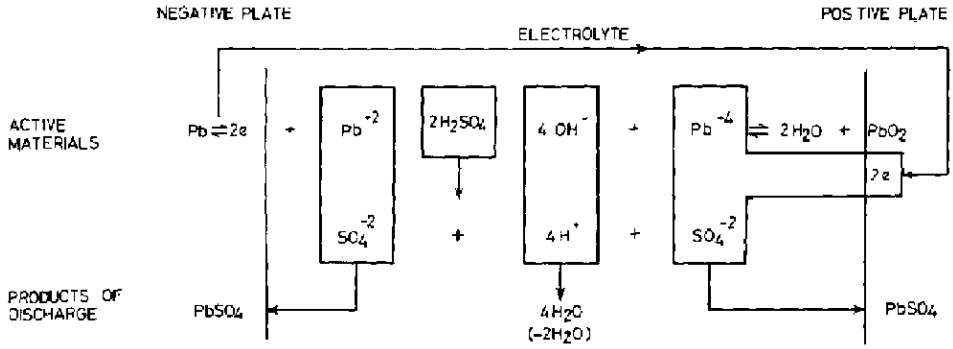

Fig. 54. Reactions at the plates during charge.

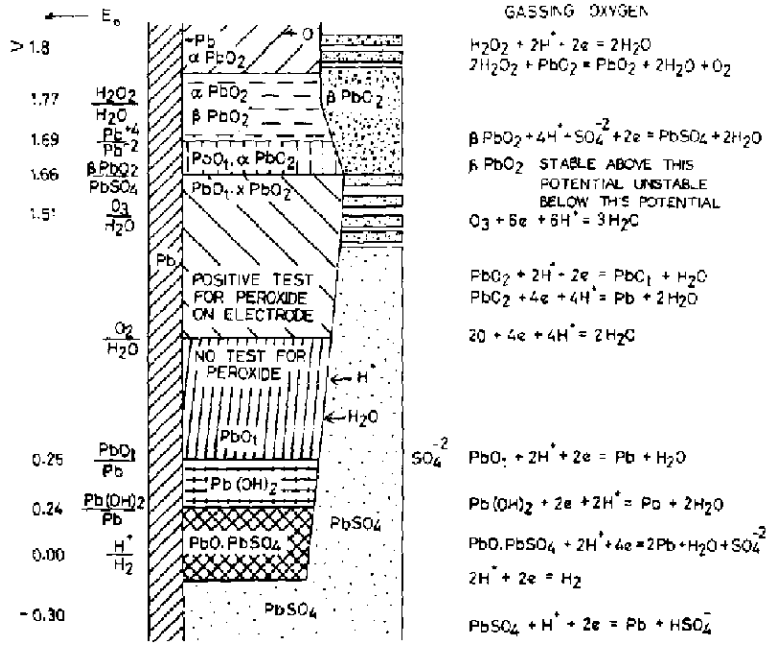

Fig. 55. Schematic cross section of Pb/H_2SO_4 interface during anodic corrosion. (Source: J. Burbank, J. Electrochem. Soc., 106 (1959) 369.)

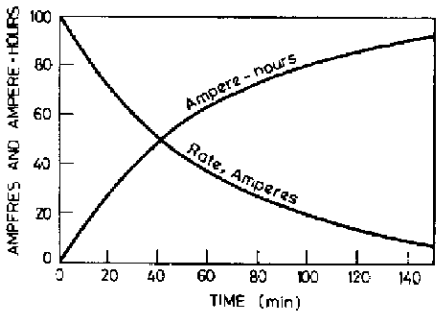

Fig. 56. Graphical illustration of the Ampere Hour Law. This graph illustrates how the theoretical charging current should fall as the battery is progressively charged according to the equation $I = Ae^{-t}$ where I is the charging current and A is the number of ampere hours previously discharged from the battery.
(Source: G. W. Vinal, Storage Batteries, Wiley, New York, 1955, p. 245.)

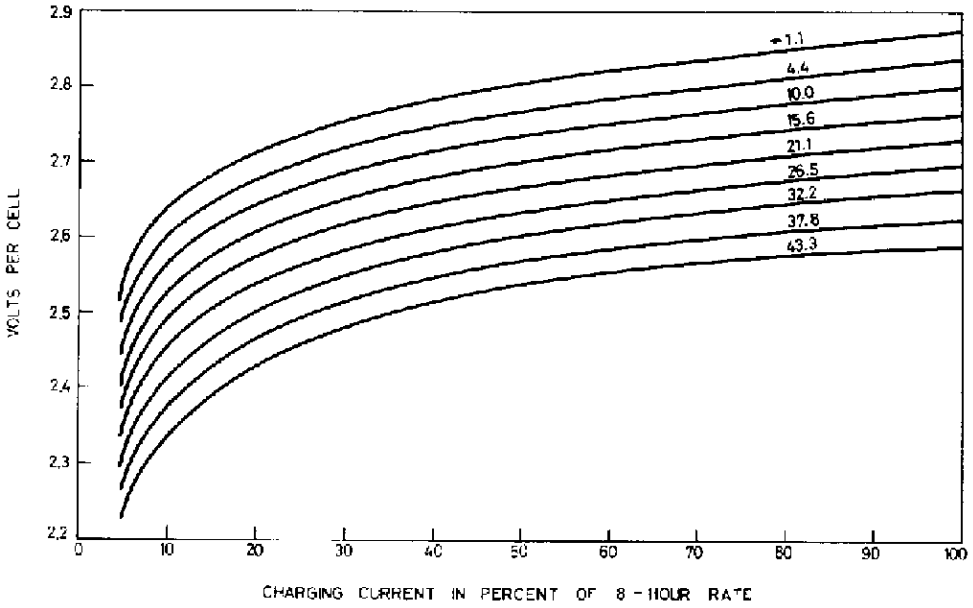

Fig. 57. Typical final charging voltages at various rates and temperatures. The values on the lines represent electrolyte temperatures in degrees Centigrade. The interval between the curves is 12.5 mV/°C. These curves apply to a typical cell but illustrate the need to compensate for the temperature variations if voltage relays are to be employed to terminate the charging of a battery.
(Source: G. W. Vinal, Storage Batteries, Wiley, New York, 1955, p. 244.)

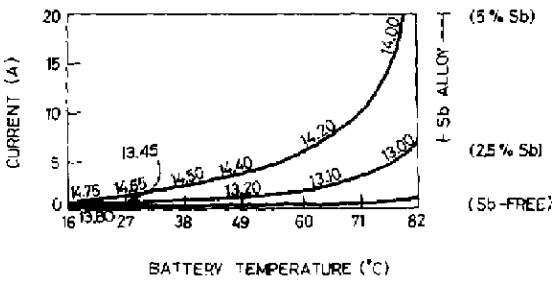

Fig. 58. Current acceptance of automotive battery as a function of temperature. The values in the graph refer to voltage regulator levels to which the 12V battery was subjected. (Source: V. M. Halsall, Proc. BCI Convention, 1974, p. 67.)

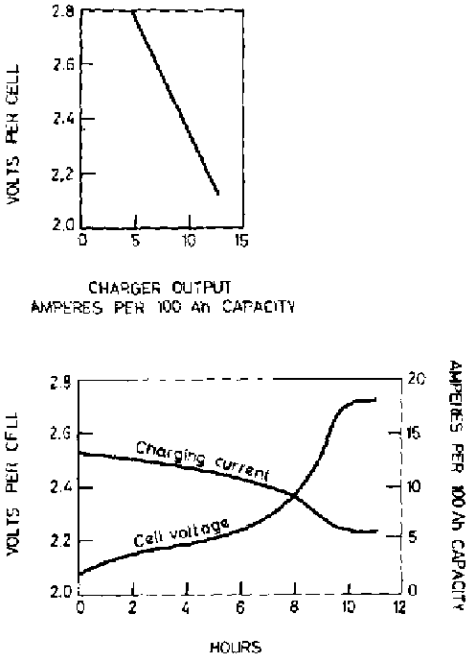

Fig. 59. Typical charger and battery characteristics for a single-step taper charge. (Source: G. Smith, Storage Batteries, Pitman, London, 1964, p. 86.)

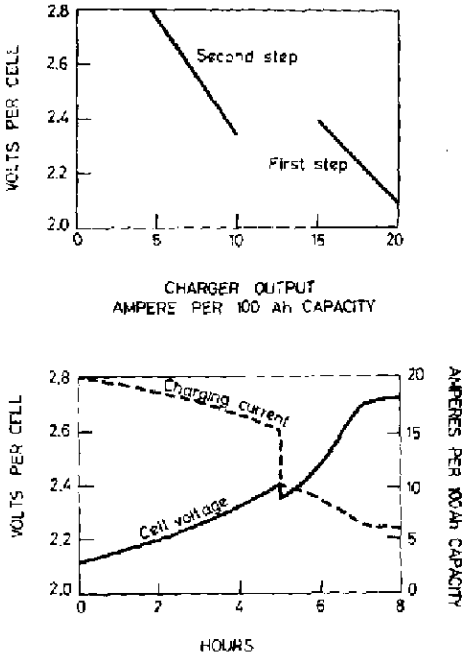

Fig. 60. Typical charger and battery characteristics for a two-step taper charge. (Source: G. Smith, Storage Batteries, Pitman, London, 1964, p. 86.)

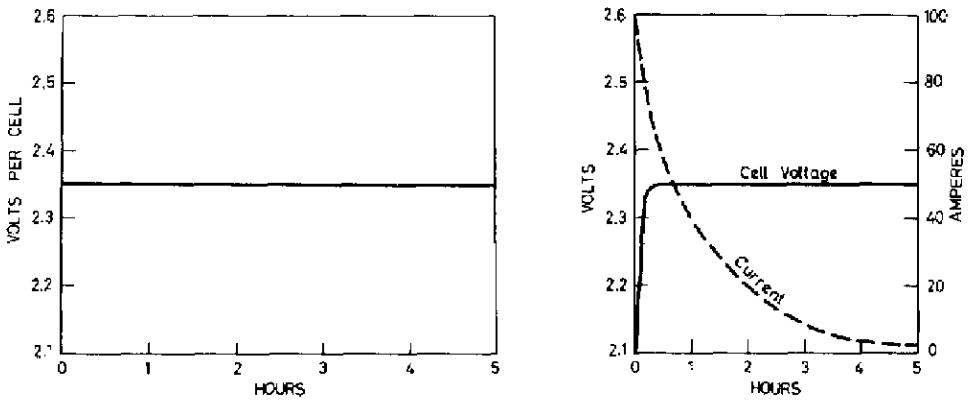

Fig. 61. Typical charger and battery characteristics for constant potential charging.

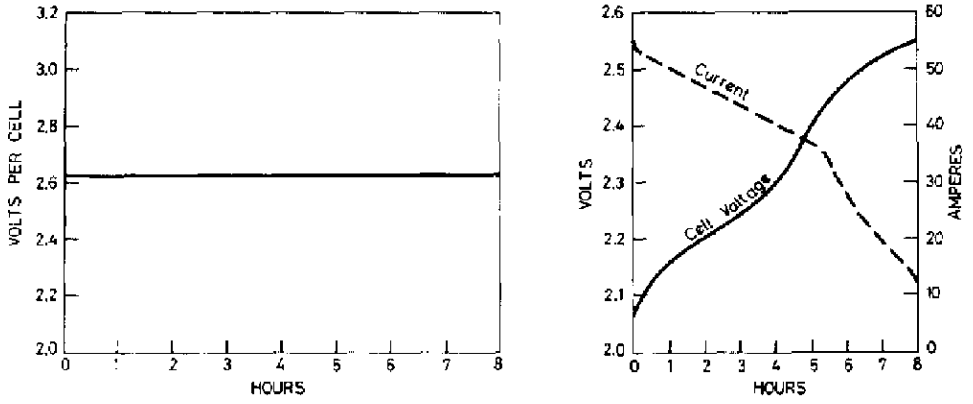

Fig. 62. Typical charger and battery characteristics for modified constant potential charging. In this method the charger voltage is constant as in constant potential charging, but the inclusion of a series resistor limits the initial current through the previously discharged cell to safe values.

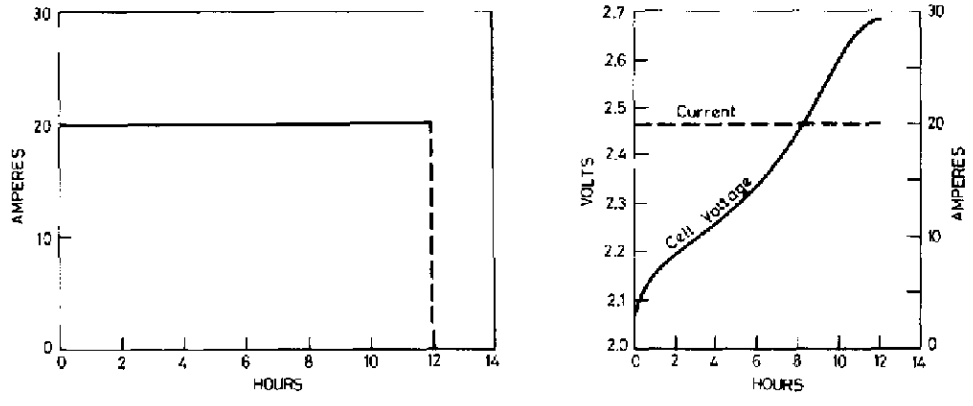

Fig. 63. Typical charger and battery characteristics for constant current charging.

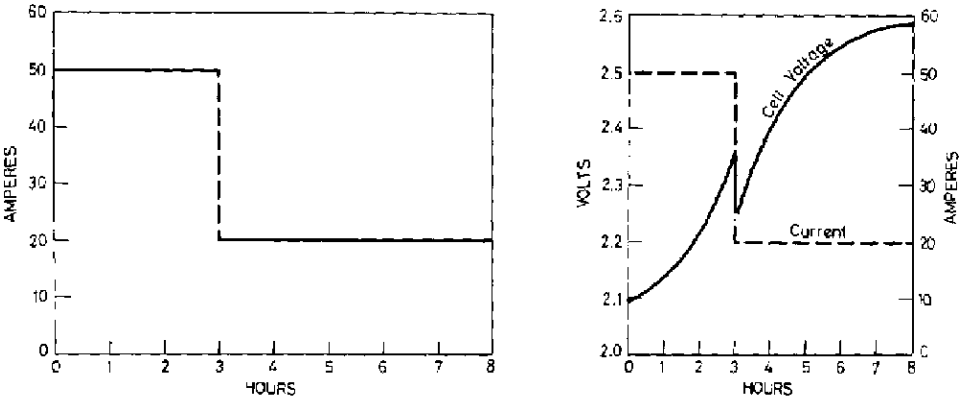

Fig. 64. Typical charger and battery characteristics for two-step constant current charging.

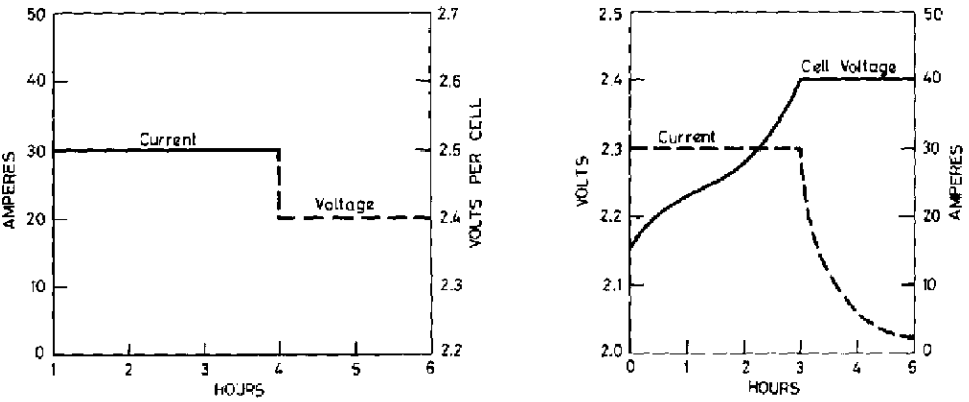

Fig. 65. Typical charger and battery characteristics for constant current–constant potential charging.

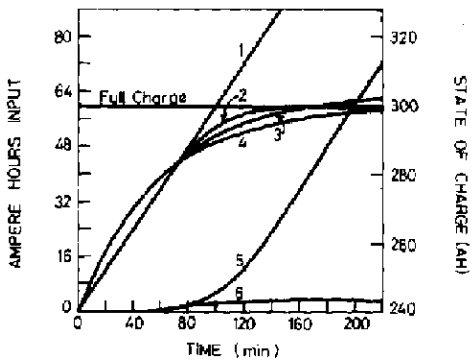

1. Ampere-hours (CC)
2. State of Charge (CC)
3. Ampere-hours (CP)
4. State of Charge (CP)
5. Gas Ampere-hours (CC)
6. Gas Ampere-hours (CP)

Fig. 66. State of charge and ampere hours input during constant potential and constant current charging of lead batteries.
Constant current (CC) charging with 36 amps and constant potential (CP) charging at 2.25 V were done after 2 h of discharge at 30 amps. of a 300 Ah capacity battery. The lowermost curves represent the ampere hours wasted in gassing.
(Source: J. L. Woodbridge, Rly. Elec. Engr., 9 (1918) 6.)

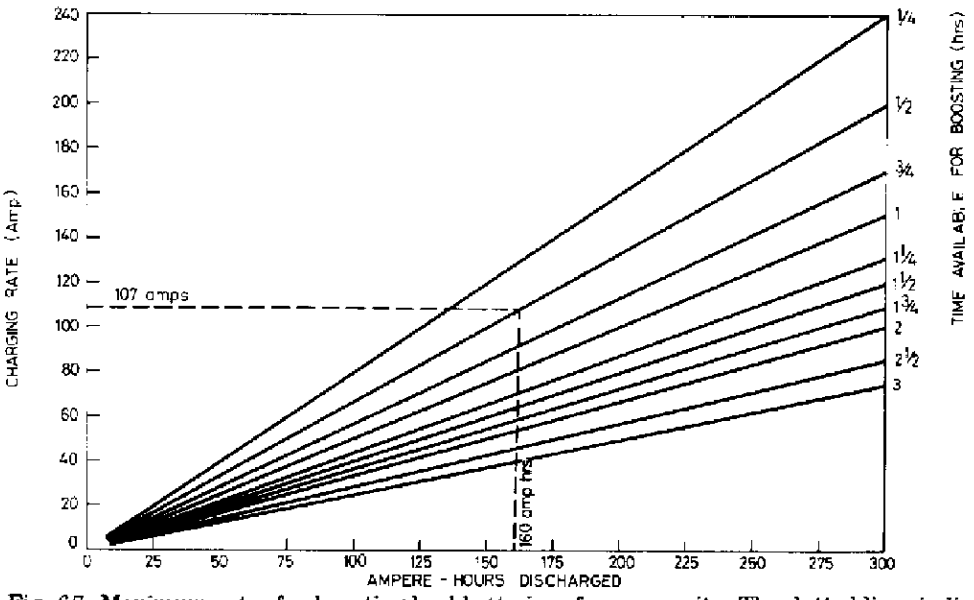

Fig. 67. Maximum rates for boosting lead batteries of any capacity. The dotted lines indicate that a current of 107 amps for half an hour will have to be used for boost charging a battery which has lost 160 Ah during previous discharge.
(Source: G. W. Vinal, Storage Batteries, Wiley, New York, 1955, p. 254.)

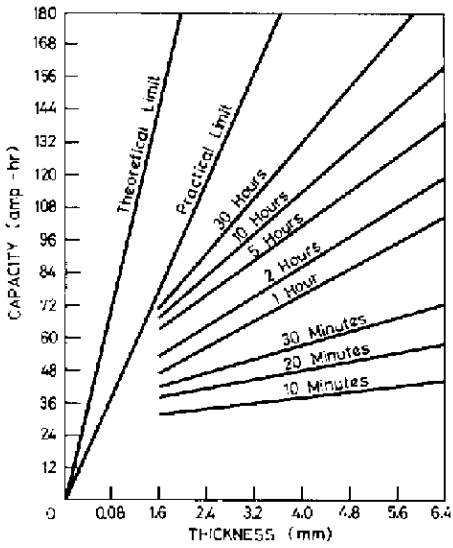

Fig. 68. Dependence of capacity on the thickness of the plates. The durations appearing in the above graph refer to the rates of discharge. The above graph also reveals the great differences in the discharge capacities of a typical 13-plate cell at high as well as low rates for plates of the same thickness. (Implicit in the above graph is Peukert's equation relating the current to the time of discharge through the relationship $I^n t = C$, where n and C are constants for any cell or battery, and I and t are respectively the current and time of discharge.
(Source: G. W. Vinal, Storage Batteries, Wiley, New York, 1955, p. 212.)

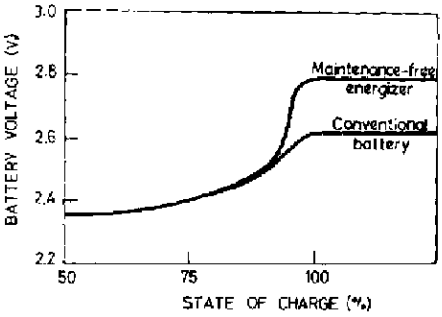

Fig. 69. Charging voltage *vs.* state of charge of conventional and maintenance free batteries (constant current of 5 A at 26.7 °C).
(Source: J. W. Barrick, Proc. BCI Convention 1974, p. 78a.)

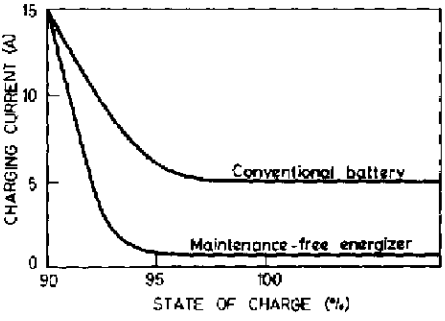

Fig. 70. Charging current *vs.* state of charge of conventional and maintenance free batteries (constant current of 15 A at 26.7 °C).
(Source: J. W. Barrick, Proc. BCI Convention 1974, p. 78a.)

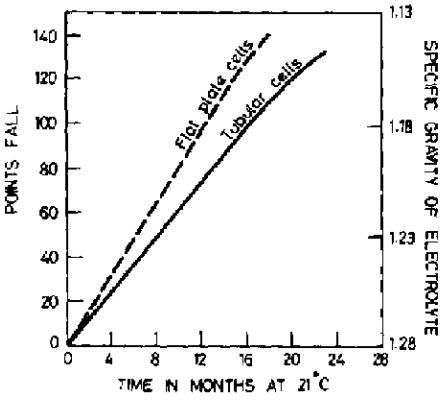

Fig. 71. Typical changes in specific gravity of tubular and flat plate cells on standing. This graph refers to motive power cells. The tubular cells were manufactured by Electric Power Storage Ltd., U.K.
(Source: C. J. Bushrod, LEAD 68, Ed. Proc. 3rd Int. Conf. on Lead, Pergamon, Oxford, 1969, p. 189.)

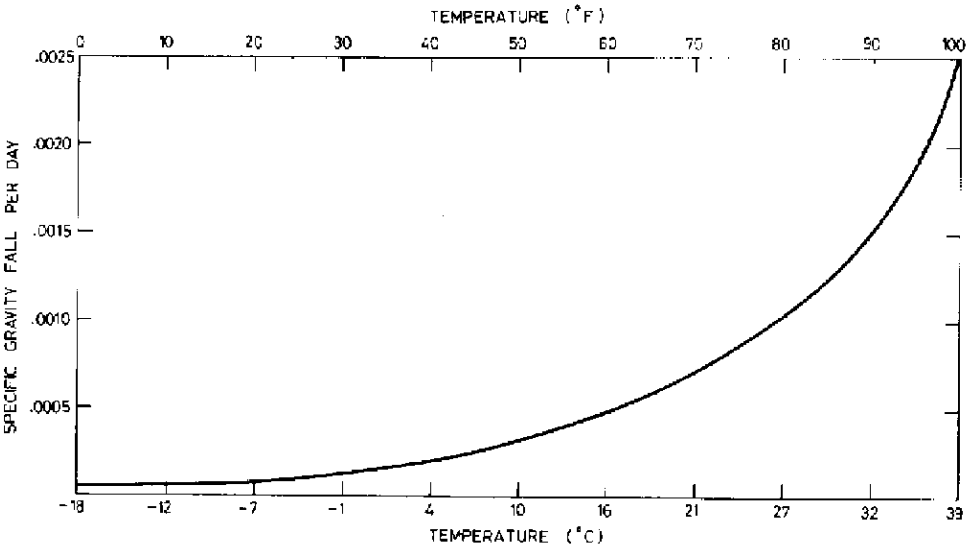

Fig. 72. Fall in specific gravity per day vs temperature. This graph indicates the average performance of new, fully charged batteries with 6% antimony in the grids.
(Source: Storage Battery Mfg. Manual, IBMA 1973, p. 35.)

8. MISCELLANEOUS

TABLE 59

PROPERTIES OF SEPARATORS

	Cellulose	*PVC*	*Rubber*	*Microporous polyethylene*		*Nonwoven polypropylene*
				Standard	*Thin*	
Pore size (μm):	25	20	1	0.03		12
Purity:	fair	good	good	good		excellent
Corrosion resistance:	fair	excellent	excellent	excellent		good
Mechanical strength:	fair	good	fair	excellent		good
Backweb thickness (Mils):	20	14–20	20	18–20	10–12	20
Porosity (%):	60	45	60	60	60	60
Electrical resistance (mohm cm^{-2})	3.72	3.25	3.72	3.72	1.86	2.79
Cold start voltage (5 s, 280 A, −18 °C(0°F))	7.7	7.8	7.7	7.7	8.3	8.0
Flexibility:	brittle	slightly brittle	brittle	excellent		excellent
Sealing:	no	excellent	no	good		excellent

(Source: N. I. Palmer, BCI Convention, April 1975, p. 108.)

TABLE 60

PROPERTIES OF COMMERCIAL THERMOPLASTIC MATERIALS

Property	*Polyethylene high density*	*Polypropylene*		*ABS Heat resistant*	*PVC*	
		unmodified	*copolymer*		*unmodified*	*impact modified*
1 Modulus of elasticity (10^3 kg cm^{-2})	5.97–11.25	0.10–0.12		—	29.24	24.96
2 Tensile strength (kg cm^{-2}):	218–386	302–386	204–316	492–562	562	492
3 Ultimate elongation (%):	15–100	>220	200–700	1–20	36	110
4 Yield stress (kg cm^{-2}):	169–352	345		281–633	921	675
5 Yield strain (%):	5–10	15	—	—	1.66	3.45
6 Rockwell hardness:	R30–50	93	R50–96	R110–115	—	—
7 Notched Izod impact strength (kgm cm^{-1}):	0.081–1.09	0.05	0.04–0.065	0.11–0.22	0.04	1.52
8 Specific gravity:	0.941–0.965	0.90	0.90	1.06–1.08	—	
9 Burning rate:	slow	medium	medium	slow	slow	slow
10 Heat distortion temp. °C (18.6 kg cm^{-2})	—	—	—	115–118	89	89
11 Specific heat (cal g^{-1}):	0.55	0.50	0.50	0.3–0.4	—	—
12 Linear thermal coefficient of expansion (10^{-5}, °C):	11–13	5.8–10	8–10	6.0–6.5	—	—
13 Max. continuous service temp. (°C):	92–200	—	190–240	88–110	—	—
14 Chemical resistance to strong mineral acids:	excellent	excellent	excellent	good	—	—
15 Resistivity (ohm-cm):	$>10^{15}$	$>10^{15}$	$>10^{15}$	10^{17}	$\sim10^{15}$	$\sim10^{15}$

(Source: Handbook of Chemistry and Physics, Chemical Rubber Co. Press, 55th edn., 1974, p. C-765; and Huseby, Bell Syst. Tech. J., (1970) 1359.)

TABLE 61

PROPERTIES OF NATURAL AND SYNTHETIC RUBBERS

Property	*Natural rubber*	*Styrene–butadiene copolymer*	*Butadiene–Acrylonitrile Copolymer (acrylonitrile content)*		
			Low	*Medium*	*High*
1 Density:	0.92	0.94	0.96	0.98	1.0
2 Specific heat (cal g^{-1}):	0.452	0.454	—	—	—
3 Tensile strength (kg cm^{-2}):	274	211	211	246	281
4 Elongation (%):	780	650	400	450	400
5 Stress 300% (kg cm^{-2}):	98	84	105	105	105
6 Brittle point (°C):	—56	—60	—40	—30	—1
7 Insulation resistance (ohm-cm):	10^{17}	10^{15}	10^{10}	10^{10}	10^{10}
8 Resilience (%):	90	75	—	74	63
9 Creep, 70 °C:	26	14.6	—	17	—
10 Relative permeability to hydrogen:	50	—	—	20	—

(Source: Lange's Handbook of Chemistry, McGraw-Hill, New York, 11th edn., 1973, p. 7/453.)

TABLE 62

ELECTRODE POTENTIALS OF REFERENCE HALF CELLS AT 25 °C

Half cell	*Potential* (V) *vs. NHE*
Hg/Hg_2Cl_2, KCl (Sat)	0.2412
Hg/Hg_2Cl_2, KCl (1 *N*)	0.2801
Hg/Hg_2Cl_2, KCl (0.1 *N*)	0.3337
Ag/AgCl, KCl	0.2220
Hg/Hg_2SO_4, SO_4^{-2}	0.6150
$Pb/PbSO_4$, SO_4^{-2}	−0.3563
Pt, $PbO_2/PbSO_4$, SO_4^{-2}	1.6849

(Source: D. J. G. Ives and G. J. Janz, Reference Electrodes, Academic Press, New York, 1961.)

TABLE 63

STANDARD REDUCTION POTENTIALS OF SELECTED SYSTEMS AT 25 °C

Electrode Reaction	E°(V)
$Ag^+ + e^- = Ag$	+0.7991
$Au^{+3} + 3e^- = Au$	+1.50
$Br_2 + 2e^- = 2Br^-$	+1.0652
$Cl_2 + 2e^- = 2Cl^-$	+1.3595
$Cd^{+2} + 2e^- = Cd$	−0.403
$Co^{+2} + 2e^- = Co$	−0.277
$Cr^{+3} + e^- = Cr^{+2}$	−0.41
$Cr^{+3} + 3e^- = Cr$	−0.74
$Cu^+ + e^- = Cu$	+0.521
$Cu^{+2} + e^- = Cu^+$	+0.153
$Cu^{+2} + 2e^- = Cu$	+0.337
$Fe^{+2} + 2e^- = Fe$	−0.440
$Fe^{+3} + e^- = Fe^{+2}$	+0.771
$2H^+ + 2e^- = H_2$	0
$Hg_2^{+2} + 2e^- = 2Hg$	+0.789
$2Hg^{+2} + 2e^- = Hg_2^{+2}$	+0.920
$I_2 + 2e^- = 2I$	+0.5355
$Mn^{+2} + 2e^- = Mn$	−1.18
$Mn^{+3} + e^- = Mn^{+2}$	+1.51
$Ni^{+2} + 2e^- = Ni$	−0.250
$O_2 + 2H^+ + 2e^- = H_2O_2$	+0.682
$O_2 + 4H^+ + 4e^- = 2H_2O_{(l)}$	+1.229
$Pb^{+2} + 2e^- = Pb$	−0.126
$PbO_2 + 4H^+ + 2e^- = Pb^{+2} + 2H_2O$	+1.455
$PbO_2 + SO_4^{-2} + 4H^+ + 2e^- = PbSO_4 + 2H_2O$	+1.685
$PbSO_4 + 2e^- = Pb + SO_4^{-2}$	−0.356

(Source: W. Latimer, The Oxidation States of the Elements and their Potentials in Aqueous Solutions, Prentice Hall, London, 2nd edn., 1952.)

TABLE 64

THERMAL E.M.F. FOR CHROMEL P-ALUMEL THERMOCOUPLE
(EMF values in mV)

Temp. (°C)	*0*	*10*	*20*	*30*	*40*	*50*	*60*	*70*	*80*	*90*
0	0.00	0.40	0.80	1.20	1.61	2.02	2.43	2.85	3.26	3.68
100	4.10	4.51	4.92	5.33	5.73	6.13	6.53	6.93	7.33	7.73
200	8.13	8.54	8.94	9.34	9.75	10.16	10.57	10.98	11.39	11.80
300	12.21	12.63	13.04	13.46	13.88	14.29	14.71	15.13	15.55	15.98
400	16.40	16.82	17.24	17.67	18.09	18.51	18.94	19.36	19.79	20.22
500	20.65	21.07	21.50	21.92	22.35	22.78	23.20	23.63	24.06	24.49
600	24.91	25.34	25.76	26.19	26.61	27.03	27.45	27.87	28.29	28.72
700	29.14	29.56	29.97	30.39	30.81	31.23	31.65	32.06	32.48	32.89

(Source: Handbook of Chemistry and Physics, Chemical Rubber Co., 55th edn., 1975, p. E-106.)

TABLE 65

SIEVE DATA
(Based on ASTM E 11-61, Adopted 1961)

Sieve design		*Wire diameter*	*Sieve design*		*Wire diameter*
Standard (mm)	*Alternate (No.)*	(mm)	*Standard* (mm)	*Alternate (No.)*	(mm)
26.9	1.06 in.	3.90	0.707*	25	0.45
22.6*	7/8 in.	3.50	0.595	30	0.39
16.0*	5/8 in.	3.00	0.500*	35	0.34
11.2*	7/16 in.	2.45	0.420	40	0.29
8.0*	5/16 in.	2.07	0.354*	45	0.247
6.73	0.265 in.	1.87	0.297	50	0.215
5.66*	3½	1.68	0.250*	60	0.180
4.76	4	1.54	0.210	70	0.152
4.00*	5	1.37	0.177*	80	0.131
3.36	6	1.23	0.149	100	0.110
2.83*	7	1.10	0.125*	120	0.091
2.38	8	1.00	0.105	140	0.076
2.00*	10	0.90	0.088*	170	0.064
1.68	12	0.81	0.074	200	0.053
1.41*	14	0.72	0.063*	230	0.044
1.19	16	0.65	0.053	270	0.037
1.00*	18	0.58	0.044	325	0.030
0.841	20	0.51	0.038	400	0.025

*These sieves correspond to those proposed as an International (ISO) Standard.
(Source: Lange's Handbook of Chemistry and Physics, McGraw-Hill, New York, 1956, p. 931.)

TABLE 66

RESISTIVITY AND TEMPERATURE COEFFICIENT OF RESISTIVITY OF SOME ELEMENTS

Element	*Temperature* (°C)	*Resistivity* (μohm-cm)	*Temperature coefficient of resistivity (per °C)*
Aluminium	20	2.6548	0.00429
Carbon (graphite)	0	1375.0	−0.00028
Copper	20	1.6730	0.0068
Nichrome	20	110.0	0.0004–0.00003

(Source: Handbook of Chemistry and Physics, Chemical Rubber Co., 1953, p. F-159 and International Critical Tables, McGraw-Hill, New York, Vol. 6, p. 159.)

TABLE 67

VARIATION OF TEMPERATURE, PRESSURE AND DENSITY OF THE ATMOSPHERE WITH ALTITUDE

Elevation (km)	*Summer*			*Winter*		
	Temp. (°C)	*Pressure* (mm of Hg)	*Density, dry air* (g cm^{-3})	*Temp.* (°C)	*Pressure* (mm of Hg)	*Density, dry air* (g cm^{-3})
20.0	−51.0	44.1	0.000092	−57.0	39.5	0.000085
19.0	−51.0	51.5	0.000108	−57.0	46.3	0.000100
18.0	−51.0	60.0	0.000126	−57.0	54.2	0.000117
17.0	−51.0	70.0	0.000146	−57.0	63.5	0.000137
16.0	−51.0	81.7	0.000171	−57.0	74.0	0.000160
15.0	−51.0	95.3	0.000199	−57.0	87.1	0.000187
14.0	−51.0	111.1	0.000232	−57.0	102.1	0.000220
13.0	−51.0	129.6	0.000270	−57.0	119.5	0.000257
12.0	−51.0	151.2	0.000316	−57.0	140.0	0.000301
11.0	−49.5	176.2	0.000366	−57.0	164.0	0.000353
10.0	−45.5	205.1	0.000419	−54.5	192.0	0.000408
9.0	−37.8	237.8	0.000470	−49.5	224.1	0.000466
8.0	−29.7	274.3	0.000524	−43.0	260.6	0.000526
7.0	−22.1	314.9	0.000583	−35.4	301.6	0.000590
6.0	−15.1	360.2	0.000649	−28.1	347.5	0.000659
5.0	−8.9	410.6	0.000722	−21.2	398.7	0.000735
4.0	−3.0	466.6	0.000803	−15.0	455.9	0.000821
3.0	+2.4	528.9	0.000892	−9.3	519.7	0.000915
2.5	+5.0	562.5	0.000942	−6.7	554.3	0.000967
2.0	+7.5	598.0	0.000990	−4.7	590.8	0.001023
1.5	+10.0	635.4	0.001043	−3.0	629.6	0.001083
1.0	+12.0	674.8	0.001100	−1.3	670.6	0.001146
0.5	+14.5	716.3	0.001157	0.0	714.0	0.001215
0.0	+15.7	760.0	0.001223	+0.7	760.0	0.001290

(Source: Handbook of Chemistry and Physics, Chemical Rubber Co., 1953, p. 3087.)

TABLE 68

VAPOUR PRESSURE OF WATER AT DIFFERENT TEMPERATURES

Temp. (°C)	*Vapour pressure* (mm Hg)	*Temp.* (°C)	*Vapour pressure* (mm Hg)
0	4.579	55	118.04
5	6.543	60	149.38
10	9.209	65	187.54
15	12.788	70	233.70
20	17.535	75	289.10
25	23.756	80	355.10
30	31.824	85	433.60
35	42.175	90	525.76
40	55.324	95	633.90
45	71.88	100	760.00
50	92.51	–	–

(Source: Handbook of Chemistry and Physics, Chemical Rubber Co., 1975, p. D-159.)

9. USEFUL FORMULAE

Ampere hour capacity

$= \int_0^t i\mathrm{d}t$, where i is the instantaneous current and t is the time of discharge.

Ampere hour efficiency

$$= \frac{\text{Ampere hours output}}{\text{Ampere hours input}} = \frac{\int_0^{t_d} i_d \mathrm{d}_t}{\int_0^{t_c} i_c \mathrm{d}_t}$$

where i_d and i_c are discharging and charging currents respectively, and t_d and t_c are discharging and charging periods respectively.

Ampere hour for forming

$\Sigma X_j A_j/e$ where X_j is the fraction by weight of active material, j and A_j is the theoretical ampere hours required for its oxidation or reduction, and e is the forming efficiency.

Charging current

$(E_L - E_B)/r$, where E_L and E_B are the line and battery voltages respectively, and r is the internal resistance of the cell.

Coefficient of charge

1/Ampere hour efficiency.

Coefficient of use of active material

$$\frac{\text{Actual capacity obtained}}{\text{Theoretical capacity based on complete utilisation of active material}}$$

Current through an external resistance

$$\frac{N_s N_p E}{N_p R + N_s r}$$

where N_s and N_p represent the number of cells in series and parallel respectively, E the e.m.f. of the cell, R the external resistance, and r the internal resistance of the cell.

Degree Baume

$$145 - \frac{145}{\text{specific gravity}}$$

Degree Twaddell

$$= 200 \text{ (specific gravity} - 1)$$

Discharge rate

$$= \frac{\text{Ampere hour capacity}}{\text{Discharge current}}$$

Diffusion rate

$$= \frac{DA(C_0 - C_i)}{L}$$

where D is the diffusion coefficient, A the area of cross section, C_0 and C_i are concentrations of electrolyte outside and within the pores respectively, and L is the distance through which the acid diffuses.

Energy Density

$$= \frac{\text{Watt hours}}{\text{Weight of the battery}}$$

Gassing rate of maintenance-free battery

$$g = \frac{i \times 10.4}{v}$$

where g is the volume in cm^3 of gas evolved per min per cm^3 of electrolyte above the plates during charging, i is the charging current in amperes during overcharge, and v the volume in cm^3 of electrolyte above the plates. This equation applies to a current acceptance test on a 12 V battery performed at a constant voltage of 14.1 V and 51.7 °C. The current (i) is measured after it reaches equilibrium. (Source: R. L. Bennet, Proc. B.C.I. Conv., 1974, p. 62.)

Faraday Constant

$$= 96487 \text{ coulomb} = 26.8 \text{ ampere hour.}$$

Ficks' Laws

$$1.\ \text{Flux} = D \frac{\partial c}{\partial x}$$

where D is the diffusion coefficient, c is concentration, and x is the distance travelled.

$$2.\ \frac{\partial c}{\partial t} = D \frac{\partial^2 c}{\partial x^2}$$

where t is the time.

Gibbs–Helmholtz equation:

$$\Delta G = \Delta H + T\left(\frac{\partial \Delta G}{\partial T}\right)_p$$

where ΔG is the free energy change and ΔH is the enthalpy change for the reaction, T is the absolute temperature and p is the pressure.

Impedance

$$= \frac{\text{Amplitude of voltage}}{\text{Amplitude of current}}$$

Internal resistance of the battery

$$= \frac{E - E^1}{i}$$

where E is the open circuit voltage, E^1 is the voltage during discharge and i is the current during discharge of the battery. (Also = R_p/n, where R_p is the resistance between a pair of plates in the charged condition and n is the number of plate pairs.)

Mean pore radius of the separator

$$= \left(\frac{8KL^2}{Ed^2}\right)^{1/2}$$

where K is the permeability constant, L is the true length of the pores, d is the thickness of the separator and E is the porosity of the separator.

Nernst equation

$$E = E_0 + \frac{0.059}{n} \log \frac{a_{Cu^{+2}}}{a_{Zn^{+2}}} \quad \text{for } Zn + Cu^{+2} \rightleftharpoons Zn^{+2} + Cu,$$

where E and E_0 are EMF and standard EMF of the cell, n is the number of electrons transferred, and a's are the respective activities at 25 °C.

Ohm's law

$$i = \frac{E}{R}$$

where i is the current, E is the voltage and R is the resistance.

Oxygen requirement for curing

= 0.05915 × weight in grams of lead in the paste.

Peukerts' equation

$C = i^n t$, where n and C are constants characteristic of the battery, useful in determining the duration of discharge (t) or current (i).

Permeability constant of separator

$$= Q \frac{d\eta}{A \Delta P}$$

where Q is the flow rate ($cm^3\ sec^{-1}$), d is the thickness of the separator, η the viscosity of air, A is the area of the separator and ΔP is the pressure required (dynes cm^{-2}).

pH

= — log (activity of hydrogen ions)

Porosity of the plates

$$= 1 - \frac{\text{Apparent density}}{\text{True density}}$$

Pore diameter

$$= \frac{-4\sigma \cos \theta}{P}$$

where σ is the surface tension of liquid, θ is the wetting angle and P is the pressure of mercury as determined by Winslow and Shapiro's method.

Power loss

$= i^2R$ where i is the discharge current and R is the resistance of the circuit.

Resistance for boosting

$$= \frac{E_L - 2.5N}{5i_n}$$

where E_L is the line voltage, N is the number of cells and i_n is the normal rate of charging.

Resistance for constant current charging

$$= \frac{E_L - E_s N}{i_c}$$

where E_L is the line voltage and E_s is the voltage of the battery at the start of charge, N is the number of cells and i_c is the charging current. (Minimum resistance = $(E_L - E_e N)/i_c$ where E_e is the voltage at the end of charge.)

Resistance of conductors in series

$$= R_1 + R_2 + \ldots\ldots$$

Resistance of conductors in parallel

$$= \frac{1}{(1/R_1) + (1/R_2) + \ldots\ldots}$$

Short circuit current of the battery

$$= \frac{\text{cell voltage} \times \text{number of cells}}{\text{internal resistance of the battery} + \text{line resistance}}$$

Specific conductivity

$$= \frac{1}{R}\frac{l}{a}$$

where R is the resistance, l is the length of the conductor and a is its area of cross section.

Specific resistance

$$= \frac{1}{\text{specific conductivity}}$$

Specific surface area of the separator

$= 14/\rho(E^3/(1-E)^2K)^{1/2}$, where ρ is the true density, E is the porosity and K is the permeability constant of the separator.

Tafel equation

$\eta = a + b \log i$, where η is the overpotential, i is the current and a and b are constants characteristic of the electrode reaction defined by

$$a = \frac{\pm RT}{\alpha n F i_0} \text{ and } b = \frac{\pm RT}{\alpha n F}$$

where α is the transfer coefficient and i_0 is the exchange current density of the electrode reaction involving transfer of n electrons. (Cathodic current is taken as positive and anodic current as negative.)

Temperature coefficient of EMF

$$= \frac{(E + \Delta H/nF)}{T}$$

where E is the EMF of the cell, ΔH is the enthalpy of the electrode reaction, n is the number of electrons transferred and T is the temperature in degrees absolute.

Test current

$$= \frac{\text{Ampere hour capacity}}{\text{Time rating}}$$

Transport number $= \dfrac{|Z_i|C_i u_i}{\Sigma|Z_i|C_i u_i}$

where Z_i and C_i and u_i are the valency, concentration and mobility of the ith ion respectively.

Volt efficiency

$$= \frac{\text{Average voltage on discharge}}{\text{Average voltage on charge}}$$

Voltage during discharge

$= E - ir$, where E is the open circuit voltage, i is the discharge current and r is the internal resistance of the battery.

Water loss of maintenance free-battery

$= 0.0056\ it$(ml), where i is the overcharge current in amperes and t is the time in minutes, at standard temperature and pressure.

Watt hour capacity

$$= \int_0^t iE\ \mathrm{d}t,$$

where i and E are the instantaneous current and voltage at time t.

Watt hour efficiency

$$= \frac{\text{Watt hours obtained during discharge}}{\text{Watt hours put in during charge}}$$

$$= \text{Ampere hour efficiency} \times \frac{\text{Average voltage during discharge}}{\text{Average voltage during charge}}$$

Weight of acid decomposed (or formed) during discharge (or charge) of a battery:

$= 3.66$ g $\times$ number of ampere hours discharged (or charged).

Weight of water formed (or decomposed) during discharge (or charge) of a battery:

$= 0.672$ g $\times$ number of ampere hours discharged (or charged).

Net change in weight of electrolyte during discharge (or charge) of a battery:

$= 2.987$ g $\times$ number of ampere hours discharged (or charged).

Weight loss $= \dfrac{W_f - W_i}{A}$

where W_f and W_i are final and initial weights of the specimen of area A.